Comprehensive Study of the Chemical Reactions Resulting from the Decomposition of Chloroform in Alkaline Aqueous Solution

A DISSERTATION
SUBMITTED TO THE FACULTY OF THE GRADUATE SCHOOL
OF THE UNIVERSITY OF MINNESOTA
BY

Jorge Estevez Mews

IN PARTIAL FULFILLMENT OF THE REQUIREMENTS
FOR THE DEGREE OF
DOCTOR OF PHILOSOPHY

Jiali Gao

November 2009

Acknowledgements

This is the most important part of this manuscript, as I have had the very best of luck with the people who became part of my life during my Ph.D. study at the University of Minnesota in the Twin Cities. Their actions serve as a role model for the rest of my life. It breaks my heart when I think about all that I put my research advisor through. I walked into his office for the first time with an extremely low level of confidence in my ability to do research, which severely lowered my goals and my motivation. I cannot name anyone else who would have put the same amount of effort into helping me learn how to succeed. Thus, in accepting me into his research group, professor Jiali Gao took on a challenge larger than any of us knew at the time, but he was always willing to support his graduate students through the difficulties of pursuing a doctoral degree. Dr. Jiali Gao also worked hard to help his graduate students help each other. He has had to make sacrifices throughout his life in order to obtain and maintain his tremendous amount of knowledge and in order to make the time to be there for us, which I will never forget. In addition, Jiali knew when we needed the support the most and did everything in his power to help, which is what only best friends do. Thank you Jiali!

I have the greatest fortune to have one of the brightest and most caring persons be a top friend and collaborator. A lifetime of thankfulness will not suffice for all she did for me. Yan Zhou is one of the most complete human beings I have ever met. To this day I do not know how she can achieve so much every day. Yan helped me hundreds of times with the most difficult problems and never stopped smiling and caring for me.

One of my very best friends is very special. For Dr. Kin-Yiu Wong science is the most beautiful thing there is on earth. His devotion to physics has nearly become an obsession and is driving him to making great contributions to society. Kiniu has another passion which very few people understand fully. He is always willing to do anything to help the people around him. No one has helped people in our laboratory more than Kiniu has. It is so large, that I cannot arrive at even a rough estimate of the number of hours that Kiniu sacrificed for helping just me. Even more astonishing is the amount of thought that he gave to my problems in order to find a solution to each and every one of them. Just to mention one example, it was through discussions with Kiniu, in which he forced me to take notes, that half of the knowledge of the second chapter of this thesis sank into my head. He fought against my fear and stubbornness when I resisted the start of the most important computations. He also had to go beyond what any person would go to help me when I was not willing to make the writing of this dissertation a priority. I would not be where I am today, and would not know what I know now had Kiniu not been such an unusually devoted and caring friend. Thank you!

Professor Shu-Hua Ma of the University of Wisconsin – Stevens Point is among two hands full of people who I consider the most altruistic persons to ever cross my path. Shu-Hua was born to help others and I bet you that is what she is doing right now as you read this line. Her bright mind, hard work, tremendous knowledge, motivating smile, and endless supply of will to assist people are to be recognized by anyone working in Jiali Gao's computational chemistry lab during the years that she was here.

When very few people ever thought that I could make it through the toughest challenge, someone believed in me and decided to invest her time to help. She is one of the most interesting persons that I have ever met, is an extremely intelligent scientist, and one of my very best friends. It is humbling how much time she has devoted to teach me how to write clearly. The level of detail to which she reviewed parts of this manuscript is astounding. I will always be thankful to her, for how she motivated, changed, and saved my life. Thank you! You are one of the most amazing people in the world!

Even though the name speaks for itself, no length of writing will suffice to describe Dr. Kong-Hauw Sarwa-Bakti Tan. First and foremost, he is, and has been my best friend for over a decade. He is one of the most altruistic persons to ever be part of my life. He is an extremely intelligent and considerate person who has always been there for me whenever I needed help, even through very long times during which I could not return the favor. His friendship, help, wise advice and laughter are inseparable from my experience at the University of Minnesota. It is not just that I would not be where I am if it were not for Sarwa, but I would not be who I am, since I shared with him for half of my adult life the values driving my life. Unfortunately, there is only one like Sarwa.

I shared a dream to shake hands with one of my best friends in front of the colossal Northrop auditorium of the University of Minnesota the day that both of us graduate. He kept that dream alive, helped, and motivated me through the most challenging of times. At one time many years ago I almost quit, but Dr. Jun Kyung Chung was confident that I could do it and encouraged me to continue. We will shake hands soon.

Dr. Yuri Tserlukewich and Dr. Ilona Babenko have not heard from me for a while, but I will make sure I hunt them down to tell them how they changed my life during the first two years of my stay in Minnesota. They are the most balanced couple I have ever met.

Francesc Domenech Molins has been an exceptional friend who helped me at two of the most crucial times, and who was always there to enjoy every other time. His calm and affectionate temperament, great love for science and devotion to people make him as unique as his name, and I am looking for many great years of friendship to come!

Dr. Jingzhi Pu and Dr. Alessandro Cembran made me enjoy being part of the research group a whole lot more with their warm temperaments and incredible wit. Pu is one of the most intelligent and balanced persons I have ever met and so is Alessandro. They helped me a lot and their personalities and care for others serve as much as a role model as the power of their minds. Pinsker Lin's endless encouragement and help at key moments is priceless. Dr. Yao Fan helped me avoid entering repetitive input and was always an example for me. Professor Mireia Garcia Viloca, Dr. Kwangho Nam, Dr. Lakshmi S Devi-Kesavan gave me a great start in a new research environment. Nam taught me a lot through informal discussions. Dr. Shudeep Bhattacharyya, Dr. Xavier Prat Resina, Jake Kilian, and Dr. Christian Hensen made lasting impressions on me. I am really grateful to those who made this research group a home away from home.

There is a person who changed my life from the very first day that I spent in Minnesota and who at one point in time was one of the very few people who knew of and saw

value in my teaching skills. Professor Paul Ellis unfortunately left us before I had a chance to properly thank him. Thus, the only recourse left to me is to continue fighting for the same principles that he fought for and to treat my students with the same level of respect and encouragement that he did. He strived to make every decision fair to all.

I am particularly thankful to Professor Oriol Valls for caring for me since I set foot in Minnesota and for making sure I left in a much better position. I will never forget him. Neither will I loose track of one of my very best friends in Minnesota, Professor John Broadhurst, who is exactly the type of person and professor who I want to be. Big Hug! I will always be indebted to Professor Edgar Arriaga for taking on the task of being part of my final thesis defense committee and reading my whole doctoral thesis in its worst shape and for his excellent recommendations to improve it. Professor Charles Campbell will always be in my list of favorites for his support during both my oral and final thesis defense. His appreciative nature and wisdom will always stay with me. Professor Yuichi Kubota is the best Director of Graduate Studies in the whole world. Professor Benjamin Bayman has been my idol for over a decade. It is not just his exceptional understanding of physics, but his moral nature, care for others and friendship to Professor Broadhurst that make me want to never loose touch with him.

Sarah Burson, Nick Onorato, Kate Raach, Cristiane Zampieri have been an immeasurable source of support and will to succeed. Gbemonde (Yves) Adjallah, Bin Wu, Jeffrey Slava Thaler and Neil Graf deserve a lot more of my attention than they have received lately, but their presence in my life has been very enjoyable and cheerful.

I want to thank Professors Mikhail Shifman, Kenneth Heller, and Roger Rusack for finding and expressing value in my teaching skills and for feeding my dream to teach.

The following Professors saved my life by not just expressing appreciation for my teaching, but also communicating it in written form to prospective employers, thus helping me land the job of my life. I am indebted to these special friends for life. They are Professor Mech Johnson, who also helped me start a new life as a lecturer in the University of Wisconsin at Washington County, and Professor Wayne Schaefer who also made UW-WC the most welcoming new place I had ever been to. I admire their determination to make every sacrifice for the success of students. I was just one more of many Teaching Assistants for Professor James Eckert of Harvey-Mudd College in California who teaches at the University of Minnesota every summer. His nature and devotion to students opened his attention to their appreciation of their special TA.

Professor Roger Peterson and Dr. David L. Nixon of the University of Wisconsin at Washington County were vital to my self-esteem and changed my life forever. Their encouragement and appreciation when I needed it the most will never be forgotten.

Professors Mike Hencheck and Heidi Fencl of the University of Wisconsin at Green Bay will have to deal with me for the rest of their lives because I will not rest until I have returned the equivalent of their astronomically-sized gift of the job of my life.

Last but not least, my family overseas knows how much I miss and appreciate them.

Dziekuje!

Abstract

Chloroform ($CHCl_3$) is a volatile liquid, which has a rather slow rate of decomposition in ground water. It is a known carcinogen and one of the most common contaminants found at toxic waste sites. The dominant degradation process for chloroform in both the atmosphere and the groundwater is the reaction with the hydroxyl radical or hydroxide ion. This process triggers a sequence of reactions which ultimately yield carbon monoxide, hydrogen chloride, and formic acid. The rate of chloroform degradation is considerably larger in solution than that in the gas phase and it increases dramatically with increasing pH. However, only one of the viable reactions had been studied previously at a high level of theory in solution. It is of great interest to gain a deeper understanding of the decomposition reaction mechanism.

Quantum mechanical methods are well suited for studying the mechanism of organic reactions. However, a full quantum mechanical treatment of the entire fluid system is not computationally feasible. In this work, combined quantum mechanical and molecular mechanical (QM/MM) methods are used for studying chemical reactions in condensed phases. In these calculations, the solute molecules are treated quantum mechanically (QM), whereas the solvent molecules are approximated by empirical (MM) potential energy functions. The use of quantum mechanics and statistical sampling simulation is necessary to determine the reaction free energy profile.
In the present study, the ab initio Hartree-Fock theory along with the 3-21G basis set was used in the quantum mechanical calculations to elucidate the reaction pathways of

chloroform decomposition, with a focus on basic reaction conditions. Statistical mechanical Monte Carlo approach was then applied in molecular mechanical simulations, employing the empirical TIP3P model for water.

We employed state-of-the-art electronic structure methods to determine the gas-phase inter-nuclear potential energy profile for all the relevant reactions. Each gas-phase potential energy profile obtained at a high level of theory was used as a post-correction of the corresponding reaction free energy profile in aqueous solution. A detailed picture of the actual mechanism driving the decomposition pathway of chloroform has emerged from these simulations.

Table of Contents

List of Tables

CHAPTER 1

Introduction

1.1 General Remarks

This dissertation describes the most rewarding research project of my Ph.D. study. It was carried out with the unwavering support and candid guidance of Professor Jiali Gao. The objective of this work is to understand the reaction pathways and to estimate the associated reaction rates in the chloroform decomposition in aqueous solution under basic reaction conditions. It requires a detailed understanding of the reaction mechanism, and knowledge of the free energies of activation for all the steps of decomposition of chloroform. The sequence of reaction steps selected for explicit solvent simulation are shown in Table 1.1 below. This mechanism is described in detail in chapter 3.

Table 1.1 Chloroform aqueous alkaline dehalogenation reaction mechanism producing carbon monoxide.

Step #	Rate	
I	slow	$CHCl_3 + OH^- \rightleftharpoons CCl_3^- + H_2O$
II	fast	$CCl_3^- \rightleftharpoons CCl_2 + Cl^-$
III	?	$CCl_2 + H_2O \rightarrow CHCl_2OH$
IV	Fast	$CHCl_2OH + OH^- \rightarrow CHClO + Cl^- + H_2O$
V	Fast	$CHClO + OH^- \rightarrow CO + Cl^- + H_2O$

We first studied these reactions in the gas-phase to obtain an understanding of the intrinsic properties of the inter-nuclear potential energy surface. We employed Density Functional Theory (B3LYP), and second order Møeller-Plesset Perturbation Theory (MP2) and Coupled-Cluster (CCSD(T)) high level ab-initio theoretical methods to accurately determine the gas-phase potential energies, enthalpies, and free energies. We compared the values obtained with available experimental values for validation of these methods. We proceeded to conduct extensive statistical sampling in Monte Carlo simulations of the solvated system to obtain the one-dimensional and two-dimensional free energy profiles for the five reactions in explicit water solutions. Validation of our methods was achieved through comparison of the net reaction energies obtained with experimental findings based on the pK_a values and free energies of solvation of the constituent molecules. The results are shown in chapter 4.

1.2 Chlorinated Hydrocarbons

Chloroform belongs to the family of chlorinated hydrocarbons (CHCs). Many CHCs are among the most common contaminants found at hazardous waste sites and are either known or suspected carcinogens.[1,2] Chlorinated hydrocarbons can be degraded by both biotic and abiotic processes. In general, the chemical stability of CHCs tends to increase with the number chlorine atoms in the molecule.[3] This trend is reflected in the large half-life values of fully chlorinated hydrocarbons. Experimental hydrolysis rate constants for chlorinated methanes, ethanes, ethenes, and propanes have been measured in dilute aqueous solution within the temperature range of 0-180 ºC and pH range of 3-14. The corresponding half-life values range from a few days to 10^{10} years.[4] As a

result of the slow rate of decay of many CHCs under neutral conditions, few studies of their abiotic chemical decomposition have been published, and disagreement still exists regarding the reaction mechanisms and rates.[2]

1.3 Differences and Similarities Between Chloroform and Other Chloromethanes

Among the chlorinated hydrocarbons, chloromethanes are the chlorine derivatives of methane. Table 1.2 lists the four chloromethanes and the nomenclature.

Table 1.2 The Chloromethane Family (Nomenclature)

Formula	IUPAC Name	Common Name
CH_3Cl	Monochloromethane	methyl chloride
CH_2Cl_2	Dichloromethane	methylene chloride
$CHCl_3$	Trichloromethane	chloroform
CCl_4	Tetrachloromethane	carbon tetrachloride

Chloromethanes find broad industrial applications primarily as chemical intermediates, as well as solvents. They are released into the environment through sources both anthopogenic and natural in origin. More than 300,000 metric tons per year were produced of each type of chloromethane worldwide in 1993. The first three chloromethanes exhibit a solubility ranging from 1.9 to 7.3 g/kg in water at 25 ºC. Tetrachloromethane is an order of magnitude less water soluble than the other chloromethanes, since it has no dipole moment as a result of its tetrahedral symmetry. All four chloromethanes are thermally stable, volatile, and exhibit surface tension values ranging from 16×10^{-3} to 29×10^{-3} N/m (1/5 to 2/5 that of water) at 20 ºC. The first three chloromethanes are officially considered harmful, whereas tetrachloromethane is considered poisonous.[5]

Monochloromethane is the only chloromethane that is flammable. It is released into the atmosphere through natural processes in larger amounts than higher chlorinated chloromethanes. Monochloromethane is hydrolyzed by water at an elevated temperature to produce methanol and hydrogen chloride, neither of which is toxic in solution. This process is greatly accelerated by the presence of alkali. Dichloromethane undergoes microbiological decomposition and therefore is either completely absent, or present in very low concentrations in water sources.[5]

In contrast, both trichloromethane (chloroform) and tetrachloromethane can be detected in many water supplies, and are fairly stable compounds with respect to both biotic and abiotic transformations.[1,5] Chloroform is more susceptible to photolysis in the air when exposed to radiation at visible frequencies than tetrachloromethane. Tetrachloromethane is only subjected to decomposition by high frequency UV radiation. For these two chloromethanes, hydrolysis is so slow that it may not be considered a noteworthy dehalogenation process in water. Based upon experimentally determined rate constants, the half-life of chloroform in water at 25 ºC ranges from 1,850 to 3,650 years at pH 7, and from 25 to 37 years at pH 9.[4,6,7] Estimates for the half-life of tetrachloromethane in water have been reported to range from forty years[4] to seven thousand years, and to be independent of pH.[8] However, the dehalogenation rate of tetrachloromethane is highly dependent on the solvent composition. I. Fells and E. Moelwyn-Hughes reported a four-fold increase of the rate of alkaline hydrolysis when the reaction was carried out in 10% methyl alcohol. They measured the half-life of

tetrachloromethane to be 11 days in acidic solution, and 3 days in alkaline solution.[9] Unfortunately, tetrachloromethane hydrolysis remains extremely slow in neutral solutions and thus continues to pose a problem for its removal from water bodies. The hydrolysis of trichloromethane in acidic aqueous solution is about nine times slower than that of dichloromethane, 1800 times slower than that of monochloromethane, and the rate constant four orders of magnitude smaller than that of tetrachloromethane.[9]

Volatilization is the fastest removal process for both trichloromethane and tetrachloromethane from surface waters. The environmental problem remains unsolved for ground water, which is exposed to neither air nor light. Unfortunately, these compounds are not absorbed into soil, and thus are transported from the surface directly into aquifers underground.

The atmospheric concentrations of trichloromethane and tetrachloromethane in urban areas are two orders of magnitude larger than those of mono- and dichloromethane.[5] In the troposphere, the high reactivity of each of the first three chloromethanes with photochemically generated OH radicals is responsible for their short half-life of 15 weeks.[5] The same estimate for chloroform was made twenty years later, based on a typical hydroxide radical concentration in the atmosphere of 1×10^6 hydroxyl radicals/cm^3.[7] OH radicals do not affect tetrachloromethane, which is essentially inert in the troposphere, where it displays an estimated lifetime surpassing 330 years.[8] As a result, like other fully halogenated methanes, tetrachloromethane can reach the stratosphere, where ultraviolet radiation ultimately breaks it down. Nevertheless, this

photolytic process is slow, leading to a lifetime of CCl_4 in the stratosphere of 60 to 100 years.[8] The photolysis of CCl_4 releases Cl atoms which are thought to play a role in the chemical depletion of ozone. Some of the properties described in the text are summarized in Table 1.3.

Table 1.3 The Chloromethane Family: Properties at pH 7 and 25 ºC[5]

	Half-Life(yrs)*	Sol(g/l H_2O)	Hazard	Photolysis	Phosgene	Biodegrad.
CH_3Cl	1.1	7.3	Harmful	yes	yes	low
CH_2Cl_2	700	1.9	Harmful	yes	no	HIGH
$CHCl_3$	1,850-3,650	3.8	Harmful	yes	yes	low
CCl_4	40-7,000	0.8	Poison	UV	yes	low

(*) [4,6-8,10]

Over 90% of the tetrachloromethane produced worldwide in 1983 was used in the synthesis of the following chlorofluorocarbons (CFC): Freon-11 (CCl_3F), and Freon-12 (CCl_2F_2). These chlorofluorocarbons were employed as refrigerants, foaming agents, special solvents, and aerosol propellants.[5] Freon-11 has the highest ozone depleting potential of any refrigerant. The production of Freon-12 and Freon-11 was banned in the United States in 1994 and 1995, respectively. However, since the early 1980's there has been a slight increase in the demand for CCl_4 in the production of fluorocarbons.[5] Approximately 98% of the total trichloromethane produced in the United States since 1990 was used to synthesize monochlorodifluoromethane ($HCClF_2$), which also is named Freon-22, or HCFC-22.[11] $HCClF_2$ is the product of the reaction of chloroform with hydrogen fluoride in the presence of antimony pentahalides.[5] $HCClF_2$ is chemically less stable and more likely to break down in the lower atmosphere than fully halogenated methanes.[3] 70% of the Freon-22 produced in the United States is used as a refrigerant instead of the ozone depleting Freon-12, and the remaining 30% as a

precursor in the production of polytetrafluoroethylene PTFE (Teflon).[12] However, it is expected to be eliminated from industrial use in the United Stated by the year 2020,[11] as part of a trend to replace chlorine-containing fluorocarbons[12] with hydrofluorocarbons (HFC), which have even shorter life spans in the troposphere. Chloroform is a good solvent for cleaning, degreasing, and paint removal. But, since it is an expected human carcinogen, it is being replaced by the less toxic and easily biodegradable dichloromethane.[3,5]

When exposed to air, trichloromethane and tetrachloromethane can be degraded to produce phosgene (CCl_2O) via two different mechanisms: 1) Photochemical oxidation through exposure to light in the case of chloroform, or high frequency ultraviolet radiation in the case of tetrachloromethane. 2) Thermal decomposition when heated above 500 ºC or placed in contact with a flame. The main product of both photochemical and thermal decomposition mechanisms is phosgene (CCl2O), a colorless poisonous gas used in World War I as a chemical weapon. In the case of chloroform, toxic fumes of hydrochloric acid are produced as well. These chemical reactions can be catalyzed by the presence of iron.[5]

Methane-fermenting (methanogenic) bacteria are the subject of several research efforts on toxic bioremediation. The interest arises in the ability of this kind of bacteria to degrade some chloromethanes at low concentrations, and in the absence of heavy metals, or toxic solvents. The biodegradation of tetrachloromethane to chloroform was confirmed two decades ago.[7] Tetrachloromethane is subject to biotransformation only

in the absence of oxygen. The main degradation products of this anaerobic biotransformation of carbon tetrachloride are chloroform and carbon dioxide. This transformation can be affected by the presence of elemental iron.[13,14]

After having described each of the chloromethanes, and the similarities and differences that they share with chloroform, we focus our studies on the decomposition pathways of chloromethane (chloroform). The care devoted to tetrachloromethane was vital to our discussion due to its ability to serve as a source of chloroform through the action of methanogenic bacteria. *In situ* dehalogenation of tetrachloromethane under either iron- (Fe) or sulfate- (SO_4) reducing conditions may also lead to chloroform production[11] or to the enhancement of bacterial decomposition.[13] Reduction of tetrachloromethane via synthetic magnetite also leads to the production of carbon monoxide and chloroform.[15] Employing carbon as an electrode, and methanol to stabilize the product (chloroform), it is possible to electrochemicaly reduce tetrachloromethane to trichloromethane with high selectivity and current efficiency adequate for industrial application.[16] Even though the dehalogenation of tetrachloromethane has been observed to proceed through both biotic and abiotic pathways, the former is likely to be the predominant mechanism in the environment.[11] Since there are multiple feasible ways to degrade tetrachloromethane to trichloromethane (chloroform), the efforts need to be aimed at finding a way to degrade the latter. Thus, for the remaining portion of this dissertation we focus all of our attention to chloroform and its dehalogenation reactions.

1.4 General Properties of Chloroform

For the rest of this thesis we will employ the common name "chloroform" whenever we are referring to trichloromethane (IUPAC name) ($CHCl_3$). Other names for this compound are formyltrichloride, methyltrichloride, methane trichloride, Freon-20, and R-20 refrigerant.[17] Chloroform is a chemically stable alkyl halide. It is a colorless, highly volatile, neutral liquid with a boiling point of 62 ºC at standard conditions of pressure and temperature. Chloroform dissolves easily in water, with a solubility of 8.2g/l. It is 50% more dense than water.[5] Chloroform has a pleasant, nonirritating odor. A person can smell it in the air, even at concentrations as low as 133 parts per million (ppm). Chloroform is estimated to possess 40 times the sweetness of table sugar.[18] Like other solvents it stimulates a positive response in the brain. Since a small amount was enough to produce such a reaction, it was used to make pills and toothpaste more pallatable.[17]

1.5 History of Chloroform

Chloroform is believed to have been first discovered in the United States by Samuel Guthrie in 1831. After giving up on being a doctor, Guthrie bought himself a chemistry laboratory and was trying to discover new products which to sell. Upon reading an article in a medical journal about a liquid with very unusual properties called "Dutch liquid" ($C_2H_4Cl_2$), which was very hard and expensive to make and could have soothing qualities, he tried to make it by mixing chlorine based hen house disinfectant (bleaching powder) with whisky (ethanol). Instead, the result was chloroform solvated in ethanol, which he bottled up and sent to the author of the original article.[17,18]

Pure chloroform was synthesized independently by J. von Liebig and M. Soubeirain in 1831. In 1835 J. Dumas demonstrated that chloroform contained only one hydrogen atom and showed alternative reactions that produce it. V. Regnault prepared chloroform by chlorination of monochloromethane. Today, successive chlorination of methane is used exclusively in the production of chloroform and the other chloromethanes. The use of chloroform as an inhaled anesthetic became widespread after its adoption by Scottish physician Sir J. Simpson in 1847.[5] It was the first substance to produce general anesthesia.[3] Its popularity increased, and just a few years later, in 1853, Queen Victoria of England was administered chloroform while she was in labor. Chloroform replaced the flammable compound ethyl ether, which was harder to handle and to administer to patients, whose throats it would irritate.[17] Many patients died because the average lethal dose of chloroform was only 30 ml. There were other adverse health effects (see text below). The medical use of chloroform declined with the discovery of less toxic general anesthetics such as Halothane ($CF_3CHClBr$) and Desflurane.[3,19] The use of chloroform as an anesthetic was banned in the U.S. after World War II.[12]

1.6 Environmental Presence

Chloroform is one of the volatile organic compounds detected most frequently in ground water by the U.S. Geological Survey's National Water-Quality Assessment program. It is also reported to be the most frequently detected volatile organic compound in a nation-wide study of both ground and surface sources of drinking water.

Frequencies of detection of chloroform are higher beneath urban and residential areas than beneath agricultural or undeveloped areas. Chloroform has been observed to travel substantial distances in the subsurface.[11]

The Environmental Protection Agency (EPA) identifies and keeps a record of the most contaminated toxic waste sites in the nation in its National Priorities List (NPL). Varying concentrations of chloroform have been detected in at least 717 of 1430 NPL sites, the number of which may increase as more sites are evaluated. Most of the chloroform found in large concentrations in the environment comes from industry,[7] even though it might only constitute 10% of the total global input to the hydrologic system. Natural sources include volcanic gases, biomass burning, marine algae, and soil microorganisms.[11]

1.7 Anthropogenic Sources of Chloroform

Paper (and pulp) mills and chemical companies are responsible for the largest portion of anthropogenic emissions of chloroform. The largest documented releases of chloroform to the environment in 2001 were reported by the paper industry, which constituted 56% of the total.[11] 565 million lbs of chloroform were produced in the United States in 1994. U.S. exports exceeded 220 million lbs of the material in the year 2000.[12] Chloroform is formed as an unintended byproduct in the process of chlorination of water containing organic molecules. Thus, chloroform is present in small concentrations in drinking water, and in much larger concentrations in waste water from sewage treatment plants.[7,12,20] These sources may account for a large portion of the remaining fraction of the total man-made chloroform released. Persons working at

wastewater and other treatment plants can be exposed to elevated concentrations of the chemical. The National Occupational Exposure Survey indicated that a total of 100,000 workers potentially were exposed to significant levels of the chloroform.[7,12] Inadvertent release of chloroform into the environment also takes place during irrigation of lawns and gardens with chlorinated tap water.

1.8 Human Exposure

Human health can be affected by chloroform primarily through three routes of exposure: ingestion, inhalation, and skin absorption.

Ingestion of contaminated water is expected to be a primary source of chloroform entry into the body. Chloroform is present as a contaminant in the sources of drinking water. Chloroform is produced as an unintended result of water chlorination when chlorine reacts with organic molecules. Thus, the concentration of chloroform in drinking water increases with time from around 2 to 68 ppb (parts per billion).[12] Typical concentrations range from 2 to 40 ppb,[7] but cases in which the concentration of chloroform in public water supplies reached above 300 ppb have been reported.[20] Drinking water originating from both well and ground water sources near a hazardous waste site contained 1,900 ppb of chloroform.[7] In addition, chloroform is used in medical procedures such as dental root canal surgeries.[12]

Exposure to chloroform via inhalation results in 60 to 80 % absorption.[12] Due to its high volatility, most of the chloroform in water bodies exposed to the surface eventually enters the atmosphere. Even though typical concentrations of chloroform in the air only

range from 0.02 to 0.05 ppb, concentrations as high as 610 ppb have been measured in air at a municipal landfill.[7,20] The solubilities of monochloromethane and dichloromethane in water at 60 ºC are more than 70% lower than in water at 15 ºC.[5] Thus, the use of heated tap water inside the home may be responsible for significantly larger concentrations of chloroform in indoor air than those in the atmosphere. Average concentrations in indoor air were measured to be between 2 and 5 times larger.[5]

Water temperature has been demonstrated to exert a very strong effect on the absorption of chloroform while bathing. The mean concentrations of chloroform exhaled by subjects in a study bathing at 40 ºC was 35 times higher than that exhaled by those bathing at 30 ºC.[12] It is not clear which process is responsible for the largest fraction of the chloroform absorption in this case, inhalation, or dermal contact. Higher levels of chloroform are inhaled while showering if the water is hot enough for chloroform to evaporate.[7] A different study involving two students swimming for two hours in a chlorinated pool was conducted. In that particular case dermal absorption of chloroform made a larger contribution than inhalation, since the chloroform breath concentrations of the two students were two times the maximum possible concentrations attainable solely through inhalation.[12]

1.9 Possible Impact on Human Health

Ingestion of two teaspoons of chloroform is enough to cause death in humans. Once inhaled, chloroform is very quick to enter the bloodstream and the brain.[17] It tends to accumulate in tissues with high concentrations of lipids. Adipose, brain, liver, and

kidney tissue fall in this category.[20] Chloroform does not significantly bioaccumulate in living organisms and a large portion of it leaves the body during exhalation. In humans, chloroform is metabolized to produce carbon dioxide among other metabolites. Unfortunately, some of the metabolites may attach to other chemicals inside of cells and cause harm if they accumulate in significant enough amounts in the body. In large concentrations it can severely affect the liver, the kidneys, and the central nervous system, of which the brain is a part.[7]

In 1976, the National Cancer Institute published a report of the carcinogenic effects of high levels of chloroform in laboratory animals. In one instance, 98% of mice exposed to a maximum of 500 mg/kg of body weight of chloroform showed signs of hepatocellular carcinoma, as compared with only 6% in the control group.[21] Nodular hyperplasia of the liver was observed in mice that had not developed hepatocellular carcinoma, since they had been exposed to lower concentrations of chloroform.[21] Since then, there have been a large number similar studies involving animal testing, which produced the same kind of adverse results to the liver and kidneys.[12]

In 1986, the EPA classified chloroform as a probable human carcinogen based on the evidence of its carcinogenicity in animals.[11] In 1998, the same agency stated that chloroform is likely to be carcinogenic to humans by all routes of exposure at concentrations high enough to cause cytotoxicity or the formation of regenerative nodules in susceptible tissues. Liver damage, however, is known to occur at chloroform levels of exposure lower than those required to cause cancer.[11]

In addition, miscarriages, as well as the presence of birth defects in offspring, occurred in rats and mice that breathed air containing elevated levels of chloroform (30 to 300 ppm) during pregnancy. In the United States, the Occupational Safety and Health Administration (OSHA) sets the maximum levels of chloroform allowed in the workplace air. A permissible occupational exposure limit is 50 ppm in air during an 8-hour workday and 40-hour workweek.[7] The U.S. Food and Drug Administration (FDA) has banned the use of chloroform in drugs, cosmetics, and food packaging.[12]

1.10 Chloroform Removal Strategies

Chloroform has also been the subject of numerous bioremediation studies, many of which are currently in progress.[7,13] The biological dehalogenation of chloroform is already taking place in the natural ecosystem, where chloroform is produced in small concentrations by marine algae and soil microorganisms. We would like to reduce the presence of chloroform at waste water treatment plants and at hazardous waste disposal sites.

Unfortunately, at high concentrations, chloroform becomes toxic to both anaerobic and aerobic microorganisms. In facilities which employ anaerobic digestion systems, sustained concentrations of chloroform near 100 mg/L proved to be elevated enough to kill the methanogenic bacteria. Even when the levels of chloroform are low enough to keep the methane fermenting bacteria alive, considerable inhibition of methanogenesis

was observed with concentrations of the chemical as low as 1 mg/L. In addition, the sites in which the bioremediation is targeted often contain appreciable levels of other contaminants, like other organic solvents, chlorinated hydrocarbons and heavy metals, all of which have proven to inhibit the biological degradation of chloroform.[7] Thus, for sites with high levels of chloroform contamination, abiotic degradation is a path that should be considered in our search for the solution to the problem.

Several processes for the chemical decomposition of chloroform have been reported in the literature.[22-25] A collaboration of researchers in Illinois and Washington states determined experimental dissociation rate constants for the thermal decomposition of chloroform. They employed a laser schlieren (LS) technique to measure the total endothermic decomposition rate of chloroform in incident shock waves at temperatures between 1282 and 1872 K. In addition, they used theoretical Rice-Ramsperger-Kassel-Marcus (RRKM) modeling of the rate constants, by means of ab-initio calcutations of the transition state, in order to compare with their experimental data. This allowed them to estimate the rate constants through a temperature range of 1200 to 2700 K.[23]
W. Choi and M. Hoffmann at Cal. Tech. explored the aqueous photocatalytic dehalogenation of chloroform experimentally. A similar reaction mechanism as the one thought to take place in the troposphere was proposed, albeit in solution. It involved the proton abstraction from $CHCl_3$ by a photocatalytically created hydroxyl radical. Of interest to us is that a dramatic enhancement of the rate of degradation of chloroform at pH larger than 11 was found.[22]

There is sufficient experimental evidence demonstrating that chloroform reacts most favorably with the hydroxide ion.[9,24,26-29] Chlorine is considerably more electronegative than hydrogen. Thus, the more hydrogen atoms that are replaced by chlorine atoms in a chloromethane, the more positive the partial charge that will be generated on the remaining hydrogen atoms. A larger hydrogen charge will result in an increased acidity of the molecule.[5] For this reason, chloroform, in which three hydrogen atoms have been substituted for chlorine atoms, is the most acidic member of the chloromethane family.[1] It is therefore not surprising that it undergoes the fastest rate of decomposition in environments of high pH.[29]

At pH values above 5.5, the hydrolysis rate is observed through experiment to be proportional to the hydroxide ion concentration.[28,29] Various reaction mechanisms involving the base-catalyzed hydrolysis of chloroform have been proposed.[1,2,9,24-28,30-33] Jack Hine elucidated the first three steps of the mechanism describing the alkaline hydrolysis of chloroform. Most of his work in this subject included both novel experiments and theoretical analysis performed in the 1950's. It included the recognition of the existence of dichlorocarbene as a reaction intermediate. He also described qualitatively the reaction rate of each of the first three steps in the dehalogenation of chloroform. He also measured the overall rate of the reaction at different hydroxide ion concentrations and different reagents.[24,26-28,30] The first structural evidence for the formation of dichlorocarbene from chloroform had been discovered by W. von E. Doering and A. Hoffmann in 1954.[34] A clear picture of the last three of the five consecutive reaction steps involved in the alkaline degradation of

chloroform was presented by J. Pliego and W. De Almeida in 1996 and 1997.[25,35]

The efforts of Yurii Borisov at the Russian Academy of Sciences and Thom Dunning's group at the Pacific Northwest National Laboratory produced a very complete set of benchmark gas-phase electronic structure calculations on the alkaline hydrolysis of chlorinated methanes.[2] It includes a number of experimental references and proved an excellent resource to validate the results for our first reaction in the gas phase. Unfortunately, it was limited to the first step in the dehalogenation process of chlorinated methanes. Their collaboration with Christopher Cramer, Jiali Gao, Jason Thompson and Donald Truhlar at the University of Minnesota, and Keiji Morokuma at Emory University lead to the most comprehensive computational study on the alkaline hydrolysis of chlorinated methanes to date. Of particular interest was a gas-phase inter-nuclear potential energy curve and a solution-phase free energy profile from simulation of the second chloroform dechlorination reaction.[1] I am particularly thankful to these authors for their contributions to the search for an answer to the environmental persistence of chloroform. Their work and recent advances in computational hardware and software have given us the opportunity to make a new contribution to this end.

1.11 Overview

The second chapter of this dissertation introduces the theoretical methods employed in this work.

In the third chapter of this dissertation we present a consistent set of gas-phase inter-nuclear potential energy profiles for each one of the reactions involved in the alkaline

degradation of chloroform in water. This study in the gas phase provides us with the best window into the energetics inherent in each reaction by excluding all interactions with the solvent. The reaction mechanism which we propose shows the steps which both experiment and theory show to be the most probable.

The fourth chapter presents the solution-phase reaction free energy profiles for each of the five consecutive reaction steps in a study analogous to what is presented in the preceding chapter for the gas-phase. This ultimately allows us to determine which one of the five has the largest free energy of activation, and is thus the rate-limiting step in alkaline aqueous solution.

The fifth chapter seeks to serve the reader's interest into the electronic structure characteristics which make our third reaction step so different from the rest. This step involves the insertion of a dichlorocarbene carbon atom into a hydrogen-oxygen bond of a nearby water molecule.

CHAPTER 2

Theoretical Background

Electronic Structure Methods

Solvation Free Energy

2.1 Electronic Structure Methods

There are three types of electronic structure methods employed in this dissertation:

1. *Ab initio* quantum mechanics
2. Density Functional Theory (DFT)[36]
3. Semi-empirical quantum methods

Semi-empirical quantum mechanics methods employ experimentally fitted parameters in the simplest theoretical models sufficient to produce approximate results at a fraction of the computational cost of DFT and ab initio calculations. Due to the marginal accuracy of the resulting inter-nuclear potential energy, we have only used these semi-empirical quantum methods in one instance in which it was absolutely apparent that no higher level method was required.

Ab initio quantum mechanics methods can be separated into Hartree-Fock (HF) and Post-Hartree-Fock; e.g. nth order Møller-Plesset perturbation theory (MPn)[37,38], Configuration interaction (CI), and Coupled cluster (CC) methods. The Hartree-Fock

method employs mean-field theory to obtain an approximate solution to the electronic repulsion problem.[39] Post-Hartree-Fock methods include specific treatment of electron-electron instantaneous repulsion increasing both accuracy and computational cost.

For the initial exploration of the inter-nuclear potential energy profile of a reaction we employed the following methods: a) B3LYP (Becke, three-parameter, Lee-Yang-Parr)[40], a very successful hybrid[41] Density Functional Theory method, b) MP2 (second order Møller-Plesset perturbation theory[38]), an *ab-initio* method at a medium level of theory.

For the most accurate potential energy estimates we used an *ab-initio* quantum mechanics method at a high level of theory CCSD(T) with the aug-cc-pVDZ basis set throughout. This method consists of a couple cluster (CC) calculation including a full treatment of single (S) and double (D) excitations, while the triple excitations ((T)) are calculated based on perturbation theory.

In electronic structure calculations the wave function is constructed as a combination of basis functions. These basis functions are provided as a basis set.
The Augmented Correlation Consistent Polarized Valence Double Zeta (aug-cc-pVDZ)[42] basis set is among the most widely used basis sets that include both polarized and diffuse functions.

2.2 Statistical Mechanics Review

In this section a simple derivation of the partition function is presented. We start with the most basic model in the first subsection, and proceed to increasingly more realistic models in the following subsections.

2.2.1 One Particle Moving in One Dimension We may start with a simple model and later expand it to apply to more realistic systems. The partition function of one particle of mass *m* restricted to move along one dimension is

$$Z_{1,1-D} = \int_{x=-\infty}^{\infty} \int_{p=-\infty}^{\infty} e^{-\frac{1}{k_B T}\left(V(x)+\frac{p^2}{2m}\right)} \frac{dxdp}{h} \tag{1}$$

The partition function is expressed in terms of a double integral over all possible values of the position x and of the momentum p of the particle. V is the potential energy of the particle, T is the absolute temperature and k_B is Boltzman's Constant: $k_B = 1.23 \cdot 10^{-23} \frac{J}{K}$

For this simple case the position and momentum integrals are separable.

$$Z_{1,1-D} = \int_{x=-\infty}^{\infty} e^{-\frac{1}{k_B T}V(x)} dx \int_{p=-\infty}^{\infty} e^{-\frac{1}{k_B T}\left(\frac{p^2}{2m}\right)} \frac{1}{h} dp \tag{2}$$

The Gaussian integral on the right has the value

$$\int_{p=-\infty}^{\infty} e^{-a \cdot p^2} dp = \sqrt{\frac{\pi}{a}}, \quad a > 0, \quad a = \frac{1}{2mk_B T} \tag{3}$$

Thus, we are left with

$$Z_{1,1-D} = \frac{1}{h}\sqrt{2\pi m k_B T} \int_{x=-\infty}^{\infty} e^{-\frac{1}{k_B T}V(x)} dx = \frac{1}{\Lambda} \int_{x=-\infty}^{\infty} e^{-\frac{1}{k_B T}V(x)} dx \tag{4}$$

where Λ is the thermal de Broglie wavelength.

$$\Lambda = \frac{h}{\sqrt{2\pi m k_B T}} \tag{5}$$

2.2.2 One Particle Moving in Three Dimensions Now we proceed to generalize our discussion to one particle moving in three dimensions. The partition function becomes

$$Z_{1,3-D} = \frac{1}{h^3} \int_{x=-\infty}^{\infty} \int_{y=-\infty}^{\infty} \int_{z=-\infty}^{\infty} e^{-\frac{1}{k_B T} V(x,y,z)} dx dy dz \int_{p_x=-\infty}^{\infty} \int_{p_y=-\infty}^{\infty} \int_{p_z=-\infty}^{\infty} e^{-\frac{1}{k_B T}\left(\frac{p_x^2 + p_y^2 + p_z^2}{2m}\right)} dp_x dp_y dp_z \tag{6}$$

The case at hand is completely isotropic. We therefore make no distinction between any of the momentum coordinates and the integral at the end of the expression above are separated into a product of three identical integrals

$$Z_{1,3-D} = \frac{1}{h^3} \int_{x=-\infty}^{\infty} \int_{y=-\infty}^{\infty} \int_{z=-\infty}^{\infty} e^{-\frac{1}{k_B T} V(x,y,z)} dx dy dz \left[\int_{p_x=-\infty}^{\infty} e^{-\frac{1}{k_B T}\left(\frac{p_x^2}{2m}\right)} dp_x \right]^3 \tag{7}$$

Solving the Gaussian integral in the same manner as before, we obtain the final expression for the partition function of one particle moving in three dimensions

$$Z_{1,3-D} = \frac{1}{\Lambda^3} \int_{x=-\infty}^{\infty} \int_{y=-\infty}^{\infty} \int_{z=-\infty}^{\infty} e^{-\frac{1}{k_B T} V(x,y,z)} dx dy dz \tag{8}$$

Where Λ is the thermal de Broglie wavelength for a particle of mass *m* of equation (5).

2.2.3 N Indistinguishable Non-interacting Particles in 3-D Because of the particles not interacting with each other and being indistinguishable the partition function is the product of three identical one-particle partition functions and the 1/N! term to correct for counting the same state twice

$$Z_{N,3-D} = \left(Z_{1,3-D}\right)^N \cdot \frac{1}{N!} \tag{9}$$

The last expression may be written fully for clarity

$$Z_{N,3-D} = \frac{1}{\Lambda^{3N}} \left[\int_{x=-\infty}^{\infty} \int_{y=-\infty}^{\infty} \int_{z=-\infty}^{\infty} e^{-\frac{1}{k_B T} V(x,y,z)} dx dy dz \right]^N \cdot \frac{1}{N!} \tag{10}$$

2.2.4 N Distinguishable Non-interacting Particles, each of Mass m_j, in 3-D

We do not need to correct for counting the same state twice since the particles are now distinguishable, which is the case in the molecular simulations which we perform. The expression is almost identical to the previous one, except for the integrals not being identical for different particles since these are now distinguishable

$$Z_{N,3-D} = \left(\prod_{j=1}^{N} \frac{1}{\Lambda_j^{\,3}} \right) \cdot \int_{x_1=-\infty}^{\infty} \int_{y_1=-\infty}^{\infty} \int_{z_1=-\infty}^{\infty} e^{-\frac{1}{k_B T} V_1(x_1,y_1,z_1)} \ldots \int_{x_N=-\infty}^{\infty} \int_{y_N=-\infty}^{\infty} \int_{z_N=-\infty}^{\infty} e^{-\frac{1}{k_B T} V_N(x_N,y_N,z_N)} dx_1 dy_1 dz_1 \ldots dx_N dy_N dz_N \tag{11}$$

There is now a different expression for the de Broglie thermal wavelength for each particle of mass m_j

$$\Lambda_j = \frac{h}{\sqrt{2\pi m_j k_B T}} \tag{12}$$

2.2.5 N Distinguishable Interacting Particles, each of Mass m_j, in 3-D

Finally we are in a position to describe the Canonical ensemble which best represents the system in our simulations. In the previous cases each particle was moving under the influence of its own potential energy function. In the current case each particle is influenced by the position of every other particle through one potential energy function. The expression for the potential energy function is the same for all, and it includes the coordinates of all the particles

$$Z_{N,3-D} = \left(\prod_{j=1}^{N} \frac{1}{\Lambda_j^{\,3}} \right) \cdot \int_{x_1=-\infty}^{\infty} \int_{y_1=-\infty}^{\infty} \int_{z_1=-\infty}^{\infty} \ldots \int_{x_N=-\infty}^{\infty} \int_{y_N=-\infty}^{\infty} \int_{z_N=-\infty}^{\infty} e^{-\frac{1}{k_B T} V(x_1, y_1, z_1, \ldots, x_N, y_N, z_N)} dx_1 dy_1 dz_1 \ldots dx_N dy_N dz_N \qquad (13)$$

2.3 Free Energy Perturbation

In this section I give a brief introduction to the statistical free energy perturbation techniques used to obtain the free energy difference between two well-defined states.

We may start by expressing the Hemholtz free energy in terms of the Canonical partition function for N distinguishable interacting particles derived above

$$F \equiv F_N = -kT \ln(Z_N) \qquad (14)$$

We want to obtain an expression for the free energy difference between an initial state and a final state, each in statistical equilibrium.

$$\Delta F = F_f - F_i = -kT\left(\ln Z_f - \ln Z_i\right) = -kT \ln\left(\frac{Z_f}{Z_i}\right) \tag{15}$$

Unity may be expressed in the following form

$$e^{-\frac{V_i}{k_B T}} \cdot e^{\frac{V_i}{k_B T}} = 1 \tag{16}$$

Writing the full expression for the partition function Z_f of the final state in equation (15) and inserting the unity from equation (16) we arrive at the following expression

$$\Delta F = -kT \ln\left(\frac{\left(\prod_{j=1}^{N} \frac{1}{\Lambda_j^3}\right) \cdot \int e^{-\frac{V_f}{k_B T}} \cdot e^{-\frac{V_i}{k_B T}} \cdot e^{\frac{V_i}{k_B T}} \left(d^3 r\right)^N}{Z_i}\right) \tag{17}$$

From the definition of the partition function, we have the expression for the probability of the system of having a potential energy V_i

$$P_i = \frac{e^{-\frac{V_i}{k_B T}}}{Z_i} \tag{18}$$

Recognizing this expression for the probability inside of equation (17) we can arrive at a more meaningful equality

$$\Delta F = -kT \ln\left(\left(\prod_{j=1}^{N} \frac{1}{\Lambda_j^3}\right) \cdot \int e^{-\frac{\left(V_f - V_i\right)}{k_B T}} \cdot P_i \cdot \left(d^3 r\right)^N\right) \tag{19}$$

The term in parenthesis is the average of $e^{-\frac{\left(V_f - V_i\right)}{k_B T}}$ over the initial ensemble, which we labeled with the suffix *i*. We arrive at the final equation in Zwanzig's 1954 paper[43]

$$\Delta F = F_f - F_i = -kT \ln \left\langle e^{-\frac{(V_f - V_i)}{k_B T}} \right\rangle_i \quad (20)$$

2.4 The Free Energy of Solvation

One of the most important properties in the study of solvent effects is the free energy of solvation. Free energies of solvation can be derived by computational methods from intermolecular interactions. The free energy of solvation ΔG_{sol} is defined as the reversible work spent in the transfer of a particle of the solute from a fixed position in the gas phase into a fixed position in solution at constant temperature, pressure, and solvent composition.[44] ΔG_{sol} incorporates both the free energy contributions related to direct solute-solvent interactions and those arising from internal changes in the solute and solvent upon solvation. The solvation process is regarded to consist of two steps, (i) the formation of a cavity in the solvent large enough to accommodate the solute, and (ii) the introduction of the solute into this cavity.[45] During the second step the forces of interaction between the solute and the solvent are 'switched on'. These forces are either electrostatic or steric in nature. The latter consist of the Pauli exchange repulsion of electronic cores of atoms at close distances and the electronic dispersion attraction. This van der Waals interaction is modeled by the Lennard-Jones potential. This leads us to the breakdown of the solvation free energy into components according to the nature of the interaction:

$$\Delta G = \Delta G_{cav} + \Delta G_{vdW} + \Delta G_{ele} + RT \cdot \ln\left(\frac{RT}{p^0 \cdot v_m}\right) \quad (21)$$

Where v_m is the molar volume of the solvent.[45]

The first term corresponds to the formation of a cavity in the solvent large enough to accommodate the solute. This free energy change is large and positive because it involves the breakdown of cohesive forces between solvent molecules as the total surface area is increased against the solvent surface tension.

The second term is the contribution from the van der Waals interactions between the solute and the solvent molecules. This free energy change is negative for a cavity of appropriate size, where the dispersion forces are stronger than the core-core repulsion forces.

The third term represents the work spent in building up the charge distribution of the solute in solution. It is made of (i) the work necessary to create the solute's gas-phase charge distribution in solution and (ii) the work required to polarize the solute charge distribution by the solvent and the subsequent polarization of the solvent. Within the framework of the linear free-energy response theory, the electrostatic free energy contribution to solvation is one-half of the solute-solvent electrostatic interaction energy.[46] It can be determined empirically that the cavitation term is proportional to the Solvent Accessible Surface Area (SASA) through a factor α. This has been reproduced via theoretical models for solutes of average radius larger than 10 angstrongs.[47] It can be shown as well that the van der Waals free energy contribution is proportional to the average of its corresponding interaction energy through another empirical factor β.

$$\Delta G = \tfrac{1}{2}\left\langle E^{sx}{}_{ele} \right\rangle + \alpha \cdot SASA + \beta \cdot \left\langle E^{sx}{}_{vdW} \right\rangle \tag{22}$$

2.5 Free Energy of Molecular Association

Whether or not molecular association occurs is largely dependent on the nature and interaction of solutes and solvent, as well as on solute concentration and temperature. The association of two solute molecules will disrupt the favorable solute-solvent electrostatic and van der Waals interactions thus making an unfavorable contribution to the complex formation. On the other hand, since the association reduces the size of the solute cavity, this will decrease the unfavorable cavitation free energy. Bimolecular association also leads to the loss of translational and internal rotational freedom which will affect the entropy of dimerization unfavorably.[46] These conclusions can be summarized below:

$$\Delta G = \Delta G_{SS}^{cav} + \Delta G_{XX}^{vdW} + \Delta G_{SX}^{vdW} + \Delta G_{SS}^{vdW} + \Delta G_{XX}^{ele} + \Delta G_{SX}^{ele} + \Delta G_{SS}^{ele} + \Delta G_{X}^{\text{int } ra} \tag{23}$$

2.6 Description of Energy Contributions to Solvation

Here we specify the energy terms playing a role in the salvation process.

a) Polarization:

$$E_{ele} = E^{0} + E^{ind} \tag{24}$$

Here E^0 is the standard Coulombic potential energy from the gas-phase electronic charge distribution, and E^{ind} is the polarization energy term.

$$E^{ind} = -\tfrac{1}{2}\sum_{i} \Delta\mu_i \cdot \mathrm{E}^{0}{}_{i} \tag{25}$$

Here $\mathbf{E^0_i}$ is the unpolarized (permanent) electric field vector.

$$\Delta\mu_i = \alpha_i \cdot \mathrm{E}_i \tag{26}$$

$\mathbf{E_i}$ is the total electric field vector:[46]

$$\mathrm{E}_i = \mathrm{E}^0{}_i + \sum_{j \neq i} T_{ij} \Delta\mu_j \tag{27}$$

b) Total energy of a solution:

$$E_T = E_{SX} + E_{SX} + E_{SS} + E_{INTRA} \tag{28}$$

Here E_{SX}, E_{SS} and E_{INTRA} are the solute-solvent, solvent-solvent, and solute intramolecular interaction energies respectively.[48]

c) The Total Solvation Energy:

$$\Delta E_{sol} \equiv \Delta E^0 = E_T - (E_{SS}{}^* + E_{INTRA}{}^{ig}) = E_{SX} + (E_{SS} - E_{SS}{}^*) + (E_{INTEA} - E_{INTRA}{}^{ig}) \tag{29}$$

Here $E_{SS}{}^*$ is the energy of the pure solvent, and the subscript *ig* denotes the ideal gas.[49]

$$\Delta E_{sol} \equiv \Delta E^0 = E_{SX} + \Delta E_{SS} + \Delta E_{INTRA} \tag{30}$$

d) The Total Solvation Enthalpy:

$$\Delta H_{sol} \equiv \Delta H^0 = \Delta E^0 + p \cdot \Delta V^0 - R \cdot T \tag{31}$$

Here –RT is the pΔV contribution of the solute in the gas-phase (ideal gas). And the partial molar volume of the solute in the solution phase:[49]

$$\Delta V_{sol} \equiv \Delta V^0 = V_T - V^* \tag{32}$$

2.7 Combined QM/MM Description of Solvation

In the hybrid QM/MM approach, the solute molecule is treated quantum mechanically, while the solvent molecules are approximated by molecular mechanical force fields.

For the QM region, the closed shell restricted Hartree-Fock wave function Φ is written as a single Slater determinant of N/2 doubly occupied molecular orbitals, $\{\psi_k\}$:[50]

$$\Phi = \left|\psi_1 \cdot \alpha(1) \cdot \psi_1 \cdot \beta(2) \cdots \psi_{N/2} \cdot \beta(N)\right\rangle \tag{33}$$

Where α and β are the electron spin eigenfunctions and the molecular orbitals are linear combinations of atomic basis sets, $\{\varphi_\mu\}$. The total effective Hamiltonian of the system is:[51,52,50]

$$\hat{H}_{eff} = \hat{H}^{0}_{QM} + \hat{H}_{QM/MM} + \hat{H}_{MM} \tag{34}$$

$$\hat{H}^{0}_{QM} = -\frac{1}{2}\sum_{m}^{M}\frac{1}{2M_m}\nabla_m^2 - \frac{1}{2}\sum_{i}^{N}\nabla_i^2 - \sum_{i}^{N}\sum_{m}^{M}\frac{Z_m}{r_{im}} + \sum_{i}^{N}\sum_{j>i}^{N}\frac{1}{r_{ij}} + \sum_{m}^{M}\sum_{n>m}^{M}\frac{1}{R_{mn}} \tag{35}$$

$\hat{H}^0_{QM/MM}$ is the Hamiltonian for the *isolated* QM molecule.

$$\begin{aligned}\hat{H}_{QM/MM} &= \hat{H}^{ele}_{QM/MM} + E^{vdW}_{QM/MM} \\ &= \sum_{s}^{S}\sum_{m}^{M}\frac{q_s Z_m}{R_{sm}} + \sum_{i}^{N}\sum_{s}^{S}\frac{q_s}{r_{is}} + \sum_{s}^{S}\sum_{m}^{M}4\varepsilon_{sm}\left[\left(\frac{\sigma_{sm}}{R_{sm}}\right)^{12} - \left(\frac{\sigma_{sm}}{R_{sm}}\right)^{6}\right]\end{aligned} \tag{36}$$

Accordingly, we define the wave functions of the gas phase Φ^0 and solution Φ respectively:[50]

$$\hat{H}_{QM}\left|\Phi^0\right\rangle = E^{(0)}\left|\Phi^0\right\rangle \tag{37}$$

$$\hat{H}_{eff}\left|\Phi\right\rangle = E_{tot}\left|\Phi\right\rangle$$

a) Total Solute-Solvent Interaction Energy:[53]

$$E_{SX} = E^{vdW}_{QM/MM} + E^{(1)} + E_{pol} \tag{38}$$

$E^{(1)}$ is the electrostatic interaction energy between the solvent and the solute gas-phase charge distribution. In other words, this is the interaction energy between the unpolarized solute and the solvent:[50]

$$E^{(1)} = \left\langle \Phi^0 \left| \hat{\mathrm{H}}_{QM/MM}^{ele} \right| \Phi^0 \right\rangle \tag{39}$$

The solute-solvent polarization energy can be described the following way:[53]

$$E_{pol} = E_{dist} + E_{stab} \tag{40}$$

Where E_{dist} , the solute electron distortion energy, is the work to polarize the solute's charge distribution:[53]

$$E_{dist} = \left\langle \Phi \left| \hat{\mathrm{H}}_{QM}^{0} \right| \Phi \right\rangle - \left\langle \Phi^0 \left| \hat{\mathrm{H}}_{QM}^{0} \right| \Phi^0 \right\rangle \tag{41}$$

and the stabilization energy E_{stab} is the net gain in the solute-solvent interaction energy between the polarized solute and the bulk solvent over that without solute polarization:[53]

$$E_{stab} = \left\langle \Phi \left| \hat{\mathrm{H}}_{QM/MM}^{ele} \right| \Phi \right\rangle - \left\langle \Phi^0 \left| \hat{\mathrm{H}}_{QM/MM}^{ele} \right| \Phi^0 \right\rangle \tag{42}$$

We may re-write the total solute-solvent interaction energy:

$$E_{SX} = E_{QM/MM}^{vdW} + \left\langle \Phi \left| \hat{\mathrm{H}}_{QM}^{0} + \hat{\mathrm{H}}_{QM/MM}^{ele} \right| \Phi \right\rangle - \left\langle \Phi^0 \left| \hat{\mathrm{H}}_{QM}^{0} \right| \Phi^0 \right\rangle \tag{43}$$

From a consideration of the following thermodynamic cycle we can obtain the target of our calculation, ΔG_{hyd}.[52]

$$\Delta G^{0}_{QM}$$

$$\begin{array}{ccc} X_g\left(\hat{\mathrm{H}}^{0}_{QM}, E^{vdW}_{g}\right) & \Rightarrow\Rightarrow & X_g\left(E^{vdW}_{g}\right) \\ \Downarrow & & \Downarrow \\ \Delta G_{hyd} \quad \Downarrow & & \Downarrow \quad \Delta G_{hyd}(vdW) \\ \Downarrow & & \Downarrow \\ X_{aq}\left(\hat{\mathrm{H}}^{0}_{QM} + \hat{\mathrm{H}}^{ele}_{QM/MM}, E^{vdW}_{gas} + E^{vdW}_{QM/MM}\right) & \Rightarrow\Rightarrow & X_{aq}\left(E^{vdW}_{gas} + E^{vdW}_{QM/MM}\right) \end{array} \tag{44}$$

$$\Delta G^{ele}_{mut}$$

Since the free energy is a **state function**, any free energy change that the system undergoes will not depend on the path used. Thus we can obtain a free energy change in terms of the sum of the free energy changes obtained in an alternative path with the same starting and end points:[52]

$$\begin{aligned} \Delta G_{hyd} &= \Delta G^{0}_{QM} + \Delta G^{vdW}_{hyd} - \Delta G^{ele}_{mut} \\ &= \Delta G^{vdW}_{hyd} - \left(\Delta G^{ele}_{mut} - \Delta G^{0}_{QM}\right) \\ &= \Delta G^{vdW}_{hyd} - \Delta\Delta G^{ele}_{mut} \end{aligned} \tag{45}$$

We can obtain an expression for the target free energy of hydration ΔG_{hyd} of our solute X in terms of an alternative path in the thermodynamic cycle involving the gas-phase free energy $\Delta G^{0}_{QM,}$ the free energy of hydration ΔG^{vdW}_{hyd} of the solute's Lennard-Jones potential, and the free energy change ΔG^{ele}_{mut} upon stepwise annihilation of the solute's QM/MM interaction Hamiltonian in solution by means of a coupling parameter λ. We can subtract from the Hamiltonian for the mutation in solution the gas-phase mutation energy (computed via ab initio separately), since adding a constant term to the energy

will not affect the sampling during the free energy perturbation simulation. Here we assume the solute internal entropy to be the same in the gas phase as in solution. This procedure is shown below:[52]

$$\hat{\mathrm{H}}(\lambda) = \hat{\mathrm{H}}_{QM}^{0} + E_{QM/MM}^{vdW} + \lambda \cdot \hat{\mathrm{H}}_{QM/MM}^{ele} + \hat{\mathrm{H}}_{MM} - E^{(0)} \tag{46}$$

Using this Hamiltonian to calculate the energy difference in one step of the mutation we obtain

$$\begin{aligned} &\left\langle \Phi^{\lambda_{i+1}} \left| \hat{\mathrm{H}}(\lambda_{i+1}) \right| \Phi^{\lambda_{i+1}} \right\rangle - \left\langle \Phi^{\lambda_i} \left| \hat{\mathrm{H}}(\lambda_i) \right| \Phi^{\lambda_i} \right\rangle \\ &= \left\langle \Phi^{\lambda_{i+1}} \left| \hat{\mathrm{H}}_{QM}^{0} + \lambda_{i+1} \hat{\mathrm{H}}_{QM/MM}^{ele} \right| \Phi^{\lambda_{i+1}} \right\rangle - E^{(0)} - \left[\left\langle \Phi^{\lambda_i} \left| \hat{\mathrm{H}}_{QM}^{0} + \lambda_i \hat{\mathrm{H}}_{QM/MM}^{ele} \right| \Phi^{\lambda_i} \right\rangle - E^{(0)} \right] \end{aligned} \tag{49}$$

The last expression may be rewritten the following way

$$\begin{aligned} &\left\langle \Phi^{\lambda_{i+1}} \left| \hat{\mathrm{H}}(\lambda_{i+1}) \right| \Phi^{\lambda_{i+1}} \right\rangle - \left\langle \Phi^{\lambda_i} \left| \hat{\mathrm{H}}(\lambda_i) \right| \Phi^{\lambda_i} \right\rangle \\ &= \left\langle \Phi^{\lambda_{i+1}} \left| \hat{\mathrm{H}}_{QM}^{0} \right| \Phi^{\lambda_{i+1}} \right\rangle - \left\langle \Phi^{0} \left| \hat{\mathrm{H}}_{QM}^{0} \right| \Phi^{0} \right\rangle - \left[\left\langle \Phi^{\lambda_i} \left| \hat{\mathrm{H}}_{QM}^{0} \right| \Phi^{\lambda_i} \right\rangle - \left\langle \Phi^{0} \left| \hat{\mathrm{H}}_{QM}^{0} \right| \Phi^{0} \right\rangle \right] \\ &+ \left\langle \Phi^{\lambda_{i+1}} \left| \lambda_{i+1} \hat{\mathrm{H}}_{QM/MM}^{ele} \right| \Phi^{\lambda_{i+1}} \right\rangle - \left\langle \Phi^{\lambda_i} \left| \lambda_i \hat{\mathrm{H}}_{QM/MM}^{ele} \right| \Phi^{\lambda_i} \right\rangle \end{aligned} \tag{50}$$

Upon realization of the meaning of each term, we arrive at[52]

$$\left\langle \Phi^{\lambda_{i+1}} \left| \hat{\mathrm{H}}(\lambda_{i+1}) \right| \Phi^{\lambda_{i+1}} \right\rangle - \left\langle \Phi^{\lambda_i} \left| \hat{\mathrm{H}}(\lambda_i) \right| \Phi^{\lambda_i} \right\rangle = E_{dist}^{\lambda_{i+1}} - E_{dist}^{\lambda_i} + \left(\lambda_{i+1} E_{stab}^{\lambda_{i+1}} - \lambda_i E_{stab}^{\lambda_i} \right) \tag{51}$$

Upon further abbreviation we can write

$$E_{i+1} - E_i = \Delta E_{dist}(\lambda_i) + \Delta E_{stab}(\lambda_i) \tag{52}$$

The final expression for the energy difference makes use of the knowledge of the parts of which the solute-solvent interaction energy is comprised of

$$E_{i+1} - E_i = \Delta E_{SX}(\lambda_i) \tag{53}$$

In order too obtain the hydration free energy we employ equation (45) $\Delta G_{hyd} = \Delta G^{vdW}_{hyd} - \Delta\Delta G^{ele}_{mut}$. We make use of Zwanzig's expression for free energy perturbation, equation (20), where we mutate the solute-solvent energy:[50,52,53]

$$\Delta\Delta G^{ele}_{mut}(\lambda_i) = \sum_{i}^{steps} \Delta G_{SX}(\lambda_i) = \sum_{i}^{steps} \ln\left[\left\langle \exp\left(-\beta \cdot \Delta E_{SX}(\lambda_i)\right)\right\rangle\right] \tag{54}$$

CHAPTER 3

Gas-Phase Study

Choice of Electronic Structure Method and Basis Set for the Solvated System Simulation.

3.1 Introduction

Chlorinated hydrocarbons are the most common contaminant found at toxic waste sites. Many of these compounds are either known or suspected carcinogens. Most chlorinated hydrocarbons, unlike simple hydrocarbons, are resistant to biodegradation, and are thus difficult to treat with conventional microbiological technologies.[1,2] Strategies such as reaction with Fenton's reagent, ozone, UV radiation, and the use of ultrasound have been studied for the degradation of chlorinated compounds, but have proved ineffective or need additional reagents. Alternative approaches which are actively being pursued include electrocatalytic hydrogenation and photocatalytic degradation.[22,54] Chlorinated hydrocarbons can also degrade by abiotic chemical processes such as dehydrochlorination, hydrolysis and nucleophilic substitution. Unfortunately, the number of studies of the reactions of chlorinated hydrocarbons reported in the literature is very limited, and there is still disagreement about the mechanisms and rates of many of the key reactions.[1]

Chloroform is a persistent pollutant in the environment. This is especially the case in underground aquifers, where it can neither volatize nor react with photocatalitically

generated hydroxyl radicals.[5,11,12] Based upon experimentally determined rate constants, the half-life of chloroform in water at 25 ºC ranges from 1,850 to 3.650 years at pH 7, and from 25 to 37 years at pH 9.[4,6,7] The purpose of this research is to explore the ways of facilitating the removal of chloroform and the products of its decomposition from contaminated groundwater. We have explored new ways to chemically decompose chloroform in aqueous solution. In particular, we are proposing a mechanism for the abiotic degradation of chloroform in an alkaline aqueous environment.

The reaction with the hydroxyl ion OH^- has been demonstrated to be the dominant process involved in the degradation of chloroform in aqueous solution. The proton transfer (PT) to the hydroxyl ion is the primary reaction pathway.[1,2,9,24-30] There has been some debate on whether there is a significant increase in the rate of chloroform hydrolysis in acidic solution over that of a neutral solution.[28,29] The rate constant for the alkaline hydrolysis of chloroform has been measured to be in between three and four orders of magnitude larger than the rate constant for the acidic hydrolysis.[9,28,29] In alkaline aqueous solution, the reaction between chloroform and the hydroxide ion takes place so rapidly, compared with the reaction with water, that the latter can be ignored.[9]

The nomenclature used to describe the molecules involved in this dissertation is the following: $CHCl_3$ (chloroform), OH^- (hydroxyl ion), CCl_3^- (trichloromethyl ion), CCl_2 (dichlorocarbene), $CHCl_2OH$ (dichloromethanol), CHClO (formyl chloride), $HCOO^-$ (formate ion).

3.1.1 PT Reaction Mechanism Resulting in the Production of Carbon Monoxide

In the 1950's Jack Hine and his collaborators performed a series of experiments on the dehalogenation of chloroform and other halomethanes in basic solution.[24,26-28,30] They concluded that the principal decomposition reaction of chloroform in alkaline solution consists in the proton transfer (PT) to the hydroxide ion. They proposed a mechanism for the chemical reactions resulting from the alkaline decomposition of chloroform in water.[24,26] Since then, more detailed versions of that mechanism have been proposed.[1,9,25,31] We conducted a thorough revision and elimination of alternative reaction steps based on their high potential energy barriers. As a result, we selected the mechanism shown on Table 3.1 for the production of carbon monoxide from chloroform.

Table 3.1 Chloroform aqueous alkaline dehalogenation reaction mechanism producing carbon monoxide.[1,2,9,24,25,55]

Step #	Rate	
I	?	$CHCl_3 + OH^- \rightleftharpoons CCl_3^- + H_2O$
II	?	$CCl_3^- \rightleftharpoons CCl_2 + Cl^-$
III	?	$CCl_2 + H_2O \rightarrow CHCl_2OH$
IV	Fast	$CHCl_2OH + OH^- \rightarrow CHClO + Cl^- + H_2O$
V	Fast	$CHClO + OH^- \rightarrow CO + Cl^- + H_2O$

The first two reactions are reversible. According to Hine *et al* step III is fast in

comparison to step II, which was thus deemed to be the rate-limiting step.[24,26] We found this to be the case in the gas-phase. However, in chapter 4 we show that the effect of the solvent is to stabilize the products considerably in step II. We found the solution-phase energy of activation for step II to be half that of step III, which we determined to be the rate-limiting step. Pliego et al deemed step III to be slow since it had a high energy of activation, whereas steps IV and V were shown to be barrierless and thus considered fast.[25]

For each chloroform molecule to be dehalogenated, three hydroxyl ions are used and, in addition to carbon monoxide, three chloride ions and two water molecules are produced. The net reaction is summarized in equation 55:

$$CHCl_3 + 3OH^- \rightarrow CO + 3Cl^- + 2H_2O \quad (55)$$

Figure 3.1 shows the reaction mechanism in more detail. The first step is a proton transfer reaction without a transition state, and thus without a barrier to the reaction in the gas phase. The proton is transferred directly from chloroform to a hydroxide ion to form water. Trichloromethyl anion is the product of the first step. The second step involves the release of a chloride ion by the trychloromethyl anion in an S_N1 type mechanism yielding a short lived dichlorocarbene molecule. During the third step the carbon atom of dichlorocarbene is inserted into the O-H bond of a water molecule to produce dichloromethanol. The fourth step consists of a proton transfer from the alcohol oxygen of dichloromethanol to a hydroxide ion to form water and a simultaneous loss of a chloride ion leaving behind a formyl chloride molecule. A

similar reaction takes place in the fifth step, where formyl chloride transfers its proton to a hydroxide ion producing a water molecule simultaneous to the release of a chloride ion. What is left is carbon monoxide.

In addition to carbon monoxide, formate ion is also produced, but in quantities an order of magnitude smaller. This is due to an activation energy to the production of the formate ion from the decomposition of formyl chloride, which is higher than that of step 5 shown in Figure 3.1.

3.1.2 PT Reaction Mechanism Resulting in the Production of Formate Ion

As a result of the alkaline hydrolysis of chloroform, in addition to carbon monoxide, small amounts of formate ion are also produced. Hine and coworkers carried out a series of experiments in which the rates of reaction of chloroform decomposition were measured in 66% aqueous dioxane for different hydroxide ion concentrations and added reagents. Depending on the reagent used in the reaction and the resulting presence of excess chloride ion in solution, the exact percentage of formate produced was not always possible to determine experimentally. They found the percentage of formate ion produced to vary between 2 and 18%.[24]

The most probable mechanism leading to the production of formate ion shares the first four steps with the mechanism producing carbon monoxide. It involves two additional steps, resulting in a total of six reaction steps.[1] All six steps are shown on Table 3.2.

Table 3.2 Chloroform aqueous alkaline dehalogenation reaction mechanism producing formate ion.[1,9,24,55]

Step #	Reaction
I	$CHCl_3 + OH^- \rightleftharpoons CCl_3^- + H_2O$
II	$CCl_3^- \rightleftharpoons CCl_2 + Cl^-$
III	$CCl_2 + H_2O \rightarrow CHCl_2OH$
IV	$CHCl_2OH + OH^- \rightarrow CHClO + Cl^- + H_2O$
V	$CHClO + OH^- \rightarrow CHClOOH^-$
VI	$CHClOOH^- + OH^- \rightarrow HCOO^- + Cl^- + H_2O$
Aternative[55]	$CO + OH^- \rightarrow HCOO^-$

For each chloroform molecule dehalogenated in this manner, four hydroxyl ions are used and, in addition to a formate ion, three chloride ions and two water molecules are produced. The net reaction is summarized in equation 56:

$$CHCl_3 + 4OH^- \rightarrow HCOO- + 3Cl^- + 2H_2O \quad (56)$$

3.1.3 S_N2 Reaction Mechanism: An alternative to the Proton Transfer Reaction

This reaction involves the nucleophilic attack of the hydroxide ion to the carbon atom of chloroform. The S_N2 reaction mechanism is less energetically favorable than the proton transfer pathway, which does not have an energy barrier to the reaction in the gas-phase. This is the case because of the favorable electrostatic interaction between the positive partial charge of chloroform's acidic hydrogen and the negatively charged hydroxide

ion oxygen atom in the intermediate structures of the proton transfer mechanism. It has been determined experimentally to play a smaller role than the proton transfer reaction pathway, which is dominant. Nevertheless, it still plays a role in competing with the proton transfer.[1,2,24,25,32,33] The chemical reactions taking place in the S_N2 reaction mechanism are shown on Table 3.3 below.

Table 3.3 Chloroform aqueous alkaline dehalogenation via the S_N2 reaction mechanism producing carbon monoxide.[1,2,24,25,32,33]

Step #	Rate	
I	Slow	$CHCl_3 + OH^- \rightleftharpoons CHCl_2OH + Cl^-$
II	Fast	$CHCl_2OH + OH^- \rightarrow CHClO + Cl^- + H_2O$
III	Fast	$CHClO + OH^- \rightarrow CO + Cl^- + H_2O$

The first reaction in of the S_N2 mechanism was studied in the gas-phase by S. Re and K. Morokuma in Japan and by the group lead by Thom Dunning at the Pacific Northwest National Laboratory and in aqueous solution by M. Valiev, B. Garrett, M. Dupuis, and collaborators in 2007. They found a 32 kcal/mol energy of activation in the gas-phase and a free energy barrier to the reaction in solution of 29 kcal/mol. As we will see later, these values are considerably higher than those obtained for the proton transfer reaction, which lacks a barrier in the gas-phase and has a much smaller barrier in aqueous solution. Their results are shown in Figures 3.4 and 3.5.

3.1.4 Purpose Since these target chemical reactions take place in the environment at constant temperature and pressure, equilibrium will be reached when the Gibbs free energy is at its minimum.

By performing a frequency analysis and employing the harmonic approximation we can obtain an estimate of the free energy of a molecule in the gas phase. However, the solvent has a large effect on the free energy of most condensed phase reactions. This is especially the case for water. Aqueous solvation of both ionic and polar solutes is highly favorable energetically. In addition, the small molecular size and the large number of accessible interaction sites per water molecule, leads to a large entropic contribution to the free energy of solvation of a solute.

The transition state plays a crucial role in a chemical reaction. It determines the barrier height responsible for the rate of the reaction. Being able to treat the solvent explicitly allows us to take into account the contributions of individual water molecules to the free energy at every stage of a chemical reaction.

The main goal of this section is to choose the most suitable electronic structure method and basis set to study the system in the condensed phase.

3.2 Method Overview

Molecular modeling allows us to determine the structure, properties, and activity of a molecule. Of particular interest to us are the following types of calculations:

1. Single point energy estimation;
2. Inter-nuclear potential energy surface (PES) and reaction path following;
3. Structure optimization: energy minimum, transition state…etc;
4. Vibrational frequency spectrum, zero point energy, and thermal energy.

The purpose of this particular study of the five reactions in the gas phase is three-fold:

1. To test the viability of several reaction mechanisms in vacuum.
2. To ascertain which quantum mechanical methods are best suited to study this specific type of reactions.
3. To determine the best balance between accuracy and computational cost in our choice of the electronic structure method and basis set to be used in the solvated system simulation.

For the initial exploration of the inter-nuclear potential energy profile of a reaction we employed the following methods: a) B3LYP (Becke, three-parameter, Lee-Yang-Parr)[40], a very successful hybrid[41] Density Functional Theory method, b) MP2 (second order Møller-Plesset perturbation theory[38]), an *ab-initio* method at a medium level of theory.

In electronic structure calculations the wave function is constructed as a combination of basis functions. These basis functions are provided as a basis set.

The Augmented Correlation Consistent Polarized Valence Double Zeta (aug-cc-pVDZ)[42] basis set is among the most widely used basis sets that include both polarized and diffuse functions. With the aug-cc-pVDZ basis set, B3LYP and MP2 served as reasonably accurate methods for introducing specific electron-electron correlation at a moderate computational cost. We compared the geometries and energies that these two methods predict.

The choice of MP2/aug-cc-pVDZ to perform accurate geometry optimization at a manageable computational cost finds wide use in the scientific community.[1,2,32] The molecular bond lengths and angles that it predicts are so close to the experimental values that this method can substitute for geometry optimization with higher level methods at a fraction of the cost. On the other hand, the less expensive alternative of employing DFT methods may lead to convergence problems during the Self Consistent Field search for an energy minimum in molecular dissociation reactions at a separation between the molecules larger than 5 Å.

For the most accurate potential energy estimates we used an *ab-initio* quantum mechanics method at a high level of theory CCSD(T) with the aug-cc-pVDZ basis set throughout. This method consists of a couple cluster (CC) calculation including a full treatment of single (S) and double (D) excitations, while the triple excitations ((T)) are calculated based on perturbation theory. CCSD(T) is often called “the gold standard of

quantum chemistry" for its excellent compromise between accuracy and computational cost. If we were able to both employ an infinite basis set and in addition include all levels of excitation into the coupled cluster calculation we would obtain an exact solution of the Schroedinger equation within the Born-Oppenheimer approximation.

For our purposes the state-of-the-art CCSD(T)/aug-cc-pVDZ method served as the first benchmark for our gas-phase energies. This method was not used to perform geometry optimization of intermediate states along a reaction path due to its high computational cost. Instead we used our high level *ab-initio* method, CCSD(T)/aug-cc-pVDZ, to obtain the (more accurate) single point energy (SPE) at the MP2-optimized geometry. This approach employing a high level SPE calculation performed on a structure optimized at a lower level of theory is abbreviated the following way: high//low. Employing this nomenclature in our case we obtain CCSD(T)/aug-cc-pVDZ//MP2/aug-cc-pVDZ. As can be seen in Tables 3.1 through 3.7 below, for every reaction studied here the potential energy difference between reactants and products calculated at the CCSD(T)/aug-cc-pVDZ//MP2/aug-cc-pVDZ level differs from that obtained through direct geometry optimization with CCSD(T)/aug-cc-pVDZ by at most half a percent of the total.

Because of the high computational costs associated with ab-initio quantum mechanical methods applied to condensed phase environments, we chose to use the Hartree-Fock method in our treatment of the solute in our QM/MM scheme. We improved the resulting free energy in solution by adding the difference between the gas-phase

reaction free energy calculated with our highest level method, CCSD(T)/aug-cc-pVDZ, and the gas-phase reaction free energy calculated with the low level method employed in the solution-phase calculation, HF/3-21+G:

$$\Delta G_{sol}^{CCSD(T)/aug-cc-pVDZ}(R_c) = \Delta G_{sol}^{HF/3-21+G}(R_c) + \Delta G_{gas}^{CCSD(T)/aug-cc-pVDZ}(R_c) - \Delta G_{gas}^{HF/3-21+G}(R_c) \quad (57)$$

Our specific choices of quantum mechanical methods and basis sets for our high level calculations were also supported by how the predicted potential energy difference compared with the experimental energy difference for the singlet-triplet splitting of dichlorocarbene (for details refer to the tables in chapter 5).

3.3 Computational Details

In this chapter, we consider the gas phase inter-nuclear potential energy of each one of the molecules which take part in each of the five target reactions. The potential energy at each nuclear configuration is the sum of the electronic energy (resulting from the electronic hamiltonian) and the nuclear repulsion energy. We employed several electronic structure methods ordered according to increasing sophistication and size of the basis set used. This was done to achieve three specific goals. The first goal is to determine the best suited of the low computational cost methods for condensed phase simulation. The second goal is to explore the results that intermediate levels of theory produce. The third goal is to use the highest level methods of practical computational cost for gas phase inter-nuclear potential energy reference and for post-correction of the solvated system free energy.

In this work we used the QM/MM method for an accurate description of the chemical reactions at hand. An introduction to the QM/MM method is included in chapter 2. Since bonds are being broken and created during a chemical reaction, we have to include a quantum mechanical treatment of the changing electronic structure of the molecules involved. In our particular case this QM region will consist of the solute(s). The rest of the system is treated at the molecular mechanics (MM) level. For this study, the MM region is made up of the solvent molecules. In practice, the level of theory used in the QM region has to be chosen carefully. We needed to establish the right balance between accuracy and computational cost.

In order to obtain the free energy difference between two different points on an inter-nuclear potential energy surface we employed statistical sampling methods. For every solvent molecule which moves within the cutoff region, a new quantum mechanical inter-nuclear potential energy of the solute has to be calculated. That potential energy includes the terms accounting for the interactions of the solute with the charges of the solvent molecules at their new locations and orientations. This implies performing millions of self-consistent-field (SCF) potential energy calculations. Thus, at this point, using a high level ab-initio molecular orbital theory or density functional theory method for the QM region would be inconveniently slow.[56] Unfortunately, this is the case for both MP2 and B3LYP.

In this work we used the 3-21+G basis set with the Hartree-Fock method for our condensed-phase calculations. This method consistently produced energies a lot closer

to the high level methods and experiment than the alternative basis sets did at the HF level of theory.

There have been several studies employing HF theory and smaller basis sets to perform exactly this type of condensed-phase free energy simulations.[1,57] For this purpose the small 3-21G basis set was calibrated at the HF level to accurately describe hydrogen bonding interactions of the solute[53,58] with Jorgensen's TIP3P water model.[59]

We improve on previous studies by adding diffuse functions to our basis set. Negative ions have charge distributions that are much more delocalized than for neutral species. The functions pertaining to basis sets developed for neutral atoms may not extend far enough to accommodate a weakly bound electron. This may lead to errors in the energies and other molecular properties. The exponents in the negative exponential diffuse functions are considerably smaller than the smallest valence exponent and therefore provide the basis set with more flexibility.[60]

In the family of split-valence basis sets developed by John Pople the addition of diffuse functions exclusively on heavy atoms is represented with a single "+" sign. The addition of diffuse functions on both heavy and hydrogen atoms is represented with the "++" sign. For the Dunning family of basis sets the addition of diffuse functions of both high and low angular momentum to both heavy and hydrogen atoms is denoted with "aug" at the beginning of the basis set name.[61]

Due to the large size of these augmented basis sets and the lack of an intermediate between the augmented and the non-augmented basis sets, a new type of minimally

augmented Dunning family basis sets were recently created to provide the intermediate size needed.[61] These new Dunning family basis sets include only diffuse functions of low angular momentum on heavy atoms.[61] Most of the times it is the heavy atoms, not the hydrogen atoms, that are negatively charged, and are thus the ones that require diffuse functions. Unfortunately, we did not have a chance to employ these minimally augmented basis sets prior to the completion of this work, which we did with the fully augmented Dunning family basis sets. We hope to make use of more efficient basis sets in the near future since for this type of calculations we did not need the full set of diffuse functions that "aug-" basis set offer.

Since the negative partial charges in our system were located on heavy atoms only, mainly chlorine, oxygen, and carbon atoms, it was not necessary to add diffuse functions to the hydrogen atoms in our systems of interest. We thus added only one single "+" sign to our basis set of choice. This is supported by the results in Table 3.2, where we show the lack of improvement in accuracy obtained with basis sets employing diffuse functions on hydrogen atoms too, those with the "++" sign, with respect to their equivalents with diffuse functions exclusively on heavy atoms.

The tables below show that the inter-nuclear potential energy differences calculated with HF/3-21+G were substantially closer to those calculated with the high level methods than the ones produced with HF/3-21G. We thus used HF/3-21+G throughout our condensed phase QM calculations.

3.4 The Inter-Nuclear Potential Energy of Individual Molecules and Molecular Complexes

It was of particular importance to verify the performance in the gas-phase of the HF/3-21+G model that we chose for the QM portion of our condensed-phase simulations. The energy values for the products relative to those of the reactants were computed in the gas phase for all of the 5 reactions. Thermal enthalpies and free energies were also calculated and the results compared with those of high level ab-initio methods and experiment for the first two reactions. In the tables that follow we can observe that HF/3-21+G is currently the most cost effective method for extensive condensed-phase free energy simulation for this specific type of reactions involving negative ions.

3.4.1 Reaction #1: $CHCl_3 + OH^- \rightleftharpoons CCl_3^- + H_2O$ In the first of the reactions in the alkaline decomposition of chloroform, a proton is extracted from chloroform by a hydroxide ion. The role that this first reaction plays in the overall reaction scheme is depicted in Figure 3.2. Figure 3.3 shows the optimized geometries before, during, and after the proton transfer. This proton-transfer reaction proceeds from reactants to products without a barrier in the gas phase.

In 2001 Yurii Borisov, Thom Dunning and his collaborators at the Pacific Northwest National Laboratory suggested two alternative pathways for the reaction of chloroform with a hydroxide ion. They explored the same two pathways for CH_3Cl and CH_2Cl_2 as well. The first pathway they studied was a concerted (opposite of stepwise) nucleophilic substitution reaction (S_N2) in which a chloride ion is released at the same

time that the hydroxide ion binds to the chloroform carbon. The second pathway consisted of a proton transfer from chloroform to a hydroxide ion. Even though they found the gas-phase reaction energy to favor the S_N2 reaction over the proton transfer reaction, the 23.6 kcal/mol barrier height which they obtained for the S_N2 reaction at the MP2/aug-cc-pVDZ level completely tips the balance in favor of the proton transfer reaction for which there is not a barrier in the gas-phase. This supported our decision to exclusively focus our attention on the proton transfer reaction. The experimental evidence presented by Hine and others further supported our choice.

In Table 3.1, we compare the inter-nuclear potential energies for different quantum mechanical methods and basis sets for our first reaction. The difference of the potential energy between the reactants and products evaluated at the CCSD(T)/aug-cc-pVDZ level is -32.3 kcal/mol. CCSD(T) is considered to be "the gold standard" of quantum chemistry because of how close its results are to those of experiment. The potential energy difference between reactants and products evaluated at the HF/3-21+G level is -46.8 kcal/mol. In contrast, the same quantity evaluated with the alternative low level methods ranges from -54.0 kcal/mol, for the larger 6-31G* basis set, to -100.5 kcal/mol for HF/3-21G. The accuracy of minimum energy geometries obtained at the MP2/aug-cc-pVDZ level are made evident by the close proximity of the energies obtained via CCSD(T)/aug-cc-pVDZ and CCSD(T)/aug-cc-pVDZ//MP2/aug-cc-pVDZ, which are -32.3 and -32.2 kcal/mol, respectively. This narrow similarity between the energies of geometries optimized at MP2/aug-cc-pVDZ and CCSD(T)/aug-cc-pVDZ levels of theory is observed in all the molecules studied here.

Table 3.4 Reaction #1: $CHCl_3 + OH^- \rightleftharpoons CCl_3^- + H_2O$
Inter-nuclear potential energy in kcal/mol of the product complex and of the separated products, relative to that of the reactants at infinity.

Method	Product Complex	Products
HF/3-21G	-111.6	-100.5
HF/3-21G*	-94.7	-81.4
HF/3-21+G	-57.9	-46.8
HF/6-31G*	-66.8	-54.0
HF/aug-cc-pVDZ	-46.7	-36.7
B3LYP/aug-cc-pVDZ	-46.1	-34.0
MP2/aug-cc-pVDZ	-42.8	-27.8
CCSD(T)/aVDZ//MP2/aVDZ	-46.0	-32.2
CCSD(T)/aug-cc-pVDZ	-46.3	-32.3
MP2/6-31+G(d,p) *Kryachko*[62]	-39.5	-25.5
CCSD(T)/CBS Borisov et al.[2]	-44.7	-32.7
Exper./Theor. Borisov et al.[2]		-31.9

In Table 3.4 we also compare the potential energies for different methods but extend the study to a wider range of basis sets and also include an estimate of the computational time. We performed a geometry optimization starting from the same structure with each method and recorded the CPU time elapsed. Only those methods which include diffuse functions produced a difference in potential energy between reactants and products of absolute value smaller than 46.8 kcal/mol. The estimate of the computational time does not reflect the actual cost of performing the QM/MM Monte Carlo condensed-phase simulation, for which the time differences are more significant.

Table 3.5 Comparison between reaction energy (Reaction #1, kcal/mol) and computational time of Single-Point-Energy (SPE) calculations for $CHCl_3$ and $CHCl_2OH$. A variety of electronic structure methods and basis set sizes were used.

		$CHCl_3$		$CHCl_2OH$	
	ΔE_{react}	# of basis func's	SPE time (s)	# of basis func's	SPE time (s)
HF/3-21G	-100.5	50	10.2	48	12.6
HF/3-21G*	-81.4	68	10.3	60	12.6
HF/3-21+G	-46.8	66	10.4	64	14.1
HF/6-31G	-66.7	50	10.0	48	12.9
HF/6-31G*	-54.0	74	10.7	72	13.3
HF/6-31+G	-43.2	66	10.4	64	12.9
HF/6-31+G*	-31.9	90	11.1	88	14.1
HF/6-311G**	-58.9	102	12.0	100	15.8
HF/6-311+G**	-35.4	118	13.0	116	17.0
HF/6-311++G**	-35.4	119	13.5	118	18.3
HF/aug-cc-pVDZ	-36.7	113	15.9	118	22.0
B3LYP/aug-cc-pVDZ	-34.0	113	19.3	118	33.9
MP2/aug-cc-pVDZ	-27.8	113	29.3	118	38.5
CCSD(T)/aug-cc-pVDZ	-32.3	113	219.4	118	950.5

In Table 3.6 below, we compare calculated gas phase reaction thermal enthalpies and free energies at 298.15K at different levels of theory with experiment. In Tables 3.3-3.6 CCSD(T) stands for its reputation as the gold standard. In Table 3.5 it yields a thermal enthalpy difference between reactants and products of -32.9 kcal/mol, whereas the average over the experimental results is -32.6 kcal/mol. Both second order Møller-Plesset perturbation theory and density functional theory produced results well within the fairly large experimental margin of error of ± 7.9 kcal/mol, -34.6 and -28.4 kcal/mol respectively. As will be the case in the Tables to follow, the hybrid B3LYP functional produces results consistently closer to those of CCSD(T) than MP2 does. All high level

calculations were performed with the use of Dunning's aug-cc-pVDZ, which seems to be sufficiently large and diffuse to meet the demands of these electronic states. The HF/aug-cc-pVDZ and HF/3-21+G methods, although clearly less accurate than B3LYP and MP2, produced values for the enthalpy less than 5 and 6 kcal/mol away, respectively, from both experimental and CCSD(T) values. The performance of the 3-21+G basis set is remarkable, considering that it only uses 66 basis functions for chloroform, in contrast with 113 that the aug-cc-pVDZ basis set employs. HF methods without diffuse functions produced results between 20 and 70 kcal/mol different from experiment.

Table 3.6 Reaction #1: $CHCl_3 + OH^- \rightleftharpoons CCl_3^- + H_2O$ Thermal enthalpy and free energy at 298.15 K in kcal/mol of the products, relative to that of the reactants.

Method	ΔH	ΔG
HF/3-21G	-100.1	-101.9
HF/3-21G*	-81.5	-83.4
HF/3-21+G	-47.5	-49.4
HF/6-31G*	-54.6	-56.3
HF/aug-cc-pVDZ	-37.4	-39.0
B3LYP/aug-cc-pVDZ	-34.6	-36.5
MP2/aug-cc-pVDZ	-28.4	-30.1
CCSD(T)/aug-cc-pVDZ	-32.9	-35.2
Experiment (Std.)	-32.6 ± 7.9[2]	-33.8 ± 3.4[63]

Values obtained from the gas phase inter-nuclear potential energy and the harmonic approximation using the results of the frequency analysis. The first reference includes experimental data from JANAF Thermochemical Tables,[64] and other sources.[65] The value in the second reference was btained from combining the parent reactions $CHCl_3 \rightarrow CCl_3^- + H^+$ and $OH^- + H^+ \rightarrow H_2O$ together, for which the free energies where measured separately.[63,66]

The same trends in the thermal free energy difference between reactants and products are observed as in the previous table, but the differences between methods are not as pronounced. The CCSD(T)/aug-cc-pVDZ level of theory produces a thermal free energy difference between reactants and products of -35.2 kcal/mol, while the experimental results are centered at -33.8 kcal/mol. B3LYP is again closer than MP2 to experiment, and both fall within the smaller experimental margin of error of ±3.4 kcal/mol. The HF/3-21+G thermal free energy difference of -49.4 kcal/mol is still considerably closer to experiment than those arising from methods without diffuse functions, results of which range between -56 and -112 kcal/mol. Nevertheless, a large gap remains between the values listed for HF/3-21+G and those of CCSD(T)/aug-cc-pVDZ. This is addressed later as a post-correction to our condensed-phase results. It is done by adding to the HF/3-21+G:TIP3P Monte Carlo QM/MM free energy the potential energy difference between the CCSD(T)/aug-cc-pVDZ and the HF/3-21+G methods at each point along the reaction coordinate. It is proven that the difference in free energy arising in the use of different potential energy functions to perform the identical calculation (through the use of different levels of theory) can be approximated by the difference in the potential energy itself.[88] The inter-nuclear potential energy difference between the CCSD(T)/aug-cc-pVDZ and the HF/3-21+G methods at several points along the reaction can be observed on figure 3.6. The value of the reaction coordinate at each point along the reaction is obtained by subtracting the transferred hydrogen-oxygen (hydroxide ion's oxygen) distance from the hydrogen-carbon distance, $r_{C\text{-}H} - r_{O\text{-}H}$, in Å.

3.4.2 Reaction #2: $CCl_3^- \rightleftharpoons CCl_2 + Cl^-$ In the previous reaction a proton is removed from chloroform by a hydroxide ion releasing a water molecule. A graphical description of the reaction in the context of the overall reaction mechanism is shown in figure 3.7. What remains, the trichloromethyl ion, now undergoes a molecular dissociation reaction through the loss of a chloride ion, leaving behind a neutral, but short-lived, dichlorocarbene molecule. Figures 3.8 and 3.9 show the reactant and intermediate geometries, respectively.

The inter-nuclear potential energy difference between reactants and products at different levels of theory for this second reaction are shown on Table 3.4 below. Table 3.4 also lists the calculated reaction thermal enthalpies at 298.15K at different levels of theory. The gas-phase experimental change in enthalpy at standard conditions of temperature and pressure is 30.8 ± 2.6 kcal/mol. We obtained a thermal enthalpy change of 29.6 kcal/mol at the CCSD(T)/aug-cc-pVDZ level of theory. Geometry optimization at the CCSD(T)/aug-cc-pVDZ level yields a reaction inter-nuclear potential energy of 29.75 kcal/mol. Using the same level of theory to perform a single point potential energy calculation on the MP2/aug-cc-pVDZ optimized structure yields 29.72 kcal/mol. As we saw before, the close agreement between these values emphasizes the reliability of the MP2/aug-cc-pVDZ method in providing the lowest energy molecular geometry. Our chosen level of theory, HF/3-21+G, yields a reaction enthalpy of 35.1 kcal/mol. MP2 and B3LYP yield 33.5 and 28.0 kcal/mol, respectively, when using the aug-cc-pVDZ basis set. The results that this density functional method produces are again slightly closer to those of our coupled cluster method than the MP2 results are.

The HF/3-21+G method overestimated the reaction enthalpy by 4.2 kcal/mol, differing from the respected MP2 results by 1.6 kcal/mol. In contrast, there is a large underestimation of the enthalpy difference between reactants and products by the HF/aug-cc-pVDZ and HF/6-31G* methods of 14 and 10 kcal/mol, respectively. This large discrepancy, even when large basis sets are used, suggests that the much better results of both HF/3-21+G and HF/3-21G* might amount to simple error cancellation. Thus the use of the mean-field approach to estimate electron-electron repulsion is not sufficient. For this system to be properly studied one should employ post-Hartree-Fock methods, at least as a post-correction. Figure 3.10 shows the inter-nuclear potential energy profile for this reaction calculated at low, intermediate, and high levels of theory.

Table 3.7 Reaction #2: $CCl_3^- \rightleftharpoons CCl_2 + Cl^-$
Inter-nuclear potential energy difference, and thermal enthalpy difference, between reactants and products at 298.15K in kcal/mol.

Method	ΔE(0K)	ΔH(298K)
HF/3-21G	43.7	43.2
HF/3-21G*	30.7	30.5
HF/3-21+G	35.5	35.1
HF/6-31G*	20.9	20.8
HF/aug-cc-pVDZ	16.9	16.8
B3LYP/aug-cc-pVDZ	28.1	28.0
MP2/aug-cc-pVDZ	33.7	33.5
CCSD(T)/aVDZ//MP2/aVDZ	29.7	
CCSD(T)/aug-cc-pVDZ	29.7	29.6
Experimental Std. ΔH		30.8 ± 2.6[67]

The size of the energy barrier to this dissociation reaction in the gas phase is considerable, but we can anticipate that this is not the case in solution. The preferable solvation of the chloride ion due to its much smaller size than the trichloromethyl ion disproportionately favors the products, thus markedly reducing this barrier. Density functional theory is known to have problems with molecular dissociation reactions. The reaction studied here is not an exception to that rule, although it is only observed when the dichlorocarbene carbon and the chloride ion are more than 6 Å apart.

3.4.3 Reaction #3: $CCl_2 + H_2O \rightarrow CHCl_2OH$ A graphical description of the third reaction in the context of the overall reaction mechanism is shown in figure 3.11. The second reaction produced a dichlorocarbene molecule. The third reaction involves the insertion of the carbon atom of dichlorocarbene into the O-H bond of a neighboring water molecule. The presence of dichlorocarbene as a reactive intermediate was first suggested by Anton Geuther[68] in 1862 and supported by other scientists. Nevertheless, its existence was only first confirmed a century later. In 1950 Jack Hine's experiments employing a kinetic analysis of the competition between the hydroxide ion and other ions narrowed the number of candidate reaction paths and product structures.[24] In 1954 W. von E. Doering and Kentaro Hoffmann reported the trapping of dichlorocarbene to an olefin.[34] An olefin is also known as alkene, an unsaturated hydrocarbon containing at least one carbon-carbon double bond.[3] The reaction of chloroform with cyclohexene (an olefin) in the presence of a base represented the first structural evidence for the formation of dichlorocarbene from

chloroform.[34] We are devoting all of chapter 5 to the electronic structure of carbenes and dichlorocarbene in particular. Thus please refer to chapter 5 for more results and computational details regarding dichlorocarbene. Dichlorocarbene is known to display a preference for reacting with a water molecule, as opposed to the hydroxide ion. The reaction takes place as the dichlorocarbene's carbon atom is inserted into one of the hydrogen-oxygen bonds of a water molecule.[31] One of the hydrogen atoms in the water molecule interacts with the carbene's lone pair, while the oxygen shares its electronic cloud with the carbene's Lowest Unoccupied Molecular Orbital (LUMO). Figure 3.12 shows the optimized geometries of the reactant complex, the transition state, and of the product of this third reaction involving the insertion of the carbene carbon atom into the O-H bond of a water molecule.

In Table 3.8 we list the inter-nuclear potential energy of the reactant complex, the transition state, and the product of this third reaction with respect to the reactants evaluated at different levels of theory. The activation energy is also listed. We found two equivalent transition state geometries at the MP2/aug-cc-pVDZ and B3LYP/aug-cc-pVDZ levels of theory respectively. The transition state energy for each of the remaining theoretical methods was obtained as a single-point-energy calculation at the MP2 transition state geometry.

The inter-nuclear potential energy of the products relative to that of the reactants calculated with CCSD(T)/aug-cc-pVDZ is -64.3 kcal/mol. The SPE CCSD(T)/aug-cc-pVDZ//MP2/aug-cc-pVDZ calculation yields -64.4 kcal/mol for the products and 16.5 kcal/mol for the transition state, relative to the reactants. Again, the close proximity

between these results for the reaction energy supports our choice of the latter method for the gas-phase inter-nuclear potential energy profile to reduce the computational cost. For this reaction, B3LYP/aug-cc-pVDZ produced values for the inter-nuclear potential energy of the products and the transition state, -63.4 and 15.7 kcal/mol, respectively, relative to the reactants, which are considerably closer to the CCSD(T) results than those of the MP2/aug-cc-pVDZ method are (-70.5 and 11.9 kcal/mol).

The HF/aug-cc-pVDZ method produces values of the inter-nuclear potential energy difference between products and reactants surprisingly close to those of CCSD(T), yielding a value of -63.5 kcal/mol. However, it overestimates the transition state energy by more than 20 kcal/mol, in spite of using the same basis set that the high level methods used above. This large discrepancy emphasizes the need for a specific electron correlation treatment for obtaining a reasonable estimate of the potential energy of this transition state. Thus, for this particular reaction we absolutely needed to employ post-Hartree-Fock methods directly, and not as a post-correction, as was the case for the other reactions. Thus, the same condensed matter free energy simulation method with HF/3-21+G for the QM part that we used for the other reactions was not used to study this reaction.

In addition, in this reaction two bonds are being made as one bond is being broken, making it impossible for the reaction path to be followed constraining only one degree of freedom. Instead, we used the inter-nuclear vibration frequencies of the transition state to obtain the geometries along an unrestricted (not a reaction coordinate of choice) reaction path away from the TS in both the reactant and product directions. This type of

intrinsic reaction coordinate (IRC) calculations employs an algorithm developed by C. Gonzalez and H. Schlegel to follow a reaction minimum energy path[69] via mass-weighted internal coordinates.[70] This reaction path following from the transition state was performed separately at the MP2 and B3LYP levels of theory with the aug-cc-pVDZ basis set. It allowed us to find the most likely path to connect the reactant complex and the product complex to the transition state. The geometries obtained this way at the MP2/aug-cc-pVDZ level of theory were used to determine the CCSD(T)/aug-cc-pVDZ//MP2/aug-cc-pVDZ inter-nuclear potential energy profile.

For the rest of this discussion, we focus on how the smaller basis sets perform with the HF method in predicting the reaction energy, for which HF/3-21G, HF/3-21G*, and HF/3-21+G yielded -86.0, -78.4, and -76.2 kcal/mol, respectively.

Unlike the rest of the steps involved in the reaction scheme proposed in this project, this reaction does not involve negative ions. Thus, for this reaction, the presence of diffuse functions in the HF/3-21+G method does improve the results over those of HF methods without diffuse functions to the same extent as it does when anions are involved. Nevertheless, its results are only 6 kcal/mol away from the results produced by the more expensive MP2/aug-cc-pVDZ method.

Table 3.8 Reaction #3: $CCl_2 + H_2O \rightarrow CHCl_2OH$
Inter-nuclear potential energy in kcal/mol of the reactant complex, transition state SPE//MP2/aVDZ, activation energy, and product, relative to the potential energy of the reactants.

Method	R.C.	TS[a]	ΔE_{act}	Products
HF/3-21G	-2.3	25.4	27.7	-86.0
HF/3-21G*	-3.9	21.6	25.5	-78.4
HF/3-21+G	-3.2	32.2	35.3	-76.2
HF/6-31G*	-3.3	34.1	37.3	-73.2
HF/aug-cc-pVDZ	-2.2	37.8	40.1	-63.5
B3LYP/aug-cc-pVDZ [b]	-3.5	15.7	19.1	-63.4
MP2/aug-cc-pVDZ	-4.6	11.9	16.6	-70.5
CCSD(T)/aug-cc-pVDZ [b]	-4.1	16.5	20.6	-64.4
CCSD(T)/aug-cc-pVDZ				-64.3
HF/DZP [25]			35.1	
B3LYP/6-311** [71]	-3.7	11.0	14.7	-66.0
CCSD(T)/cc-pVDZ//MP2/DZP [31]			14.6	
CCSD(T)/aug-cc-pVDZ//MP2/DZP [c]			16.2	
MP4/cc-pVDZ//MP2/DZP [d]			4.9	

(a) Geometry optimized at the MP2/ aug-cc-pVDZ level.
(b) This transition state was optimized at the B3LYP/aug-cc-pVDZ level and is not a SPE calculation.
(c) Estimated from MP2 & MP4.[31]
(d) Two-water reaction mechanism.[72]

In Table 3.8 above we have also included some of the results obtained by other authors. We used the transition state geometry reported by Pliego et al in 1998 as a starting structure in the initial geometry optimization.[31] They also experienced the inadequacy of the Hartree-Fock method for estimating the activation energy of this reaction, which HF/DZP overestimated by at least 15 kcal/mol. Li et al employed density functional theory and a basis set of medium size, B3LYP/6-311G**, to obtain an activation energy of 14.7 kcal/mol.[71] This value is within 10% of what Pliego et al obtained using high

level ab-initio methods on structures optimized using the fairly small DZP basis set.[31] Their values fall within 15% of the MP2/aug-cc-pVDZ values that we obtained. Our B3LYP and CCSD(T) results using the same augmented aug-cc-pVDZ basis set are somewhat higher. Since our starting structures were the same, the difference in the size of the basis set used must be solely responsible the discrepancy of the results. The last activation energy listed in the table above is much smaller than the rest. This is because a completely different reaction mechanism was used by Pliego et al. in 1999. It involves two water molecules in a cyclic transition state.[72] In the direct insertion of the carbon atom of the carbene into a H-O bond of the water molecule the hydrogen atom in that bond has to migrate a distance larger than 2Å away from the parent oxygen as the reaction proceeds from reactants to products. In the mechanism that they proposed this is not necessary as it is not the same water molecule whose oxygen bonds to the carbene which donates the hydrogen to the carbene. A proton is transferred from the first water to the second, which in turn releases one of its protons to the carbene to which the first water is attached, leaving all parties involved neutral in the end.

Figure 3.13 represents the inter-nuclear potential energy profile for this third reaction. The transition state for this reaction was optimized at both the MP2/aug-cc-pVDZ and B3LYP/aug-cc-pVDZ levels of theory. Following a frequency analysis of each transition state geometry to obtain the initial force constants, a reaction path following calculation was performed at these two levels of theory. The CCSD(T)/aug-cc-pVDZ energies were obtained through a single-point energy calculation for each geometry optimized at the MP2/aug-cc-pVDZ level.

3.4.4 Reaction #4: $HCCl_2OH + OH^- \rightarrow HCOCl + Cl^- + H_2O$ The only product of the previous reaction is a dichloromethanol molecule. Dichloromethanol is further dehalogenated through a proton transfer to a hydroxide ion and a simultaneous release of a chloride ion and a water molecule. What remains is a formyl chloride molecule. A graphical description of the fourth reaction in the context of the overall reaction mechanism is shown in figure 3.14. Figure 3.15 shows the optimized geometries before, during, and after the proton transfer. In the first reaction in our reaction mechanism, a similar proton transfer takes place, but without the simultaneous loss of a chloride ion. In this chapter focusing on the gas-phase, we completely ignore the second degree of freedom, namely the C-Cl distance. This leads to the C-Cl bond remaining pretty much constant as the reaction proceeds to separate the products. This is reflected in the small change of the inter-nuclear potential energy in the far right side of the graph shown in figure 3.16.

In chapter 4, which is devoted to the solution-phase results, two separate analyses are shown for this reaction; one ignoring that the C-Cl bond breaking takes place at all, and the second taking it into account through a two-dimensional free energy statistical sampling simulation.

In Table 3.9, we compare the inter-nuclear potential energy of the product complex and of the products relative to that of the reactants for different quantum mechanical methods and basis sets for our fourth reaction. The potential energy difference between the reactants and products evaluated at the CCSD(T)/aug-cc-pVDZ level is -58.6 kcal/mol. The same value is obtained, within less than a tenth of a kcal/mol, at the

CCSD(T)/aug-cc-pVDZ//MP2/aug-cc-pVDZ level, thus again reinforcing our confidence in the ability of MP2 to determine the lowest energy geometry of a molecule. MP2 and B3LYP yield values of -57.1 and -61.9 kcal/mol for the reaction energy, respectively, when using the aug-cc-pVDZ basis set. The same inter-nuclear potential energy difference between products and reactants evaluated at the HF/aug-cc-pVDZ and HF/3-21+G levels is -75.2 and -70.5 kcal/mol, respectively. Whereas that of HF methods lacking diffuse functions ranges from -95.4 kcal/mol, for the 6-31G* basis set, to -119.4 kcal/mol for the small 3-21G basis set. It is remarkable, not only that HF/3-21+G results are only less than 12 kcal/mol off from the gold standard, but that our alternative basis sets produce results between 30 and 60 kcal/mol different from the same CCSD(T) reference. These values again emphasize the need to add diffuse functions to the basis sets used to study reactions involving ions.

Table 3.9 Reaction #4:

$Cl_2CHOH + OH^- \rightarrow CHClO + Cl^- + H_2O$

Inter-nuclear potential energy in kcal/mol of the product complex and of the separated products, relative to that of the reactants at infinity.

Method	Prod.C.	Products
HF/3-21G	-159.4	-119.4
HF/3-21G*	-145.3	-109.7
HF/3-21+G	-105.4	-70.5
HF/6-31G*	-125.4	-95.4
HF/aug-cc-pVDZ	-101.3	-75.2
B3LYP/aug-cc-pVDZ	-92.6	-61.9
MP2/aug-cc-pVDZ	-89.8	-57.1
CCSD(T)/ aug-cc-pVDZ[$]	-91.2	-58.6
CCSD(T)/aug-cc-pVDZ		-58.6

($) Geometry optimized at the MP2/aug-cc-pVDZ level.

Figure 3.16 represents the inter-nuclear potential energy profile for our fourth reaction. All geometries were optimized at the levels of theory shown, except for CCSD(T)/aug-cc-pVDZ, which, as in the previous profiles, was obtained through a single-point energy calculation for each geometry optimized at the MP2/aug-cc-pVDZ level. As seen in figure 3.16, the appropriateness of the 3-21+G basis set for this type of reactions is evidenced in the proximity of the results to those of the much larger aug-cc-pVDZ basis set at the HF level of theory.

There is a large difference between the reaction energies listed in Table 3.9 and those which we would arrive at by following the inter-nuclear potential energy profile plotted in figure 3.16. The CCSD(T)/aVDZ//MP2/aVDZ inter-nuclear potential energy difference between reactants and products listed in Table 3.9 is -58.6 kcal/mol, whereas the inter-nuclear potential energy profile at the same level of theory remains almost flat at the product state potential energy of -91.2 kcal/mol. The reaction energies are obtained from the potential energies of the species at infinite separation, whereas the potential energies plotted correspond to the same molecules a few Å apart. Our reaction coordinate only takes into account the transfer of the proton from dichloromethanol to hydroxide, and the subsequent separation of the water produced. It does not take into account the loss of the chloride ion which takes place simultaneous to the proton transfer. The product side is mostly flat as the water molecule is drawn away. As can be observed in figure 3.16, the Cl^- ion has a favorable electrostatic interaction with the hydrogen on the formyl chloride molecule, which remains in place for all the geometries on the right side of the product complex. Extending both our reaction

coordinate and the C-Cl distance to infinity would yield the reaction energies shown in Table 3.9.

In review, the reason behind the more than 30 kcal/mol difference rests is that the potential energies correspond to two completely different structures. In Table 3.9 all three products, CHClO, H_2O, and Cl^-, are at infinite separation from each other. At the far right in the inter-nuclear potential energy profile CHClO and H_2O have moved 6 Å apart, but the Cl^- ion remains at a 2.1 Å distance from the formyl chloride hydrogen.

3.4.5 Reaction #5: $CHClO + OH^- \rightarrow CO + Cl^- + H_2O$ The previous reaction produced a water molecule, a chloride ion, and a formyl chloride molecule. Formyl chloride is dehalogenated through a proton transfer to a hydroxide ion and a simultaneous release of a chloride ion yielding carbon monoxide and water. A graphical description of this reaction in the context of the overall reaction mechanism is shown in figure 3.17. Figure 3.18 shows the optimized geometries before, during, and after the proton transfer.

In Table 3.10 we list the inter-nuclear potential energy of the product complex and of the products of this fifth reaction, with respect to that of the reactants, evaluated at different levels of theory. The inter-nuclear potential energy of the products relative to that of the reactants at the CCSD(T)/aug-cc-pVDZ level of theory is -65.7 kcal/mol. The SPE CCSD(T)/aug-cc-pVDZ//MP2/aug-cc-pVDZ calculation yields the same value

of -65.7 kcal/mol. This close agreement supports our choice of the latter method for the gas-phase inter-nuclear potential energy profile to reduce the computational cost. For this reaction, the B3LYP/aug-cc-pVDZ level for the first time produced values considerably more distant from our gold standard than MP2/aug-cc-pVDZ did. Both methods yielding reaction energies of -59.1 kcal/mol and -62.5 kcal/mol, respectively. The B3LYP method underestimated the potential energy difference of the product state by about 8 kcal/mol.

Table 3.10 Reaction #5:

$CHClO + OH^- \rightarrow CO + Cl^- + H_2O$

Inter-nuclear potential energy in kcal/mol of the product complex and of the separated products, relative to that of the reactants at infinity.

Method	Prod.C.	Products
HF/3-21G	-158.8	-136.8
HF/3-21G*	-147.5	-125.8
HF/3-21+G	-106.6	-87.7
HF/6-31G*	-122.1	-104.4
HF/aug-cc-pVDZ	-101.6	-87.4
B3LYP/aug-cc-pVDZ	-76.6	-59.1
MP2/aug-cc-pVDZ	-81.1	-62.5
CCSD(T)/ aug-cc-pVDZ[$]	-84.4	-65.7
CCSD(T)/aug-cc-pVDZ		-65.7

($) Geometry optimized at the MP2/ aug-cc-pVDZ level.

HF/aug-cc-pVDZ and HF/3-21+G predicted reaction energies of -87.4 and -87.7 kcal/mol, respectively. This clearly shows that there is not much more benefit that could have been obtained upon a further increase of the size of the basis set beyond 3-

21+G. As with every other reaction that we have studied involving negative ions, HF methods lacking diffuse functions produced results very distant from the gold standard. The reaction energies that they produced ranged from -104.4 kcal/mol, for the larger 6-31G* basis set, to -136.8 kcal/mol for the small 3-21G basis set.

Figure 3.19 represents the inter-nuclear potential energy profile for our fifth reaction, the last in our process of decomposition of chloroform. As seen in the first, second and fourth reactions, in which negative ions took part, the right balance between accuracy and computational cost seems to be reached again at the HF/3-21+G level. As observed in the last reaction, the HF/3-21+G results are remarkably close to those of the much larger aug-cc-pVDZ basis set at the HF level of theory, unlike the results obtained employing basis sets without diffuse functions. It may also be noted that the inter-nuclear potential energy of the product state is not accurately estimated without a treatment of electron-electron correlation beyond the mean-field approximation found in the Hartree-Fock method. We chose to use HF/3-21+G for our QM portion of the condensed-phase simulation and employ a post-correction based on the difference between the CCSD(T)/aug-cc-pVDZ and HF/3-21+G gas-phase potential energy reaction profiles.

The inter-nuclear potential energy in atomic units of each molecule taking part in these reactions is tabulated in appendix A. It is from those values that the reaction energies shown in the tables in this chapter are obtained. Since the same electronic structure methods are used, the numbers reported in appendix A are in exact agreement with

those for which there is an entry reported by the National Institute of Standards and Technology (NIST) at its Computational Chemistry Comparison and Benchmark Database (CCCBD). Of the molecules taking part in the reactions studied here, water, chloroform, dichlorocarbene, and carbon monoxide have entries in the CCCBD database.

3.5 Chloroform Geometry

Chloroform is an organic compound with a boiling point of 62 ºC and a dipole moment of 1.0 D. It is an alkyl halide, and its carbon atom is sp^3 hybridized. In this symmetrical setup the three chlorine atoms are equidistant to and span the same angles with their neighbors.

Table 3.11 below shows just the bond lengths present in chloroform, as the calculated values for the angles and dihedrals barely differed between methods.

As is well documented in the literature, the addition of diffuse functions to the smaller basis sets does not improve the equilibrium geometries. This is due to the small size of the exponents in the diffuse functions, which makes their contribution significant only at larger distances.

Table 3.11 Chloroform optimized geometry.

Method	C-H Bond Length (Å)	C-Cl Bond Length (Å)
HF/3-21G	1.07	1.84
HF/3-21G*	1.07	1.78
HF/3-21+G	1.07	1.84
HF/6-31G*	1.07	1.76
HF/aug-cc-pVDZ	1.08	1.77
B3LYP/aug-cc-pVDZ	1.09	1.79
MP2/aug-cc-pVDZ	1.09	1.78
CCSD(T)/aug-cc-pVDZ	1.10	1.79

3.6 Conclusion

The harmonic approximation allows us to estimate the free energy of a stable state in the gas phase. In addition we can use an implicit, or continuum solvation model to obtain a qualitative perspective on the free energy profile of a process in solution. During a chemical reaction bonds are being broken and made. Individual solvent molecules may have very strong interactions with parts of our solute with a large partial charge. This is particularly important for reactions in which ions are being transferred, as is the case for four of the five reactions studied here. Being able to model the solvent explicitly gives us the opportunity to take these strong interactions into account. This allows us to obtain a much better estimate of the contribution of the solvation effect to the free energy of a reaction. This allows us to obtain the activation free energy, from which we can determine the rate constant for the reaction in solution.

The QM/MM method allows us to treat the solute quantum mechanically and the solvent with a molecular mechanical model and to calculate the interactions between the

two parts. The cost of treating the solvent explicitly is that statistical sampling has to be used in order to obtain the free energy. For every solvent molecule which moves within the cutoff distance, an SCF energy minimization will be performed on the solute molecule(s). This leads to millions of SCF calculations per 0.4 A of reaction coordinate sampled. Thus it is crucial to choose a quantum mechanical method and basis set which are as accurate as possible, while keeping the computational costs to a minimum.

Unfortunately, post-Hartree-Fock methods are too costly for this purpose at this moment. We are thus using the Hartree-Fock method, but we still have a choice when it comes to the basis set to use with it. The need to employ a basis set with diffuse functions to study processes involving negative ions is widely documented. Here we have the chance to improve on previous studies by employing such a basis set. The tables in this chapter clearly show that the dramatic increase in accuracy obtained by adding diffuse functions to the 3-21G basis set outweighs the costs. We can also observe that the cost of increasing the size of the basis set beyond that of the 3-21+G basis set is not justified by the marginal improvement in accuracy obtained.

CHAPTER 4

Solution-Phase Study

Free Energy Simulation of the Solvent Effect on the Chloroform Alkaline Dehalogenation Reactions.

4.1 Introduction

Water is a polar solvent with a high dielectric constant. A water molecule has a considerably large dipole moment for its small size. Just a single electronic charge on an ionic solute can lead to very large electrostatic interactions with the solvent. The smaller the solute the stronger the hydrogen bonds with the waters in the first solvation shell thus increasing the electrostatic contribution. This helps explain the large negative free energy of solvation of the hydroxide ion, and why it is considerably larger than that of the larger chloride ion. We can obtain qualitative values for the free energies of solvation of the species involved by employing a continuum solvation model. These values can be used to make a first estimate on the free energy of a reaction. Experimental results are available for the free energy change for our first reaction.

It would be ideal to use ab-initio molecular orbital theory or density functional theory to calculate the total and interaction energies of the whole system, which consists of solutes and solvent. However, it is computationally impractical at the present time. In addition, free energy calculations must be carried out, which require ca. 10^6 electronic

structure calculations.[29] Nevertheless, we need a quantum mechanical description of the bond-breaking and bond-making process. In order to evaluate the inter-nuclear potential energy of such a chemical process in solution, we used a combined quantum-mechanical and molecular mechanical (QM/MM) potential.[9,26, 27, 28] In order to conduct extensive statistical sampling to simulate the free energy along one- and two-dimensional potential energy surfaces, we chose the HF/3-21+G method for the QM region. This particular combination of Hartree-Fock theoretical method and 3-21+G basis set corresponded to the best accuracy vs. computational cost ratio. for our case corresponds to the solute molecules. Figure 4.1 shows a snapshot of a simulation of the fourth reaction studied in this project.

4.2 First Reaction: $CHCl_3 + OH^- \rightleftharpoons CCl_3^- + H_2O$

In this first reaction a proton is transferred from chloroform to a hydroxide ion. As we saw in chapter 3, for this reaction in the gas-phase the products are by far more stable than the reactants. The effect of water as a solvent for this particular reaction is to favor the reactants. The largest contribution to this effect can be traced back to the small size of the hydroxide ion, our only ionic reactant, which is much smaller than that of the trichloromethyl ion, our only ionic product for this reaction. The free energies of solvation of the neutral molecules chloroform and water also contribute to the final free energy of the reaction, but to a lesser extent, as is observed in the values of Table 4.1.

Table 4.1 lists both continuum model and experimental estimates of the contribution of

the solvent to the free energy difference between reactants and products of our first reaction. The free energy of solvation of each molecule taking part in the reaction is calculated via a continuum solvation model employing the Pauling (Merz-Kollman) atomic radii for every solute atom. The free energy solvation can be separated into electrostatic, dispersion, and cavitation parts. As mentioned previously, the magnitude of the cavitation term found via such implicit solvation models is directly proportional to the solvent-accessible-surface-area SASA of the solute. The keywords PCM and Pauling were used in the Gaussian package to generate these results.

Aqueous solvation has a net stabilization effect of the reactants due to the smaller size of the hydroxide ion in comparison to the trychloromethyl ion. Thus the magnitude of the experimental free energy of solvation of OH^- is 50 kcal/mol larger than that of $CCl3^-$. The same free energy of solvation difference is estimated to be 45 kcal/mol by the PCM Pauling implicit solvation model. As mentioned above, it is this difference in free energy of solvation between the ion present in the reactants and the one present in the products which is largely responsible for the net stabilization of reactants over products by 39 kcal/mol according to the implicit model and 45 kcal/mol according to experiment.

Table 4.1 Reaction #1: $CHCl_3 + OH^- \rightleftharpoons CCl_3^- + H_2O$ Continuum model (PCM, Pauling) and experimental free energy of solvation of each molecule involved and the resulting estimates of the net solvent effect for the first reaction.

Species	CCSD(T)/aug-cc-pVDZ PCM Pauling Free Energy of Solvation (kcal/mol)	Experimental Free Energy of Solvation (kcal/mol)
$CHCl_3$	-2.9	-1.1
OH^-	-99.1	-106
CCl_3^-	-53.7	-55.7
H_2O	-9.2	-6.3
Net Reaction Solvent Effect	39.1	45.1
Reaction ΔG	5.3	

Adding the experimental estimate of the solvation effect of 45 kcal/mol to the experimental gas-phase reaction free energy of -34 ± 4 kcal/mol we can obtain a rough prediction of the experimental reaction free energy in solution, which we would expect to fall around 11 ± 4 kcal/mol. This estimate is consistent within the large margin of error with an estimate obtained from the experimental pKa of chloroform, which places the reaction free energy in solution at 12 kcal/mol. The free energy profile which we have obtained from a set of ab-initio HF/3-21+G:TIP3P QM/MM Monte Carlo simulations predicts a value of 11.7 kcal/mol. This value is obtained from the potential of mean force at the HF/3-21+G level (-2.5 kcal/mol) corrected with the difference in values for the gas-phase reaction free energy (14.2 kcal/mol) arising from two different levels of theory; CCSD(T)/aug-cc-pVDZ and HF/3-21+G. As predicted theoretically, this difference in gas-phase free energy (14.2 kcal/mol) can be approximated by the

difference in gas-phase reaction potential energy (14.5 kcal/mol).

The thin orange solid line in figure 4.2 marks the values of the solution-phase potential of mean force at the HF/3-21+G level. The thick violet dashed line is obtained from adding to the solution-phase potential of mean force in the thin orange solid line the gas-phase inter-nuclear potential energy difference between the results produced at the CCSD(T)/aug-cc-pVDZ and HF/3-21+G levels of theory.

4.3 Second Reaction: $CCl_3^- \rightleftharpoons CCl_2 + Cl^-$

Having the fairly large trichloromethyl ion as a product made the solvation effect favor the reactants in the previous reaction. Now, for our second reaction, the free energy of solvation of the trichloromethyl ion, now on the reactant side, is surpassed by that of the smaller chloride ion produced. Experiment finds these two solvation free energies to lie around -56 and -77 kcal/mol, respectively. The free energy of solvation of the neutral CCl_2 molecule, which is about -1 kcal/mol, is dwarfed by that of the two ions. Thus, the 21 kcal/mol free energy of solvation difference between the two ions is responsible for the net solvation stabilization of products over reactants by about 22 kcal/mol.

Table 4.2 Reaction #2: $CCl_3^- \rightleftharpoons CCl_2 + Cl^-$ Continuum model (PCM, Pauling, CCSD(T)/aug-cc-pVDZ SPE) and experimental free energy of solvation of each molecule involved and the resulting estimates of the net solvent effect for the second reaction.

Species	CCSD(T)/aug-cc-pVDZ PCM Pauling Free Energy of Solvation (kcal/mol)	Experimental Free Energy Solvation (kcal/mol)
CCl_3^-	-53.7	-56.0
CCl_2	-1.2	
Cl^-	-74.4	-76.5
Net Reaction Solvent Effect	-22.0	
Reaction ΔG	-0.9	

Figure 4.3 shows the large difference between the gas-phase potential energy and solution-phase free energy profiles. The thin orange solid line in figure 4.3 marks the values of the solution-phase potential of mean force at the HF/3-21+G level. The thick violet dashed line is obtained from adding to the solution-phase potential of mean force the difference between the values for the gas-phase inter-nuclear potential energy obtained at CCSD(T)/aug-cc-pVDZ and HF/3-21+G levels of theory.

It was expected due to the -22 kcal/mol solvent stabilization of products over reactants. Our implicit solvation model predicted a negative reaction free energy of less than a kcal/mol and our more accurate explicit solvation simulation produced a value a little above 2 kcal/mol higher.

In a previous study,[1] a free energy of activation of 12.7 kcal/mol for this reaction was found via similar simulation methods. The treatment of the quantum mechanical region

was performed at the HF/3-21G level of theory and the number of solvent molecules used in the solvation box was considerably smaller. We got a value of 8.6 kcal/mol, which after the post-correction with CCSD(T)/aug-cc-pVDZ becomes 7.12 kcal/mol. The solvent-induced barrier for recombination obtained in the previous study mentioned above was about 3.8 kcal/mol. Including the CCSD(T)/aug-cc-pVDZ post-correction, we found this barrier for recombination of Cl^- and CCl_2 to be slightly larger, namely 6.1 kcal/mol. Nevertheless our results are fairly close and agree qualitatively. The reaction free energy profile published in the 2002 study[1] is reproduced in figure 4.4.

4.4 Third Reaction: $CCl_2 + H_2O \rightarrow CHCl_2OH$

The third reaction represents the insertion of the carbon atom of dichlorocarbene into one of the hydrogen-oxygen bonds of a neighboring water molecule. Electrostatic attraction plays a role in the process, where the lone pair of the dichlorocarbene molecule interacts with the hydrogen. Simultaneously, the lone pair of the oxygen of the water molecule is shared with the lowest unoccupied molecular orbital (LUMO) of the dichlorocarbene.

As can be observed in Table 4.3 below, the solvent effect for this reaction is an order of magnitude smaller than what we observe for the rest of the reactions. This is because this reaction does not involve the transfer of ions. Instead, a neutral hydrogen atom changes hands while an oxygen atom forms a bond with the dichlorocarbene carbon.

Table 4.3 Reaction #3. $CCl_2 + H_2O \rightarrow CHCl_2OH$ Continuum model (PCM, Pauling, CCSD(T)/aug-cc-pVDZ SPE) and experimental free energy of solvation of each molecule involved and the resulting estimates of the net solvent effect for the third reaction.

Species	PCM Pauling Free Energy of Solvation (kcal/mol)
CCl_2	-1.2
H_2O	-9.2
$CHCl_2OH$	-6.6
Net Reaction Solvent Effect	3.8
Reaction ΔG	-60.5

Thus, the value that the continuum model predicts for the reaction free energy in solution is within 10% of what was obtained for the gas-phase calculation.

We have shown that continuum models are quite accurate predicting the free energy differences between stable and well parametrized molecules with well defined solvent accessible surface areas. This is the case for the reactants and products of our reactions, for which the continuum model we chose gave us excellent results. However, the reliability of these models to predict free energies of unstable molecular geometries is not yet well established. Nevertheless, this reaction did not involve any proton transfer, or any ionic charge transfer, so the results of this continuum model were not very far from those obtained treating the solvent explicitly.

The solvent molecules were treated explicitly via a molecular mechanics model. The partial charges of the TIP3P water model[59] used were obtained via quantum mechanics

and fitting of experimental data such as the density, enthalpy of vaporization, and free energy of solvation/mixing with other molecules.

The importance of employing an explicit treatment of the solvent lies in being able to take into account the potential energy of specific solute-solvent interactions such as hydrogen bonds. Due to their strength and specificity, these interactions may play a crucial role in the outcome of the reaction.

In chapter 3, which is devoted to gas-phase calculations, we showed that the Hartree-Fock mean field treatment of the electron-electron repulsion problem is not sufficient. The values predicted by HF methods differed from those produced by high-level post-Hartree-Fock methods by more than 15 kcal/mol, which was unacceptable. This discrepancy was independent of the size of the basis set used. Unfortunately free energy simulation requires extensive statistical sampling of geometries involving thousands of degrees of freedom of the solvent molecules and millions of SCF electronic structure calculations for the solute. Thus, at this point, employing the same direct potential of mean force calculation method as we did for the other reactions with the HF/3-21+G method was not adequate for this reaction. Therefore, we had to use the highest level post-Hartree-Fock ab-initio electronic structure method practical for our purposes, which we chose to be CCSD(T)/aug-cc-pVDZ. Chapter 3 describes the reasons behind this choice in more detail.

The transition state (TS) for this reaction was also found from the same starting

structure via two different post-Hartree-Fock electronic structure methods, yielding slightly different TS geometries. These two levels of theory used were MP2/aug-cc-pVDZ and B3LYP/aug-cc-pVDZ. From the force constants resulting from a frequency analysis of the two TS geometries found, we obtained two high-level gas-phase minimum energy paths employing Gonzalez's intrinsic mass-weighted reaction coordinate following algorithm (IRC). Thus, the geometries along these two separate gas-phase minimum energy paths were optimized at the MP2/aug-cc-pVDZ and B3LYP/aug-cc-pVDZ levels, respectively. The inter-nuclear potential energy profiles for these two paths are shown in figure 4.6 with thin dark blue and red lines, respectively. Consistent with our choice throughout this project, we conducted single point energy (SPE) calculations at the benchmark CCSD(T)/aug-cc-pVDZ level on the geometries along the minimum energy path optimized with the MP2/aug-cc-pVDZ method. The inter-nuclear potential energy profile at the CCSD(T)/aug-cc-pVDZ level is displayed with a thin light blue line in figure 4.6.

We employed a very efficient semi-empirical electronic structure method (AM1) for explicitly calculating the solvation free energy difference between consecutive geometries along the gas-phase minimum energy path in the presence of the explicitly treated solvent. The resulting AM1 free energy of solvation profile of the solutes along the reaction coordinate is shown in figure 4.6 with a thick light blue line. Semiempirical methods provide a practical procedure for free energy simulations that employ explicit electronic structure theory. Although less systematic than high-level ab initio models that include electron correlation, semiempirical methods can still provide

important insights on the reaction mechanism, and have been successfully used in numerous enzymatic reactions by several groups. [50-57] An implicit calculation of the free energy of solvation profile of the solutes via the PCM continuum solvation model yields almost identical results to those obtained via the AM1 explicit treatment. The PCM free energy of solvation profile is shown in figure 4.6 with a thin brown line connecting the points (large brown dots) along the reaction coordinate for which the free energy of solvation was calculated.

We add the AM1 solvation free energy to the CCSD(T)/aug-cc-pVDZ inter-nuclear potential energy at each reaction coordinate value to obtain the solution-phase free energy profile. The transition state plays a crucial role in a chemical reaction. The Gibbs free energy difference between the reactant complex and the transition state determines the barrier height responsible for the rate of the reaction. It is also called the free energy of activation. Figure 4.5 describes a sample one-dimensional free energy profile. The free energy is plotted as a function of the reaction coordinate.

There are several empirical mathematical relations between the Gibbs free energy of activation and the corresponding rate constant of a reaction. Transition state theory provides us with the ability to obtain the rate constant as a function of the temperature and the temperature dependent Gibbs free energy of activation.

$$k = \frac{k_B T}{h} \exp\left(-\frac{\Delta G_{act}}{k_B T} \right) \tag{58}$$

Our goal is to obtain the most accurate estimate of the free energy of activation in solution. Thus, a frequency analysis was conducted for the reactant complex and the transition state. It allowed us to obtain the gas-phase free energy difference between the reactant complex and the TS within the harmonic approximation. The difference between this gas-phase free energy difference and the corresponding inter-nuclear potential energy difference corresponds to an important post-correction added to the free energy of activation obtained from the solution-phase free energy profile. This is necessary for this reaction because we had added the CCSD(T)/aug-cc-pVDZ potential energy, not free energy, to the AM1 free energy of solvation. The value obtained for this correction to the activation free energy with the B3LYP/aug-cc-pVDZ method is 1.8 kcal/mol. This leaves us with a final free energy of activation in solution of 23.5 kcal/mol. In 1996, using the same reaction mechanism, Pliego et al obtained a free energy of activation of 26.0 kcal/mol.[31] The use of a smaller basis set (DZP) to optimize the transition state geometry with MP2 is responsible for the 2.5 kcal/mol difference in their results.

The approach of adding the free energy of solvation to the gas-phase free energy is justified by the relatively small solvent effect of this particular reaction.[31] The small solvent effect is not likely to considerably perturb the solute geometries from their gas-phase configuration. The solvation free energy profiles resulting from explicit and implicit solvation models show this to be the case. The change in solvation free energy observed via these two models along the reaction coordinate does not exceed 2 kcal/mol in magnitude, whereas the inter-nuclear potential energy drops by more than 80 kcal/mol as the system moves from the TS to the product.

4.5 Fourth Reaction: $HCCl_2OH + OH^- \rightarrow HCOCl + Cl^- + H_2O$

In this reaction dichloromethanol is dehalogenated through a proton transfer to a hydroxide ion and a simultaneous release of a chloride ion, water and formyl chloride molecules. In this reaction a chloride ion is released, whereas in our first reaction a much larger trichloromethyl ion was produced. Due to the smaller size difference between the hydroxide ion reactant and the chloride ion product, we expect a smaller reactant stabilization than the 45 kcal/mol we found for our first reaction. The experimental free energies of solvation of the hydroxide and chloride ions are about 106 and 76 kcal/mol respectively. This 30 kcal/mol contribution to the solvent stabilization of the reactants is further reduced by the two polar neutral molecules produced, water and formyl chloride, whose free energies of solvation are estimated by our implicit solvation model to be -9.2 and -7.6 kcal/mol respectively. In the end, the solvent effect favors the reactants over the products by 14.4 kcal/mol. Adding the solvent effect calculated via our implicit solvation model to the inter-nuclear potential energy difference between reactants and products at the CCSD(T)/aug-cc-pVDZ level (-58.6 kcal/mol) yields a net reaction free energy of -44.2 kcal/mol.

Table 4.4 Reaction #4: $HCCl_2OH + OH^- \rightarrow HCOCl + Cl^- + H_2O$ Continuum model (PCM, Pauling, CCSD(T)/aug-cc-pVDZ SPE) and experimental free energy of solvation of each molecule involved and the resulting estimates of the net solvent effect for the fourth reaction.

Species	CCSD(T)/aug-cc-pVDZ PCM Pauling Free Energy of Solvation (kcal/mol)	Experimental Free Energy of Solvation (kcal/mol)
$CHCl_2OH$	-6.6	
OH^-	-99.1	-106.0
HCClO	-7.6	
Cl^-	-74.4	-76.5
H_2O	-9.2	-6.3
Net Reaction Solvent Effect	14.4	
Reaction ΔG	-44.2	

Figure 4.7 corresponds to an extended set of Monte Carlo QM/MM free energy simulations performed biasing one dimension of the system via a parabolic potential energy function for each window. This method was quite successful for the first two reactions described in this thesis. However, this reaction involves the simultaneous breaking of two independent bonds while a third is being formed. One of the two bonds is represented by the carbon-chloride ion distance, which is not restrained via a parabolic potential during the simulation. For this reason the free energy profile in figure 4.7 does not represent the minimum free energy path for the reaction. As a result, an artificial barrier in the path from reactants to products is obtained.

It is worth noting that a continuum solvation model (constant dielectric) does not predict the existence of the barrier, which further enhances the argument for computing a two-dimensional free energy profile, as was done and is shown in figure 4.8.

Since two dimensions are being sampled in the 2-D free energy simulation, the number of SCF electronic structure calculations required increases by a whole order of magnitude. The resulting 2-D free energy profile for this fourth reaction is displayed below in figure 4.8. It clearly shows that the reaction is concerted. This means that both reaction coordinates, plotted along the horizontal and vertical axes, change simultaneously, and not in a step-wise fashion.

We can observe that the value predicted this way for the free energy of the reaction in solution is within 10% of that which was obtained using the continuum solvation model. These values are (- 62 + 14 = - 48) and -44 kcal/mol, respectively. The 14 kcal/mol added to the free energy of the reaction from the 2-D profile corresponds to the same high-level *ab initio* post-correction employed to correct the reaction free energy profiles obtained at a low level in solution throughout this thesis.

Figure 4.9 is a close view of the only region in our two-dimensional free energy profile in which there is a barrier present along the path from reactants to products. From it we can see that it is not larger than 2 kcal/mol.

4.6 Fifth Reaction: $CHClO + OH^- \rightarrow CO + Cl^- + H_2O$

The previous reaction produced a water molecule, a chloride ion, and a formyl chloride molecule. Our fifth and last reaction closely resembles the previous reaction. Formyl chloride is dehalogenated through a proton transfer to a hydroxide ion and a simultaneous release of a chloride ion yielding carbon monoxide and water.

The experimental free energies of solvation of the hydroxide and chloride ions are about 106 and 76 kcal/mol respectively. This 30 kcal/mol difference leads to a moderate solvent stabilization of the reactants with respect to the products. Our implicit solvation model of choice differs somewhat yielding a value of 25 kcal/mol for the reactant solvent stabilization. The neutral molecules do not alter this value considerably since the calculated solvation free energy of the neutral reactant formyl chloride is very similar to that of the water molecule produced, -7.6 and -9.2 kcal/mol respectively, and the carbon monoxide produced barely makes a contribution. In the end, the solvent effect favors the reactants over the products by 22.7 kcal/mol. Adding the solvent effect calculated via our implicit solvation model to the inter-nuclear potential energy difference between reactants and products at the CCSD(T)/aug-cc-pVDZ level (-65.7 kcal/mol) yields a net reaction free energy of -43.0 kcal/mol.

Table 4.5 Reaction #5: $CHClO + OH^- \rightarrow CO + Cl^- + H_2O$
Continuum model (PCM, Pauling, CCSD(T)/aug-cc-pVDZ SPE) and experimental free energy of solvation of each molecule involved and the resulting estimates of the net solvent effect for the fifth reaction.

Species	CCSD(T)/aug-cc-pVDZ PCM Pauling Free Energy of Solvation (kcal/mol)	Experimental Free Energy of Solvation (kcal/mol)
HCClO	-7.6	
OH^-	-99.1	-106
CO	-0.4	
Cl^-	-74.4	-76.5
H_2O	-9.2	-6.3
Net Reaction Solvent Effect	22.7	
Reaction ΔG	-43.0	

Figure 4.10 shows the reaction free energy profile for our fifth reaction. The net free energy change for the reaction obtained via QM/MM HF/3-21+G:TIP3P Monte Carlo simulation is -44 kcal/mol. The proximity of the -43 kcal/mol value obtained via the PCM Pauling implicit solvation model is fairly close. This shows how useful continuum solvation models can be in obtaining a first estimate of a reaction energy, even though they may not be helpful when dealing with a transition state. The reader may be surprised by comparing with that of the gas-phase because in the simulation the chloride ion was not completely removed from the carbon monoxide.

In the computation of the one-dimensional free energy profile shown in figure 4.10 we did not encounter the same problem we did for the fourth reaction. Even though the length of the carbon-chloride ion distance was not biased during the simulation, the path followed is very close to the path of steepest descent of the free energy. This can be observed in the two-dimensional free energy profile, which is displayed in figure 4.11.

Figures 4.11 and 4.12 display the free energy surface in a similar way to what was is done for the fourth reaction. In both cases the free energy drops dramatically without a barrier larger than 2 kcal/mol. The amount by which the free energy drops in going from reactants to products is almost identical that predicted by the continuum solvation model PCM, which employs Pauling solvation radii parameters. Where the continuum model does not prove to be useful, is to show the change in the free energy during the reaction, where bonds are being broken and formed. This is especially important for these last two reactions which involve the transfer of a proton, for which continuum models utterly fail due to the difficulty in choosing and parametrizing the solvation sphere of a proton.

4.7 Conclusion

This fourth chapter is concerned with the effect that the solvent has on the values for the net reaction free energy and the free energy of activation. The former is used to predict the direction in which the reaction proceeds. The latter determines the rate of the reaction.

4.7.1 Effect of the Solvent on the Reaction Free Energy a) Reaction #1: The experimental reaction free energy for the first reaction in the gas phase was found to be - 34 ± 3 kcal/mol, which is highly exothermic. The reaction free energy in solution found via free energy simulation of the solute in explicit solvent molecules was + 12 kcal/mol, which is endothermic. Thus the net solvent effect on the reaction free energy was to stabilize the *reactants* by about 46 ± 3 kcal/mol. Thus a step which would have

never been suspected as being the rate-limiting step from just looking at the gas-phase free energy suddenly turned into a prime suspect when taking into account the effect of the solvent. b) Reaction #2: The solvent effect is the opposite for the second reaction, which is the most endothermic step in the gas phase, with an experimental standard reaction enthalpy of + 31 ± 3 kcal/mol. We found the reaction free energy in solution to be about + 2 kcal/mol, which means that the solvent effect was to stabilize the *products* by 29 ± 3 kcal/mol. c) Reaction #3: The introduction of the solvent changed the reaction free energy less than 1 kcal/mol since there were no ions involved in this reaction. d) Reaction #4: Just based on the difference between the reaction energy in the gas-phase of - 59 kcal/mol and the reaction free energy of - 48 kcal/mol, we can conclude that the solvent stabilized the reactants by 11 ± 5 kcal/mol approximately. e) Reaction #5: Just based on the difference between the reaction energy in the gas-phase of -66 kcal/mol and the reaction free energy of -39 kcal/mol, we can conclude that the solvent stabilized the reactants by nearly 27 ± 5 kcal/mol.

Table 4.6 summarizes the net effect of the solvent on the reaction free energy.

Table 4.6 The solvent effect on the reaction free energy.

Step #	$\Delta\Delta G_{react}$
1	+ 46 ± 3
2	- 29 ± 3
3	0 ± 2
4	+ 11 ± 5
5	+ 29 ± 5

Thus we can observe that the effect of the solvent on the reaction free energy was completely decisive for the first two reactions, in which its size was enough to turn an exothermic into an endothermic reaction in one case, and turn a very strongly endothermic reaction into one without a large difference in free energy between reactants and products. Large differences were observed when considering the effect of the solvent on the free energy barriers observed and is plotted and discussed in the conclusion contained in the last chapter of this dissertation.

CHAPTER 5

Electronic Structure of Carbenes

5.1 Introduction to Carbenes

Carbenes are a class of highly reactive uncharged species characterized by the presence of a divalent carbon atom.[3] Most carbenes are very short lived. However, persistent carbenes are known. The most common carbenes are CCl_2 and CH_2.[73] They are usually named by the names of the two substituents. For example CCl_2 is called dichlorocarbene. The parent species CH_2 is called methylene.

The carbon atom has the tendency to use all of its four valence electrons in bonding. Only two of the four valence electrons are used in carbenes, resulting in very high reactivity. A carbene has both a lone pair of electrons and an empty *p* orbital, which results in the capability to react both as an electrophile (with electron rich species) and as a nucleophile (with electron poor species).[3]

The nucleophilic and electrophilic character of the carbenes is greatly affected by the pi-electron-donating or withdrawing properties of the two groups attached to the carbon. Groups or atoms with lone pairs will render the carbene more nuclephilic and usually more stable. Whereas electron-withdrawing groups will make them more electrophilic and also more reactive.[73]

The two electrons that do not participate in bonding, may have parallel spins (triplet) or antiparallel (singlet). The multiplicity of the unshared electrons is also a key role in determining the reactivity of carbenes. The singlet state has a total spin of zero. The triplet can have total spin numbers of +1, 0, or -1, since each electron can either be of spin + ½ or – ½.[3,73]

The electronic structures of the singlet and triplet carbenes are shown in the figure 5.1.

Triplet carbenes may be either linear (*sp* hybridized), or bent (sp^2 hybridized).
The carbon atom of a singlet carbene is sp^2 hybridized, with trigonal geometry, where the two unshared and paired electrons occupy one of the sp^2 hybrid orbitals. The empty *p* orbital extends perpendicularly above and below the plane of the three atoms.[3]

Singlet carbenes are bent molecules, the angle between the two groups attached to the carbon depending both on steric and electronic factors.[73] For instance, it is known that in triplet methylene, the angle between the 2 hydrogens is of 136 degrees, whereas it is 103 degrees for the singlet species.[74] In 1968, Lester Andrews found singlet dichlorocarbene to have a Cl-C-Cl angle of 100±9 degrees via infrared spectroscopy in solid argon.[75] However, more recent studies by Fujitake *et al* and Clouthier *et al* have measured the angle to be 109.2[76] and 109.3[77] degrees, respectively. Barden and Schaefer obtained a value of 109.1 degrees for this angle with the CCSD(T)/cc-pVQZ method.[78] The highest level theoretical method that we employed in this project, CCSD(T)/aug-cc-pVDZ determined the Cl-C-Cl angle of singlet dichlorocarbene to be 108.8 degrees. MP2/aug-cc-pVDZ found it to be 109.0 degrees. The small difference

of this value compared to what the benchmark CCSD(T)/aug-cc-pVDZ method produced confirms the competence of MP2/aug-cc-pVDZ as a high level geometry optimization method at a moderate computational cost. R. Schwartz et al reported values of 110.4 and 127.5 degrees for the Cl-C-Cl angle of the singlet and triplet dichlorocarbene states, respectively. They employed the MP2/6-311+G* method for these calculations.[79] The values that we obtained for the Cl-C-Cl angle of triplet dichlorocarbene range from 127 to 129 degrees, depending on the theoretical method. Barden and Schaefer obtained a value of 127.7 degrees for this angle with the CCSD(T)/cc-pVQZ method.[78]

5.2 Reactions of Carbenes

Carbenes are generated mainly in two ways. One is the photochemical or thermal disintegration of organic compounds containing certain kinds of double bonds (chiefly ketenes and diazocompounds). The other type, which comprises the reaction studied in the present work is α-elimination. In this mechanism, a four valent carbon loses a group leaving the previously shared electrons on the carbon, thus generating a carbanion. Then, another group (usually a halide) leaving with its electron pair generates the carbene.[73]

Although the most common reaction of this type is the reaction between chloroform and a base to form dichlorocarbene, other numerous examples are known.[73,80]

Carbenes exhibit a broad range of reactivity. They can add to carbon-carbon double bonds, aromatic systems, nitrogen-nitrogen double bonds. They are also capable of

inserting to C-H and O-H bonds. Carbenes, both in triplet and singlet states, can also abstract hydrogen or other atoms to yield free-radicals.

5.3 Singlet-Triplet Energy Splitting of Dichlorocarbene

Most carbenes have a sp^2 hybridized triplet ground state. Triplets carbenes tend to be the lower in energy than singlets in the gas-phase, whereas the opposite generally holds true in aqueous solution. Simple hydrocarbon triplet carbene energies are usually about 8 kcal/mol lower than their singlet carbene counterparts. Triplet CH_2 is about 11 kcal/mol lower than singlet CH_2.[73]

Studies of the infrared spectrum of dichlorocarbene trapped at low temperatures in solid argon indicate that the ground state of CCl2 is the singlet.[75] Nucleophilic substituents can donate electron pairs and thus stabilize the singlet state by delocalizing the pair into an empty p-orbital. If the energy of the singlet state is sufficiently reduced it can become the ground state. In 1999, negative ion photoelectron spectroscopy determined the singlet CCl2 to be lower in energy than the corresponding triplet by 3 ± 3 kcal/mol.[79] No other experimental studies determining the singlet-triplet (S-T) energy splitting for dichlorocarbene had been reported prior to that date.[81] However, the triplet CCl2 state presents tremendous challenges to photodetachment experiments attempting to measure the vertical detachment energy.[78] We used the CCSD(T)/aug-cc-pVDZ//MP2/aug-cc-pVDZ level of theory to obtain a value for the S-T dichlorocarbene energy splitting of 20.9 kcal/mol. Barden and Schaefer obtained a very similar result, 20.3 kcal/mol, using a very high levels of theory for both energy calculation and

geometry optimization: CCSD(T)/aug-cc-pVQZ//CCSD(T)/cc-pVTZ.[78] The very close agreement further serves to validate our choice of the CCSD(T)/aug-cc-pVDZ//MP2/aug-cc-pVDZ method as our benchmark. The 17 kcal/mol discrepancy between experimental and the highest level theoretical results is startling. Barden and Schaefer estimated the possible margin of error inherent in the approximations used in the theoretical calculations to be limited to ± 2 kcal/mol.[78] This does not come even close to explaining the large difference. Thus, the reason behind this large difference between theory and experiment remains a mystery.[78,82] Efforts to obtain a new experimental value of the S-T energy gap have succeeded in determining a lower limit of 14 kcal/mol by analyzing the laser-induced dispersed fluorescence spectrum of CCl_2.[83]

MP2/aug-cc-pVDZ and B3LYP/aug-cc-pVDZ produced S-T energy splitting values of 18.6 and 19.3 kcal/mol, respectively. These values are still acceptable, considering the lower computational cost involved, in comparison to CCSD(T). However, Hartree-Fock proves its inadequacy to properly describe the electronic structure of carbenes by producing values which underestimate the dichlorocarbene S-T energy splitting by more than 25 kcal/mol. This shortcoming of the HF method was independent of the size of the basis set used, as can be observed in Tables 5.1-5.2 below.

In Tables 5.1-5.2 we show the set of calculations of the singlet and triplet full geometry-optimization energy calculations for different theoretical methods and basis sets. These results were used to choose the most suitable level of theory and size of the basis set.

Table 5.1 Dichlorocarbene Single-Triplet Energy Splitting I.

Method	Triplet-Singlet ΔE
HF/6-31G(d)	-7.1
HF/6-31+G(d)	-6.1
HF/6-311+G(d)	-5.0
HF/cc-pVDZ	-4.1
HF/cc-pVTZ	-4.4
BLYP/6-311G(d)	21.2
BLYP/6-311+G(d)	21.9
B3LYP/6-311G(d)	17.0
BLYP/6-311+G(3df)	20.7
B3LYP/6-311+G(3df)	17.1
BLYP/cc-pVDZ	22.4
BLYP/cc-pVTZ	21.4
B3LYP/aug-cc-pVDZ	19.3
BP86/6-311+G(3df)	19.4
B3P86/6-311+G(3df)	15.5
BP86/cc-pVDZ	21.3
BP86/aug-cc-pVDZ	22.1
BP86/cc-pVTZ	20.1
Experiment	> 14

Table 5.2 Dichlorocarbene Single-Triplet Energy Splitting II.

Method	Triplet-Singlet ΔE
MP2/6-311+G(3df)	17.9
MP2/cc-pVDZ	16.2
MP2/aug-cc-pVDZ	18.6
MP2/cc-pVTZ	18.3
MP2/aug-cc-pVTZ	19.2
MP3/aug-cc-pVDZ	17.4
MP4/aug-cc-pVDZ	22.3
MP4D/aug-cc-pVDZ	19.0
MP4DQ/aug-cc-pVDZ	17.6
MP4SDQ/aug-cc-pVDZ	18.8
CCD/cc-pVDZ	16.2
CCD/aug-cc-pVDZ	18.0
CCSD/cc-pVDZ	16.3
CCSD/aug-cc-pVDZ	18.0
CID/cc-pVDZ	10.9
CID/cc-pVTZ	10.6
CISD/cc-pVDZ	11.0
CISD/cc-pVTZ	10.5
CISD/aug-cc-pVDZ	12.3
Experiment	> 14

CHAPTER 6

Concluding Remarks

The free energy profiles obtained for the five reactions can be connected to give an overall picture for the whole process. This is shown in figure 6.3. We also compare our results for the third reaction with those obtained with an alternative reaction mechanism by Pliego *et al* in 1999.[72] The novel mechanism that they proposed involved a proton transfer between two water molecules in a geometrical arrangement at the transition state which is shown in figure 6.2.

We may compare our results in solution to the inter-nuclear potential energy profile which we obtained in the gas-phase. This is shown in figure 6.4. This provides us with the ability to appreciate the magnitude of the solvent effect as a whole.

The net reaction is summarized in equation 6.1:

$$CHCl_3 + 3OH^- \rightarrow CO + 3Cl^- + 2H_2O \qquad (59)$$

The magnitude of the change in potential energy from reactants to products in the gas-phase is much larger than the difference in free energy from reactants to products in solution. This difference arises because of the free energy of solvation of the hydroxide ion (circa -100 kcal/mol), on the reactant side, is considerably larger than that of the

chloride ion (circa -75 kcal/mol) on the product side.

Based on our solution-phase results and those of Pliego et al for the two-water reaction mechanism for the hydrolysis of dichlorocarbene, we can conclude that the reaction scheme described in Table 6.1 is the most probable mechanism for the alkaline dehalogenation of chloroform in aqueous solution. Based on the values of the free energy of activation tabulated below, we conclude that either one of step I or step III, and not step II, is the rate-limiting step. The activation free energy of step III is around 23.5 kcal/mol via a direct insertion mechanism, but about 11.5 kcal/mol via a two water cyclical mechanism.[72]

Table 6.1 Chloroform aqueous alkaline dehalogenation reaction mechanism producing carbon monoxide. The free energy barrier to overcome at each reaction step is shown.

Step #	$\Delta G^{\ddagger}$ (kcal/mol)	
I	12	$CHCl_3 + OH^- \rightleftharpoons CCl_3^- + H_2O$
II	9	$CCl_3^- \rightleftharpoons CCl_2 + Cl^-$
III a)	22.0	$CCl_2 + H_2O \rightarrow CHCl_2OH$
		or
III b)	11.5	$CCl_2 + 2H_2O \rightarrow CHCl_2OH + H_2O$
IV	2	$CHCl_2OH + OH^- \rightarrow CHClO + Cl^- + H_2O$
V	2	$CHClO + OH^- \rightarrow CO + Cl^- + H_2O$

In Figure 4.6 it can be seen that the free energy barrier that has to be overcome by the system in the third reaction is fairly narrow, thus opening the possibility for tunneling to further reduce the effective height of the barrier. This tunneling effect could reduce the 11.5 kcal/mol value further, which was obtained by Pliego et al via the two water cyclical mechanism. This is not the case for the first step of the reaction, for which there was not a transition state in solution. The free energy in solution for this first reaction step increased gradually as a function of the reaction coordinate, thus not being open to any tunneling effects. Since the barrier height of step I has almost the same value as that of step III, but that of step III may be lower including tunneling effects, we may conclude that step I will most likely be the rate-limiting step in the mechanism proposed here.

Thus, assuming that the two-water cyclical mechanism put forth by Pliego et al is sound, the first step in the reaction scheme shown here will most likely be the rate-limiting step of the alkaline aqueous dehalogenation of chloroform.

Thus, future work will focus on more accurate estimates of the reaction free energy and height of the free energy barrier of the first step of the five reaction steps comprising the alkaline aqueous dehalogenation of chloroform mechanism presented here. Also it would be of interest to the authors of this manuscript to reproduce the values obtained by Pliego et al for the third reaction step via the same two-water cyclical reaction mechanism.

Figures

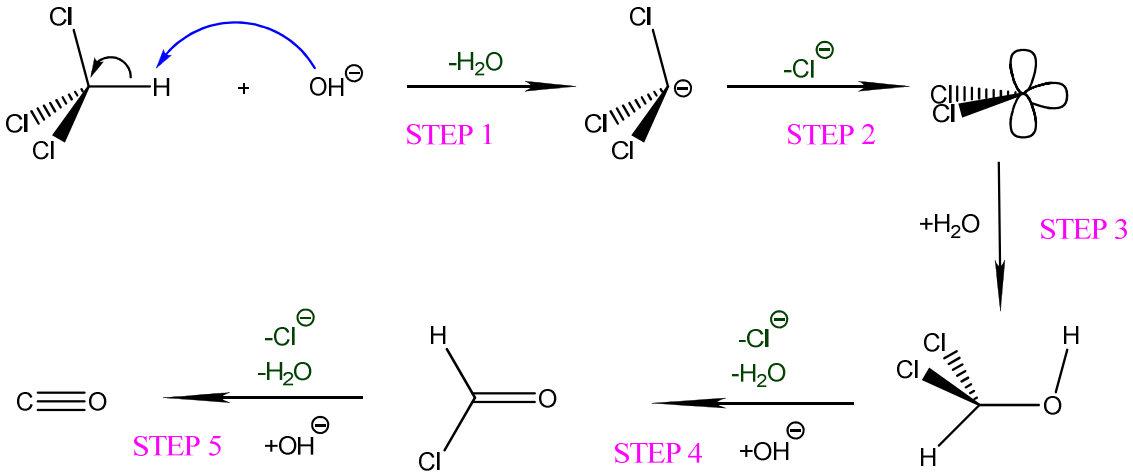

Figure 3.1 Chloroform alkaline dehalogenation reaction mechanism to produce carbon monoxide. Each step corresponds to one of the reactions studied in this project.

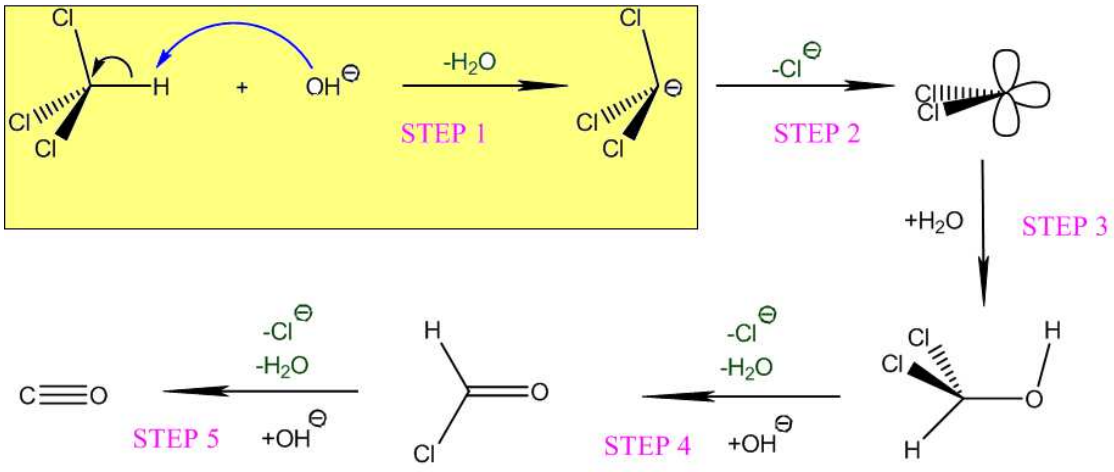

Figure 3.2 Reaction #1: $CHCl_3 + OH^- \rightleftharpoons CCl_3^- + H_2O$ Role of the first reaction in the overall reaction mechanism.

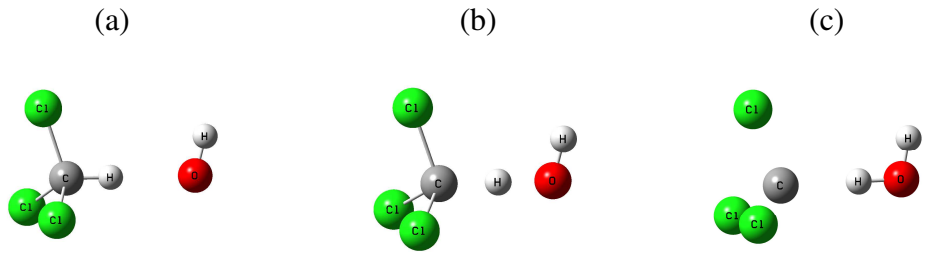

Figure 3.3 Reaction #1: $CHCl_3 + OH^- \rightleftharpoons CCl_3^- + H_2O$ Optimized geometries before (a), during (b), and after (c) the proton transfer from chloroform to the hydroxide ion. (c) corresponds to the product complex, which is the absolute potential energy minimum for the reaction. In (a), (b), and (c), the O-H distance along the forming bond is 2.09 Å, 1.25 Å, and 1.01 Å respectively. All three structures were optimized at the MP2/aug-cc-pVDZ level of theory.

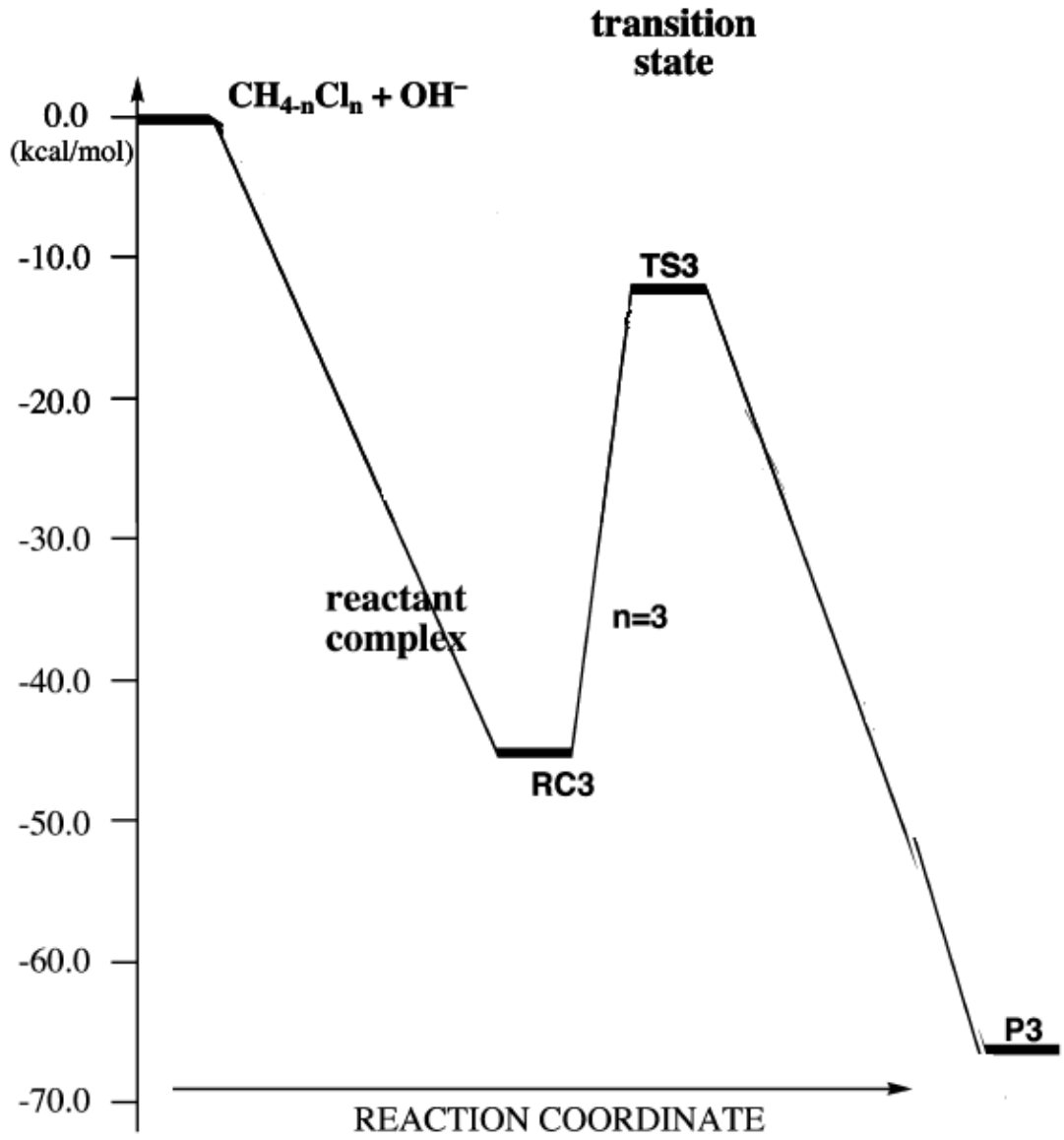

Figure 3.4 S_N2 Reaction. $CHCl_3 + OH^- \rightarrow CHCl_2OH + Cl^-$ Inter-nuclear potential energy of the reactants, reactant complex, transition state, and product states at the CCSD(T)/aug-cc-pVDZ//MP2/aug-cc-pVDZ **ΔEact = 32 kcal/mol.**[32]
CCSD(T)/CBS//MP2/aug-cc-pVDZ **ΔGact= 29 kcal/mol.**[2]

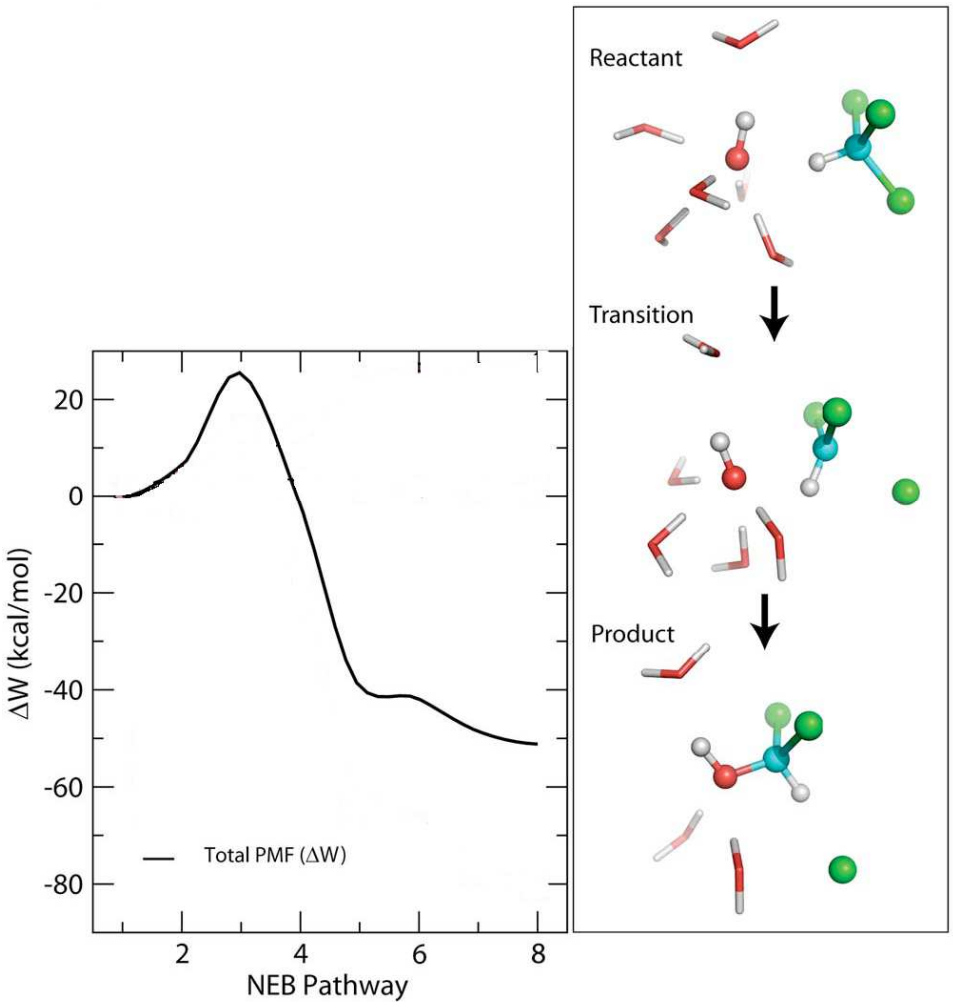

Figure 3.5 S_N2 Reaction. $CHCl_3 + OH^- \rightarrow CHCl_2OH + Cl^-$ QM/MM Free energy profile and reactant, transition, and product states in explicit aqueous solution obtained by M. Valiev et al. As can be seen in the picture on the left, the free energy of activation that they found for this first step is **ΔG‡ = 29.3 kcal/mol.**[33]

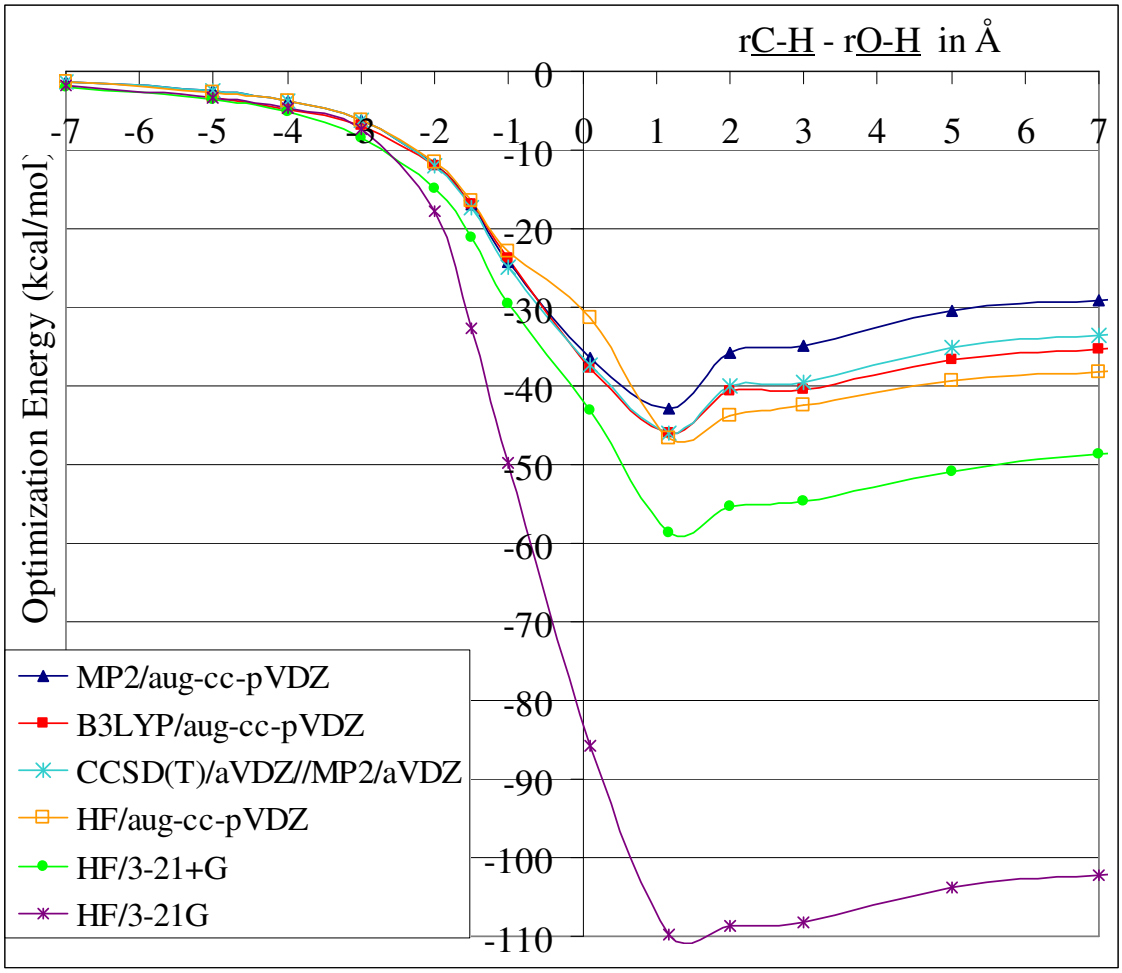

Figure 3.6 Reaction #1: $CHCl_3 + OH^- \rightleftharpoons CCl_3^- + H_2O$ Inter-nuclear Potential Energy Profile for the Proton Transfer from Chloroform to the Hydroxide Ion in the Gas-phase.

As the reaction coordinate proceeds from large negative to positive values, a proton is transferred from chloroform to the hydroxide ion to form water, which then gradually moves away from the remaining trichloromethyl ion. The reaction coordinate is obtained by taking the difference between the distances of the transferred proton to the chloroform carbon and the hydroxide oxygen, respectively: $r_{C\text{-}H} - r_{O\text{-}H}$ in Å.

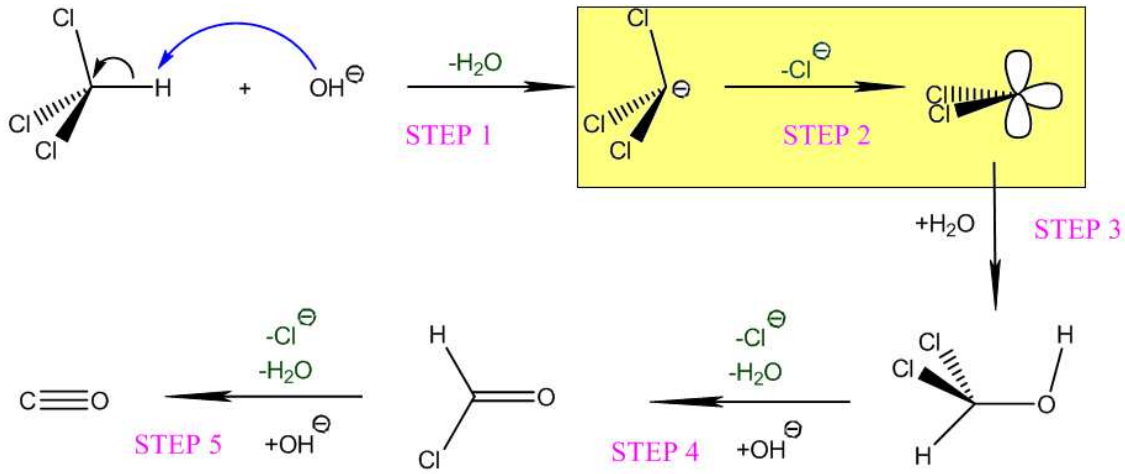

Figure 3.7 Reaction #2: $CCl_3^- \rightleftharpoons CCl_2 + Cl^-$ Role of the second reaction in the overall reaction mechanism.

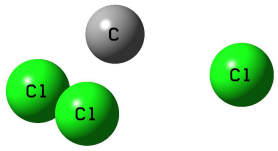

Figure 3.8 Trichloromethyl ion geometry optimized at the CCSD(T)/aug-cc-pVDZ level of theory.

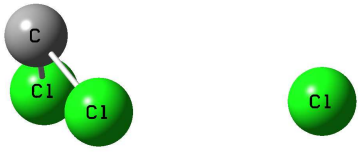

Figure 3.9 Reaction #2: CCl_3^- $\rightleftharpoons$ $CCl_2 + Cl^-$ Gas-phase intermediate geometry of the trichloromethyl ion molecular dissociation reaction in which the leaving Cl^- ion is 4.0 Å away from the dichlorocarbene carbon atom. This is structure was optimized at the MP2/aug-cc-pVDZ level of theory.

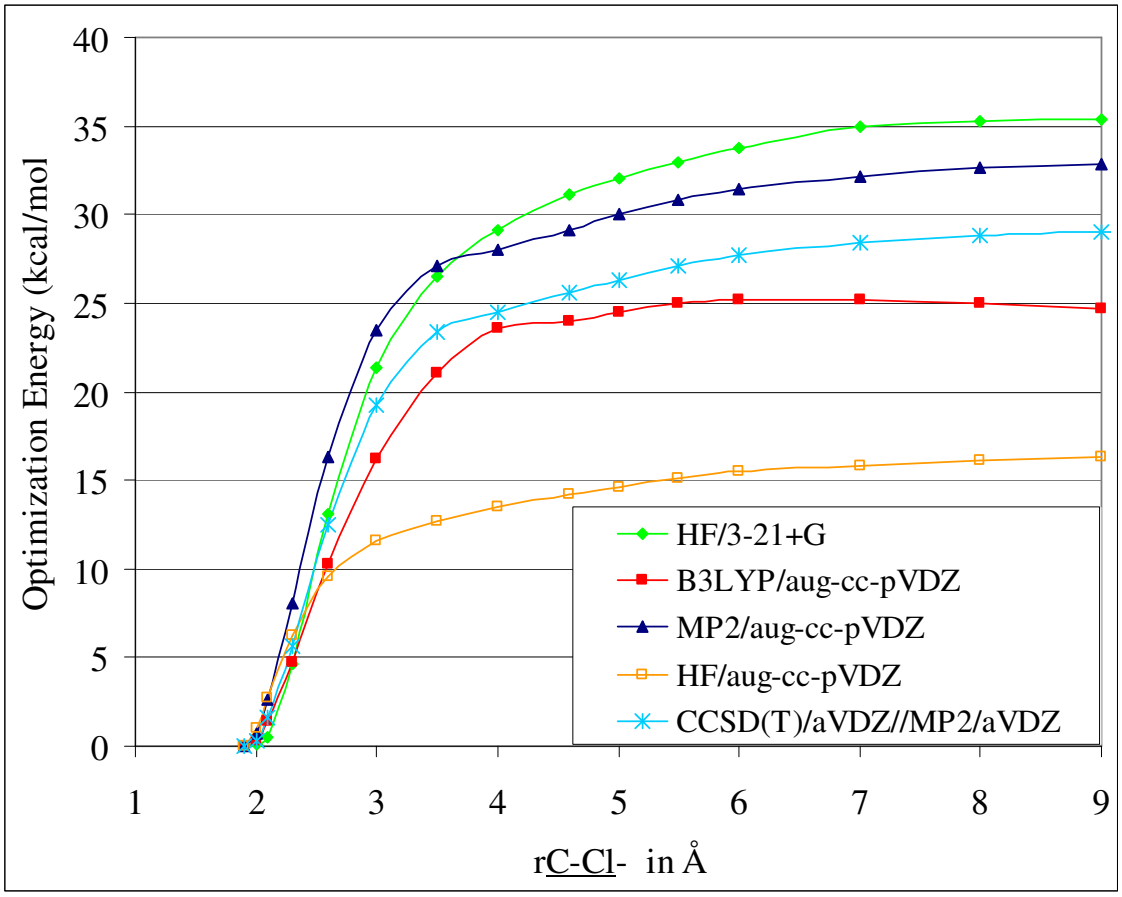

Figure 3.10 Reaction #2: CCl_3^- ⇄ $CCl_2 + Cl^-$ Trichloromethyl Ion loss of a Chloride Ion Gas phase inter-nuclear potential energy vs. carbon-chloride ion distance in Å.

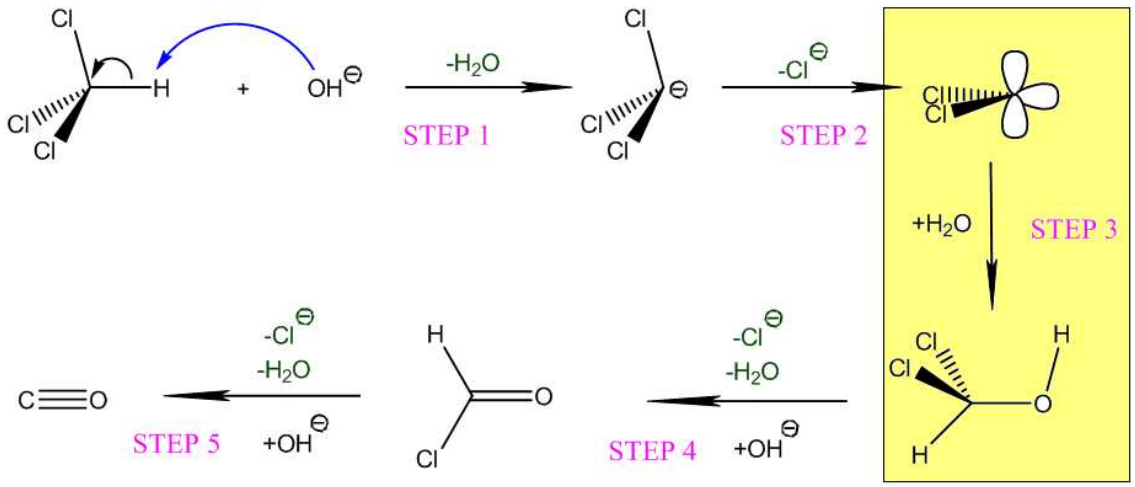

Figure 3.11 Reaction #3: $CCl_2 + H_2O \rightarrow CHCl_2OH$ Role of the thrird reaction in the overall reaction mechanism.

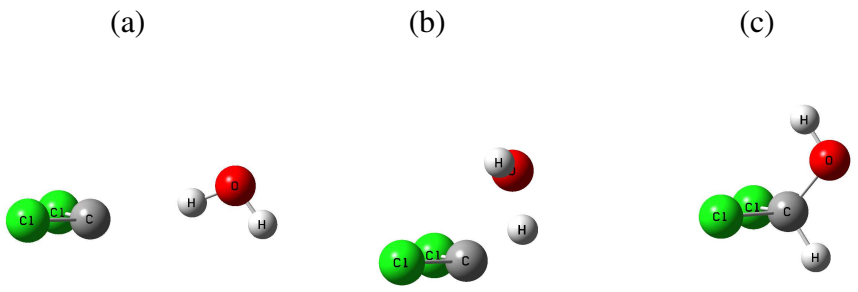

Figure 3.12 Reaction #3: $CCl_2 + H_2O \rightarrow CHCl_2OH$ Optimized geometries of the reactant complex (a), transition state (b), and product (c) of the carbene-water bond insertion reaction. All three structures were optimized at the MP2/aug-cc-pVDZ level of theory.

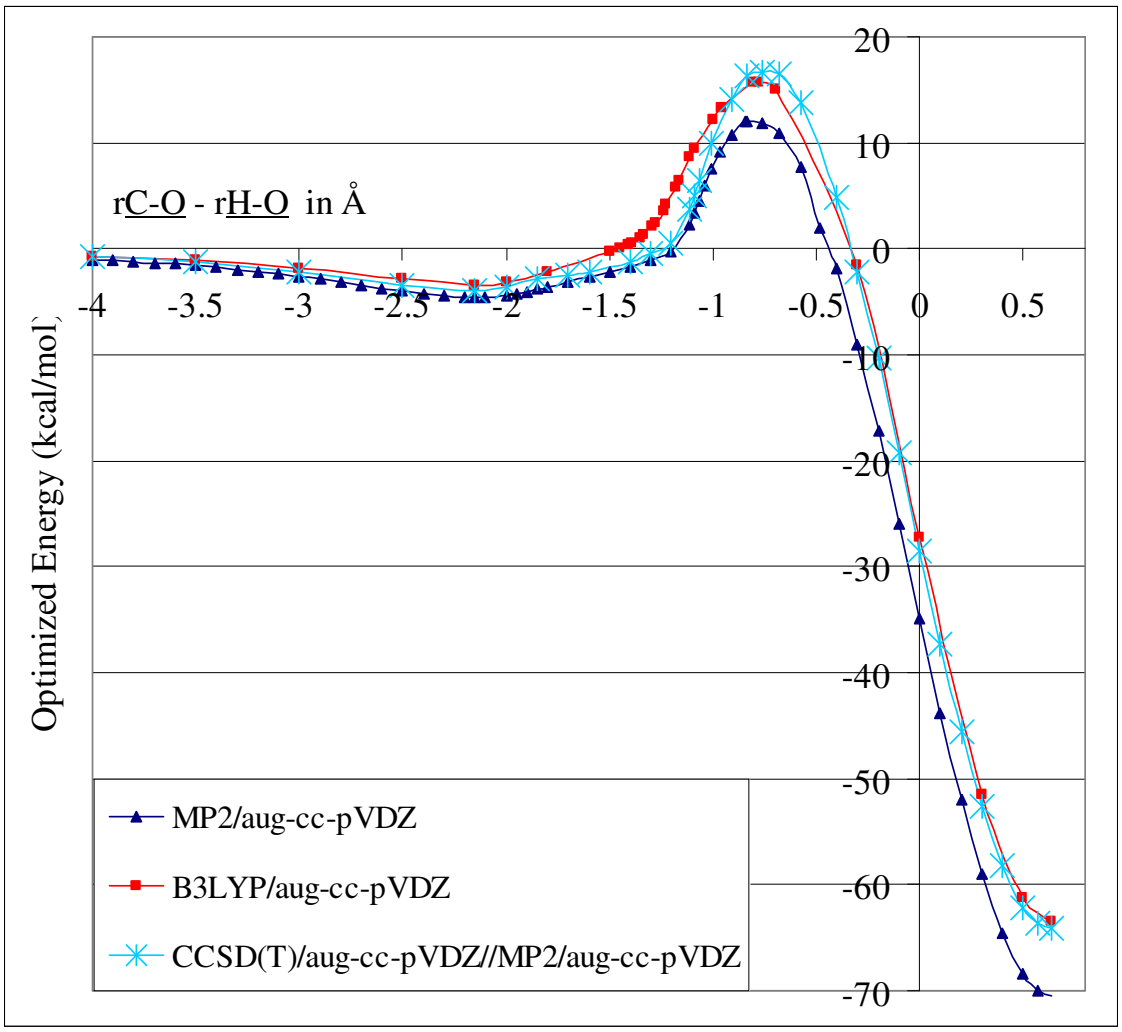

Figure 3.13 Reaction #3: $CCl_2 + H_2O \rightarrow CHCl_2OH$ Dichlorocarbene (Singlet) Water Absorption. Gas phase inter-nuclear potential energy vs. reaction coordinate (carbon-oxygen distance – hydrogen-oxygen distance), $r_{C\text{-}O} - r_{H\text{-}O}$ in Å.

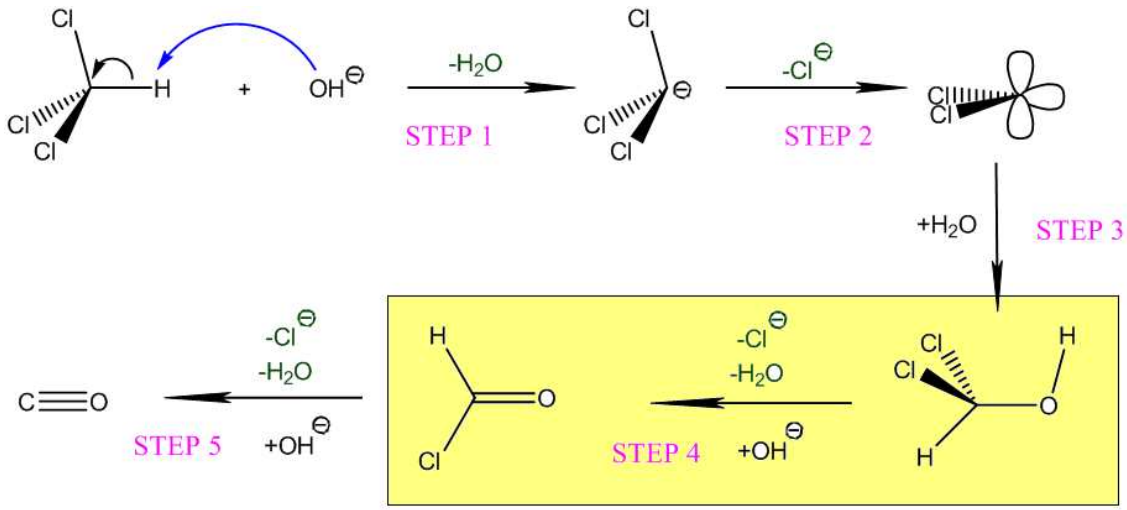

Figure 3.14 Reaction #4: $HCCl_2OH + OH^- \rightarrow HCOCl + Cl^- + H_2O$ Role of the fourth reaction in the overall reaction mechanism.

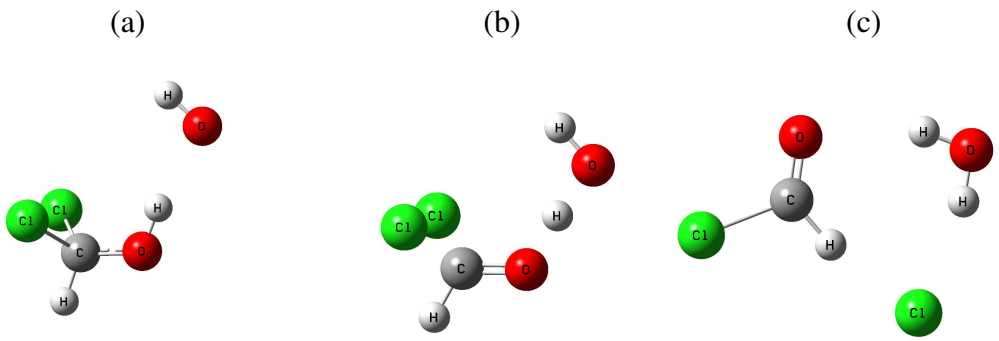

Figure 3.15 Reaction #4: $HCCl_2OH + OH^- \rightarrow HCOCl + Cl^- + H_2O$ Optimized geometries before (a), during (b), and after (c) the proton transfer from chloroform to the hydroxide ion. (c) corresponds to the product complex. All three structures were optimized at the MP2/aug-cc-pVDZ level of theory.

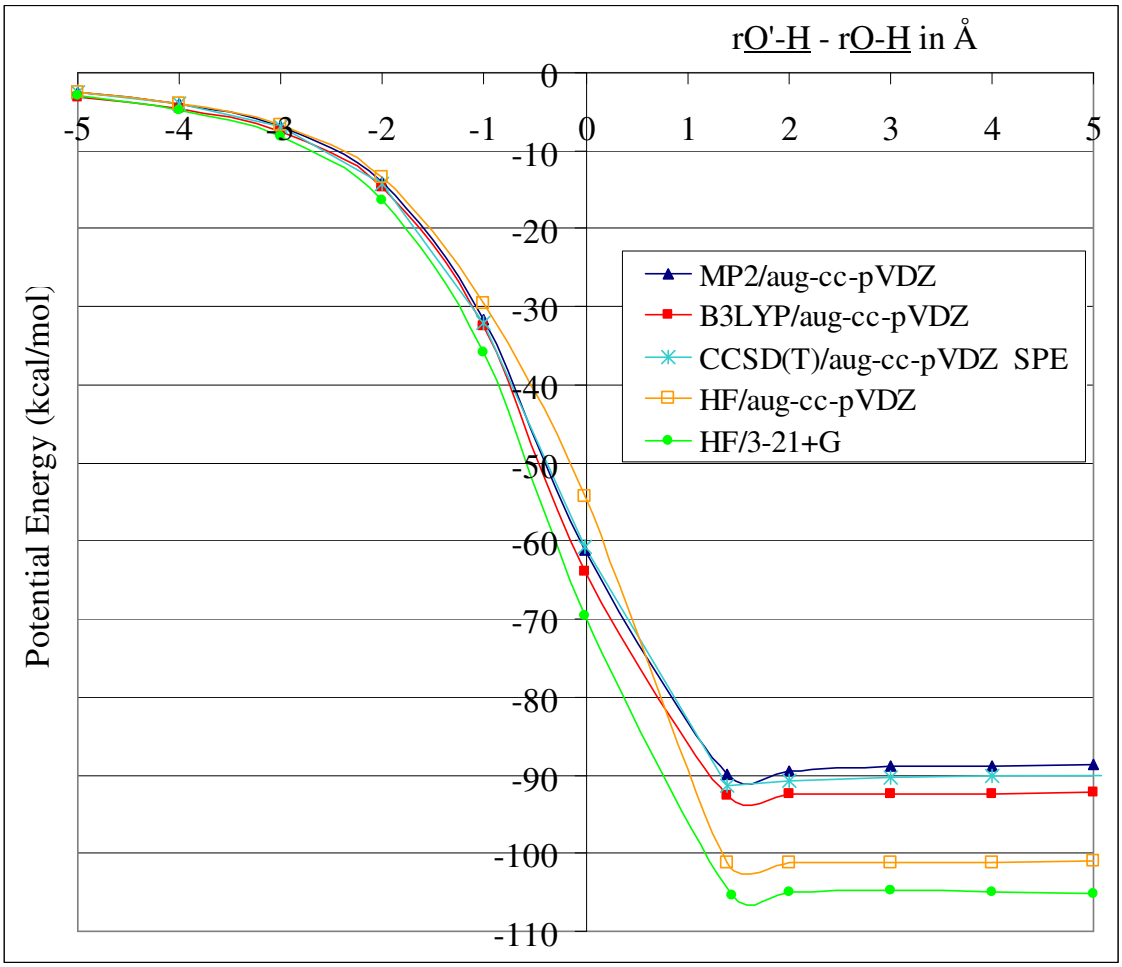

Figure 3.16 Reaction #4: $HCCl_2OH + OH^- \rightarrow HCOCl + Cl^- + H_2O$ Proton Transfer from Dichloromethanol to OH^-. Gas phase inter-nuclear potential energy vs. reaction coordinate. This is a proton transfer reaction for which the reaction coordinate is obtained by taking the difference between the distances of the transferred proton to the dichloromethanol oxygen (the proton donor) and the hydroxide oxygen (the proton acceptor), $r_{O'-H} - r_{O-H}$, respectively.

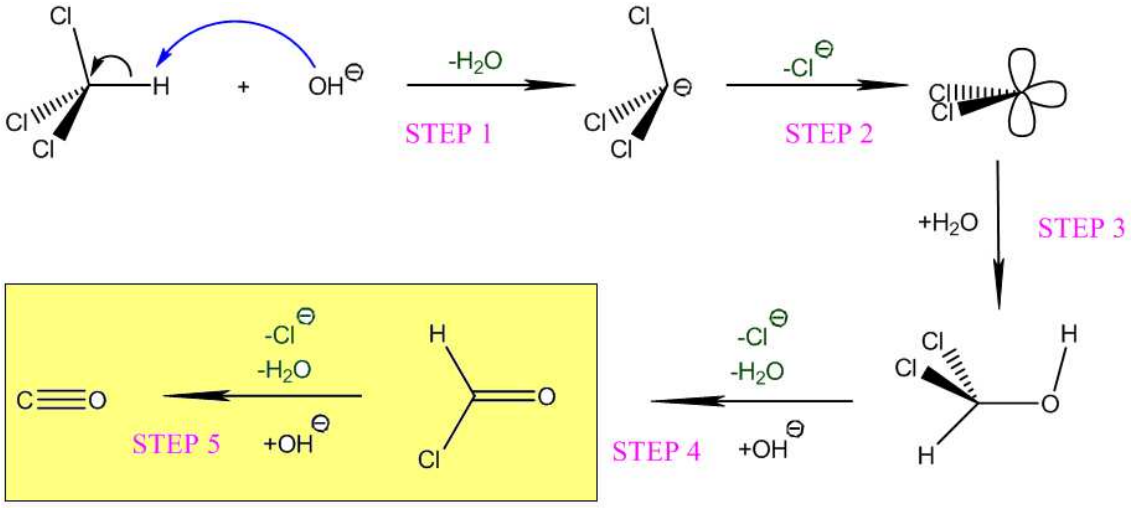

Figure 3.17 Reaction #5: $CHClO + OH^- \rightarrow CO + Cl^- + H_2O$ Role of the fifth reaction in the overall reaction mechanism.

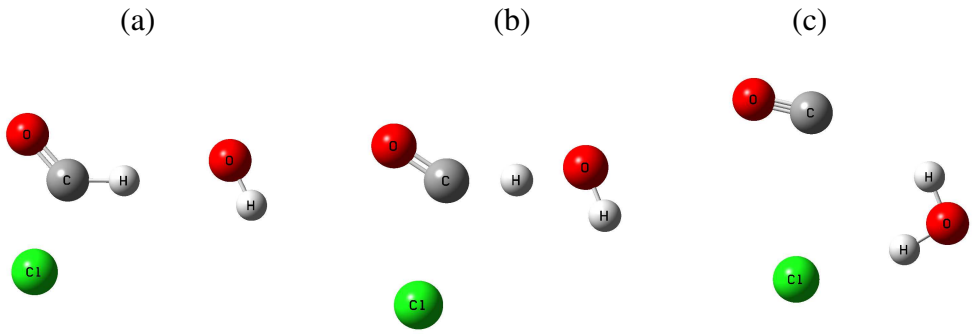

Figure 3.18 Reaction #5: $CHClO + OH^- \rightarrow CO + Cl^- + H_2O$ Optimized geometries before (a), during (b), and after (c) the proton transfer from chloroform to the hydroxide ion. (c) corresponds to the product complex. All three structures were optimized at the MP2/aug-cc-pVDZ level of theory.

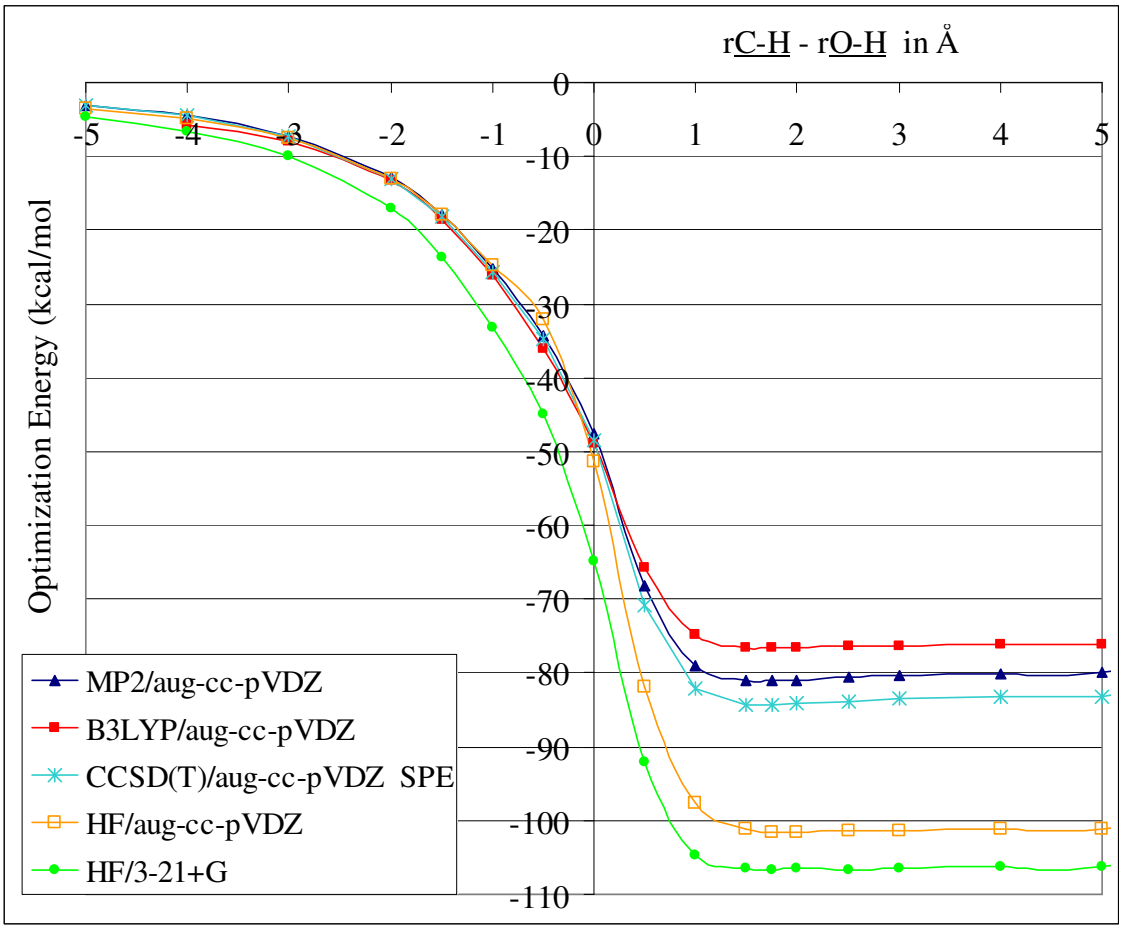

Figure 3.19 Reaction #5: $CHClO + OH^- \rightarrow CO + Cl^- + H_2O$ Proton Transfer from Formyl Chloride to OH^-. Gas phase inter-nuclear potential energy vs. reaction coordinate. In this proton transfer reaction the reaction coordinate is obtained by taking the difference between the distances of the transferred proton to the formyl carbon and the hydroxide oxygen, respectively.

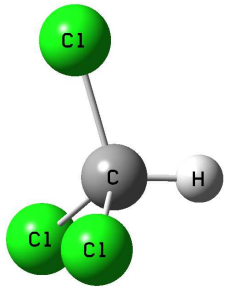

Figure 3.20 Geometry of chloroform optimized at the CCSD(T)/aug-cc-pVDZ level of theory.

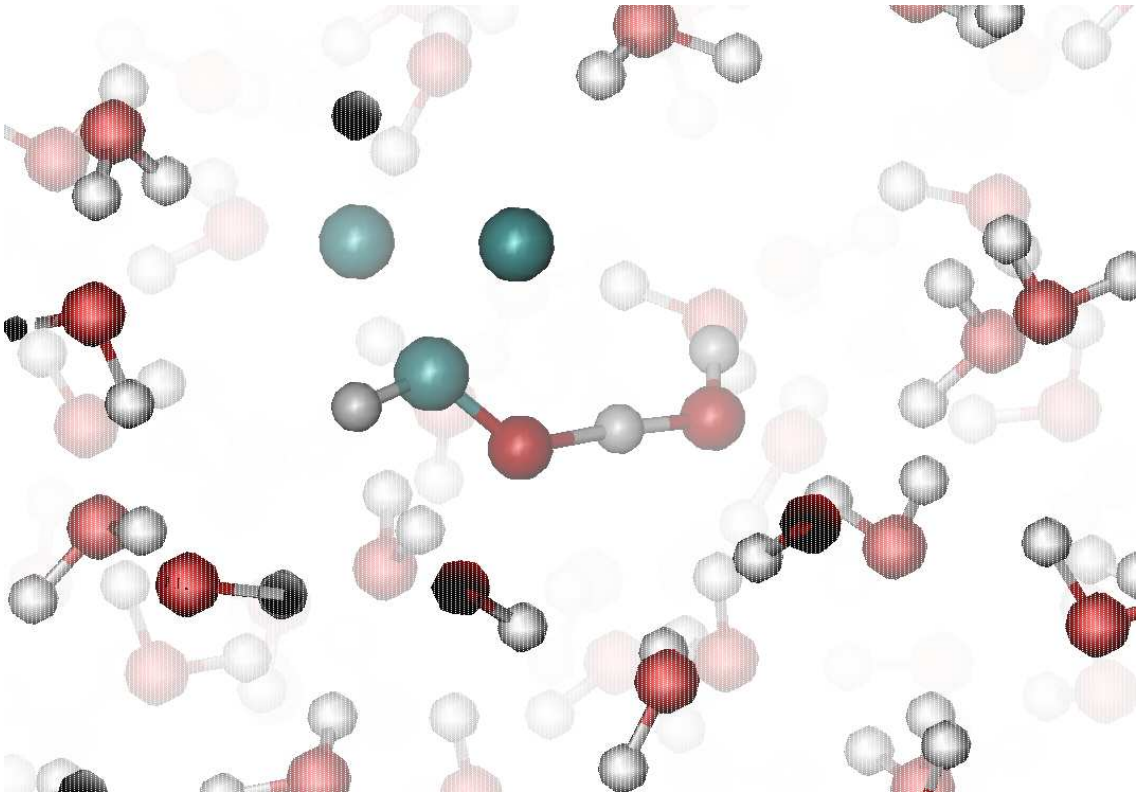

Figure 4.1 Reaction #4: $HCCl_2OH + OH^- \rightarrow HCOCl + Cl^- + H_2O$ Simulation snap shot.

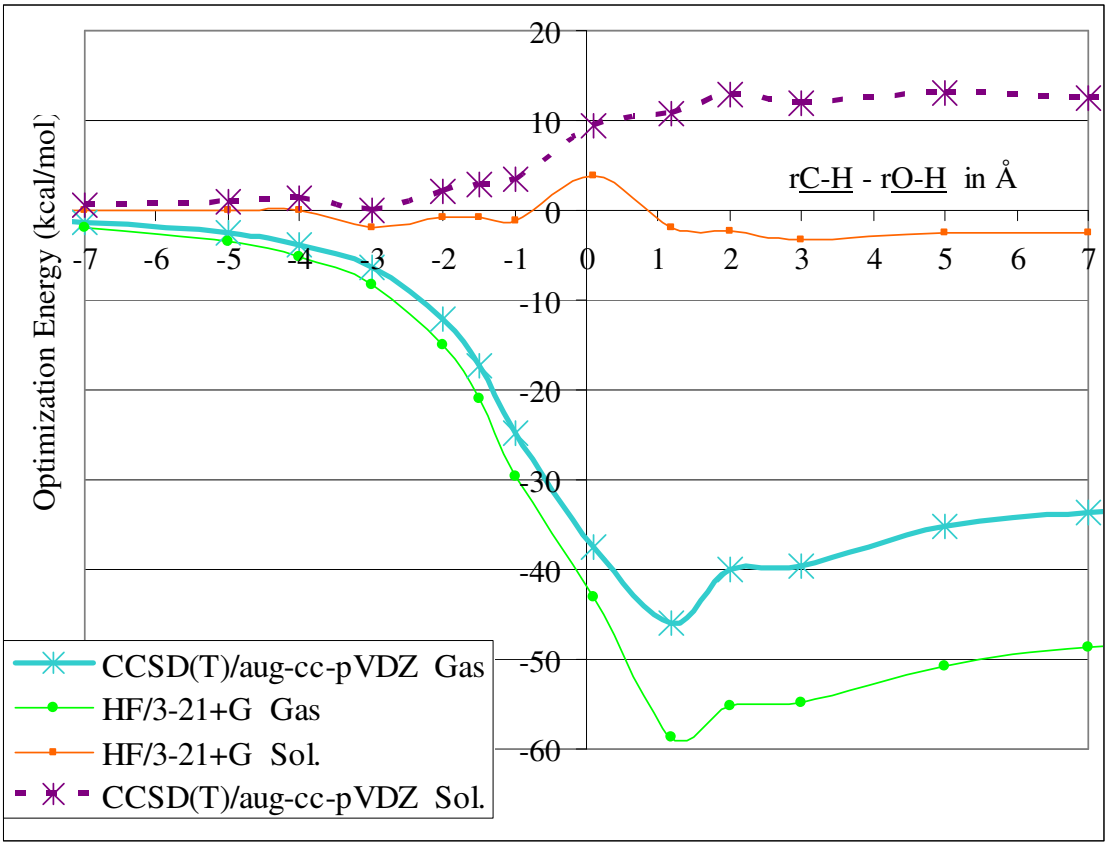

Figure 4.2 Reaction #1: $CHCl_3 + OH^- \rightleftharpoons CCl_3^- + H_2O$ Solution-phase free energy profile and gas-phase potential energy profile for the first reaction. As the reaction coordinate proceeds from large negative to positive values, a proton is transferred from chloroform to the hydroxide ion to form water and a trichloromethyl ion. The reaction coordinate is obtained by taking the difference between the distances of the transferred proton to the chloroform carbon and the hydroxide oxygen, respectively.

Reaction Free Energy (kcal/mol):

Theor.(explicit)	12
Theor.(implicit)*	5
Exper.(pKa)	-3 to 11
Exper.(Σ ΔGsol)	11 ± 4

pKa,CHCl3 = 13.6[84], 15[85], 24[86], 24.1[87]

(*) PCM (Pauling radii) CCSD(T)/aug-cc-pVDZ

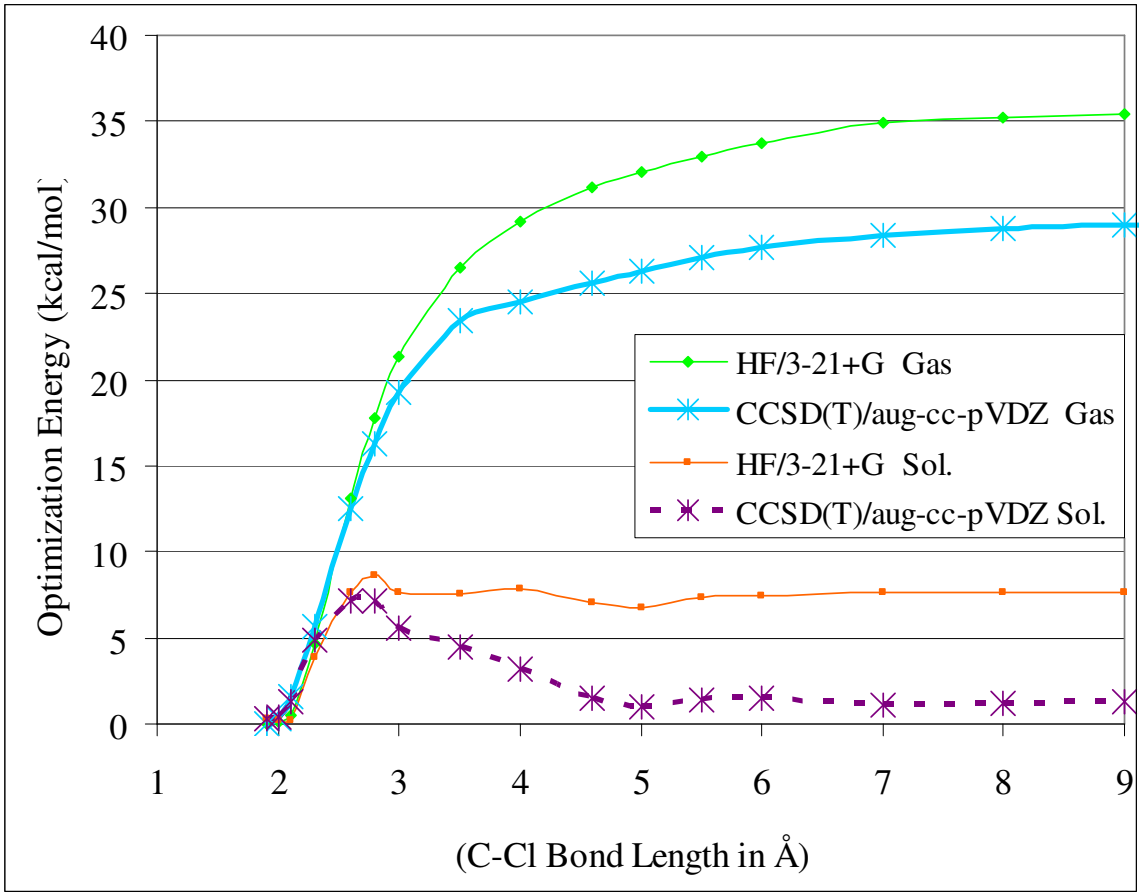

Figure 4.3 Reaction #2: $CCl_3^- \rightleftharpoons CCl_2 + Cl^-$ Solution-phase free energy profile and gas-phase potential energy profile for the second reaction.

Reaction Free Energy (kcal/mol):

Theor.(explicit)	2
Theor.(implicit)*	-1

(*) PCM (Pauling radii) CCSD(T)/aug-cc-pVDZ

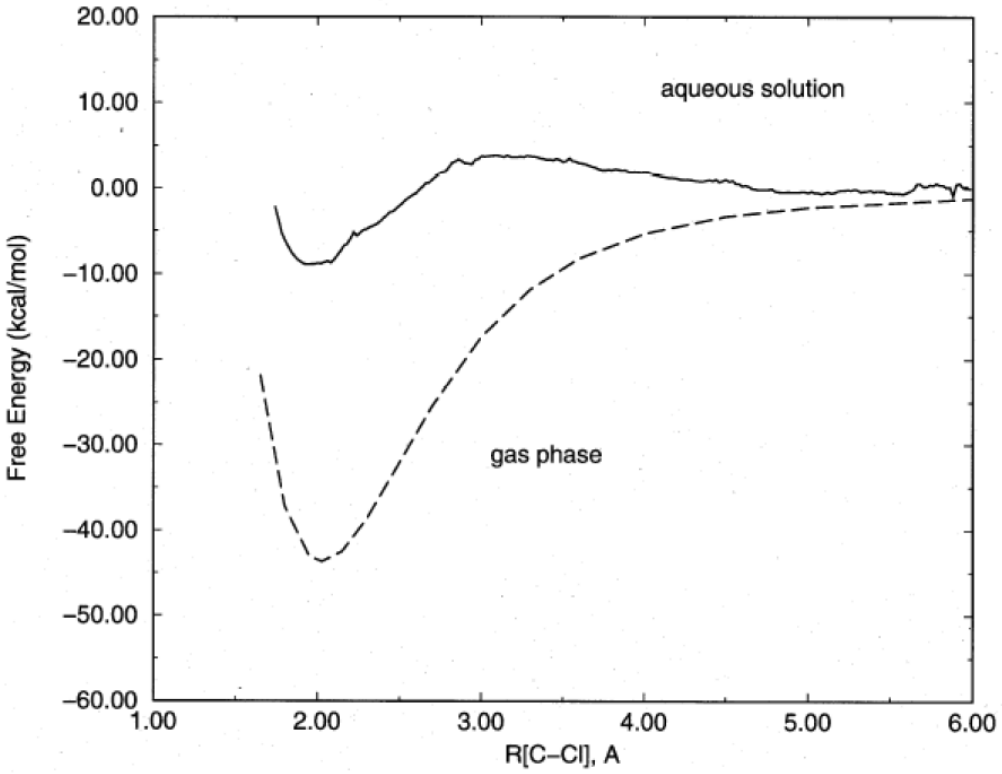

Figure 4.4 Reaction #2: $CCl_3^- \rightleftharpoons CCl_2 + Cl^-$ Reported solution-phase free energy profile and gas-phase potential energy profile for the second reaction.[1]

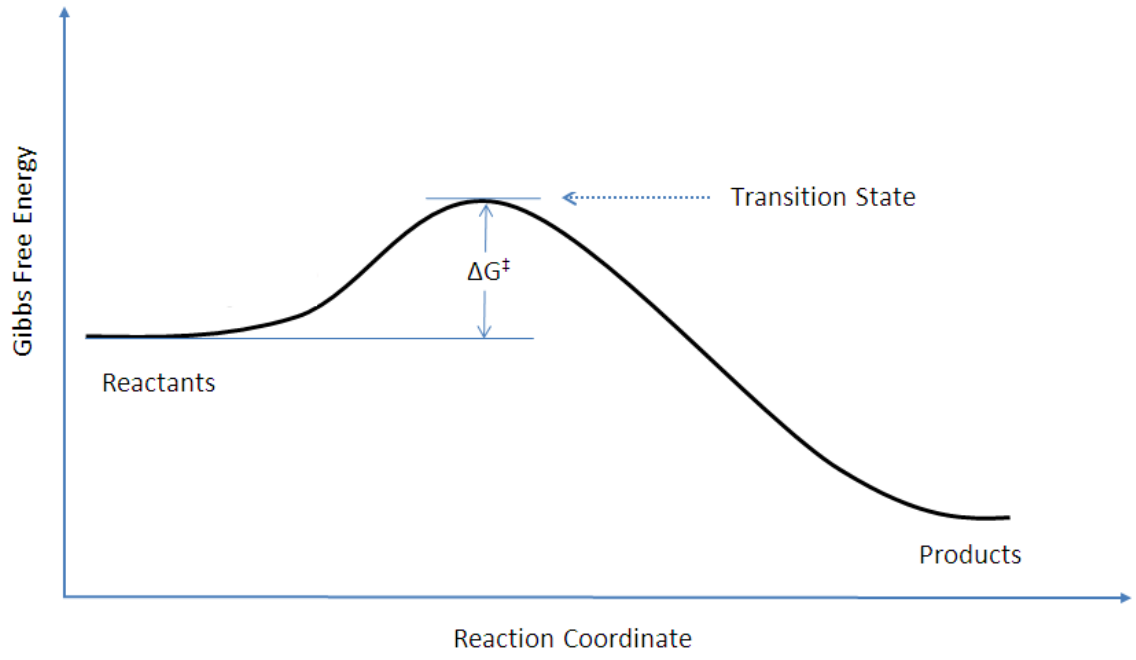

Figure 4.5 Transition State Theory: Sample plot of free energy vs reaction coordinate to aid in the explanation of transition state theory. The free energy difference between the reactant state and the transition state is called the free energy of activation for the reaction. For the remainder of this thesis, we use ΔG_{act} in place of $\Delta G^{\ddagger}$ for the Gibbs free energy of activation.

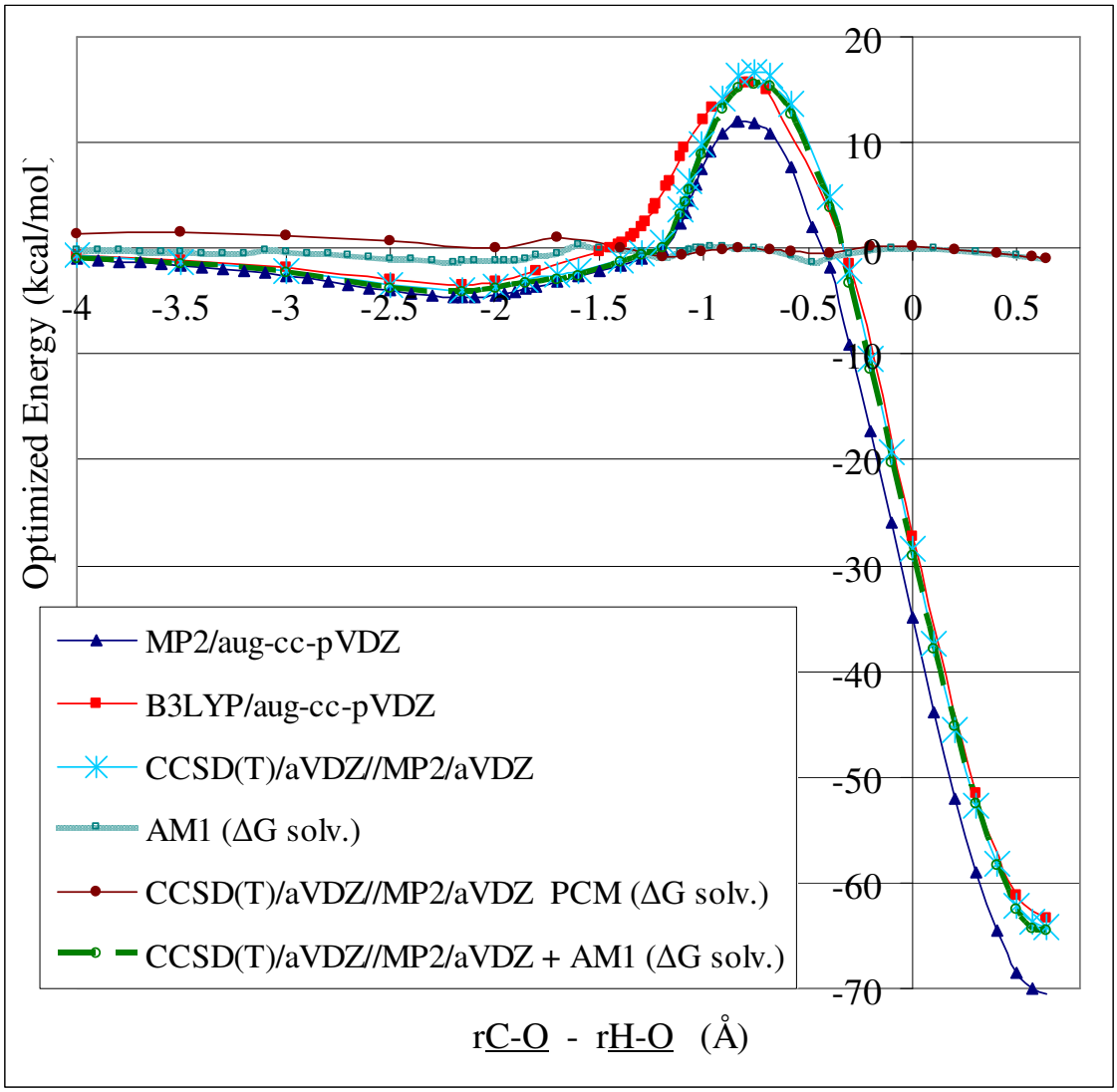

Figure 4.6 Reaction #3: $CCl_2 + H_2O \rightarrow CHCl_2OH$ Solution-phase free energy profile and gas-phase potential energy profile for the third reaction. The thick blue line represents the solvation free energy profile obtained via free energy perturbation of each gas-phase geometry to the geometries right and left of it along the reaction coordinate in the presence of the solvent. This free energy of solvation was added to the gas-phase inter-nuclear potential energy profile to obtain an estimate of free energy profile for the reaction in solution, which is shown in a dashed green line. Reaction Free Energy (kcal/mol): Theor.(explicit) -64

Theor.(implicit)* -60

(*) PCM (Pauling radii) CCSD(T)/aug-cc-pVDZ

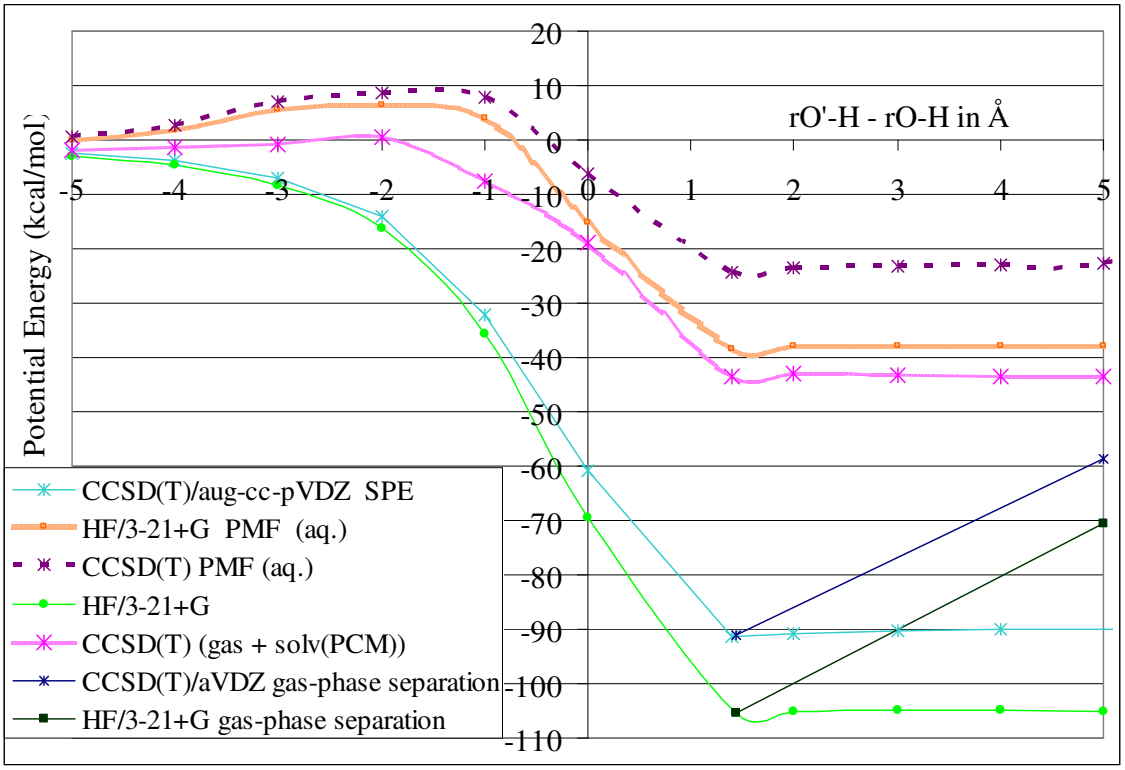

Figure 4.7 Reaction #4: $HCCl_2OH + OH^- \rightarrow HCOCl + Cl^- + H_2O$ Proton Transfer from Dichloromethanol to OH^-. Solution-phase free energy and gas-phase potential energy vs. reaction coordinate. This is a proton transfer reaction for which the reaction coordinate is obtained by taking the difference between the distances of the transferred proton to the dichloromethanol oxygen (the proton donor) and the hydroxide oxygen (the proton acceptor), $r_{O'-H} - r_{O-H}$, respectively.

The two slanted lines on the right show the gas-phase internuclear potential energy increase upon release of the chloride ion from its energy minimum location.

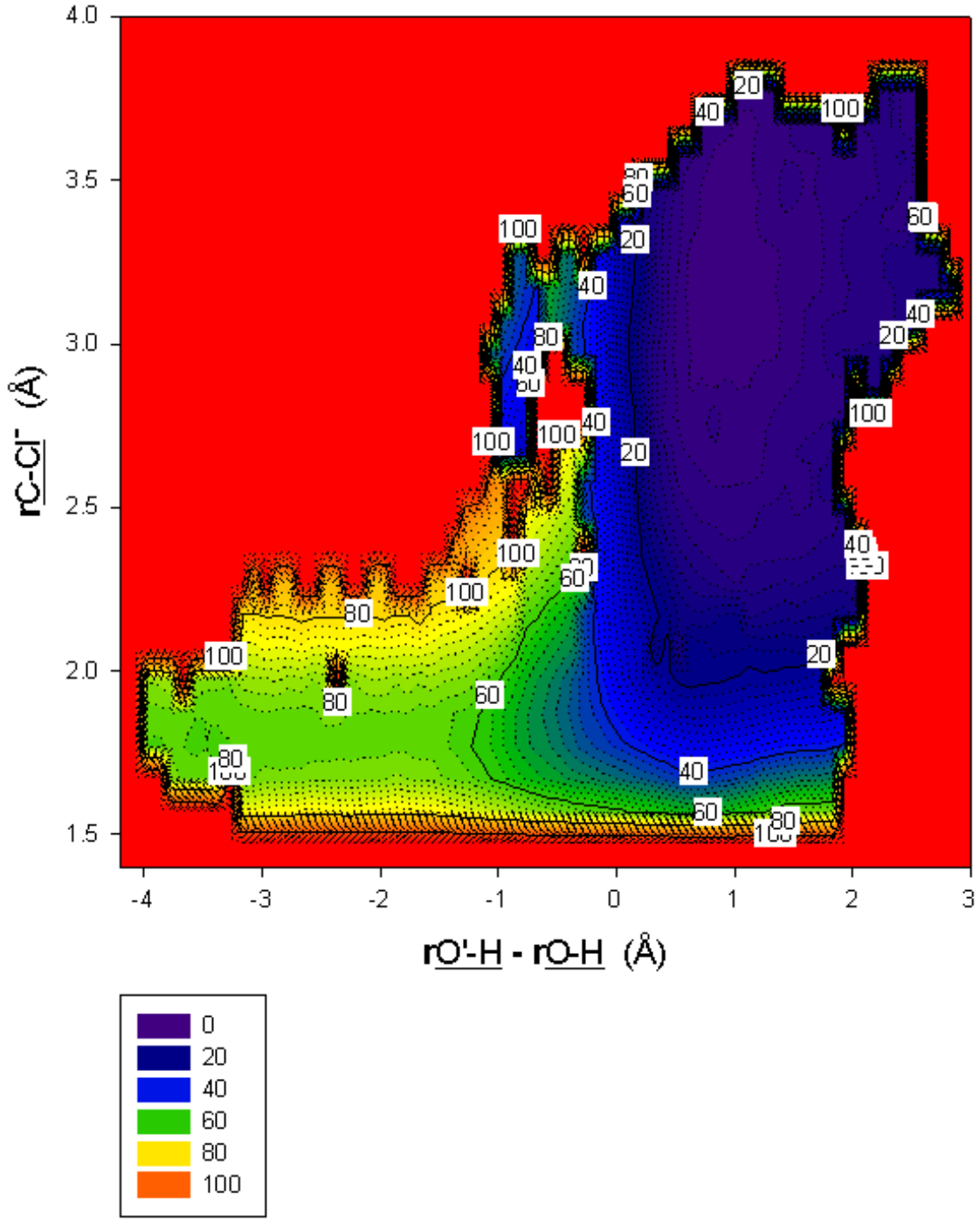

Figure 4.8 Reaction #4: $HCCl_2OH + OH^- \rightarrow HCOCl + Cl^- + H_2O$ Two-dimensional solution-phase free energy profile for the fourth reaction. The reaction proceeds from the bottom left corner to the top right of the region showed in the 2D free energy contour plot. Reaction Free Energy (kcal/mol): Theor.(explicit) = -62 + 14 = -48, Theor.(implicit)* = -44. (*) PCM (Pauling) CCSD(T)/aug-cc-pVDZ

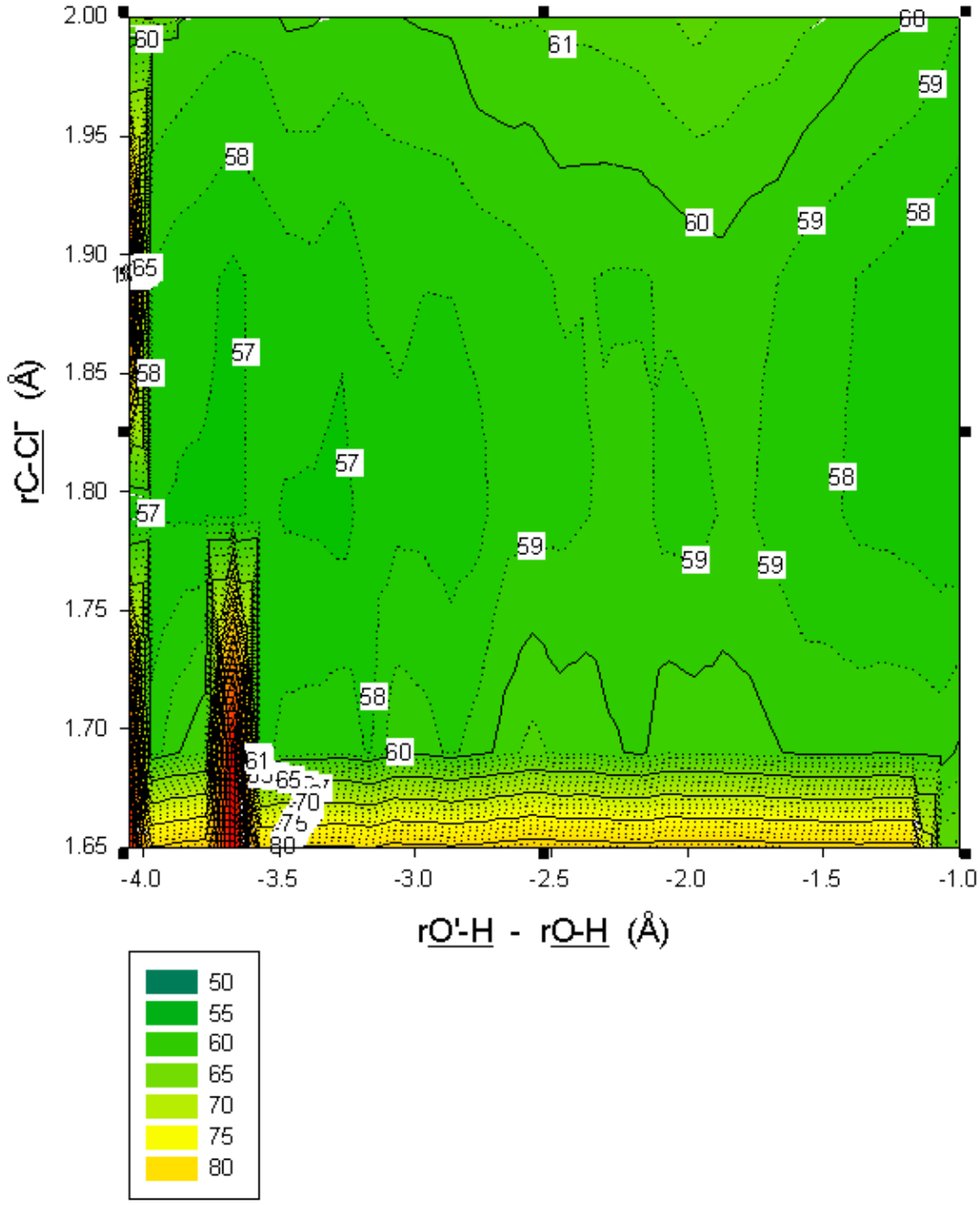

Figure 4.9 Reaction #4: $HCCl_2OH + OH^- \rightarrow HCOCl + Cl^- + H_2O$ A close-up view of the reactant channel region in the two-dimensional solution-phase free energy profile for the fourth reaction. A small barrier of 2 kcal/mol can be observed on the reactant side of the channel.

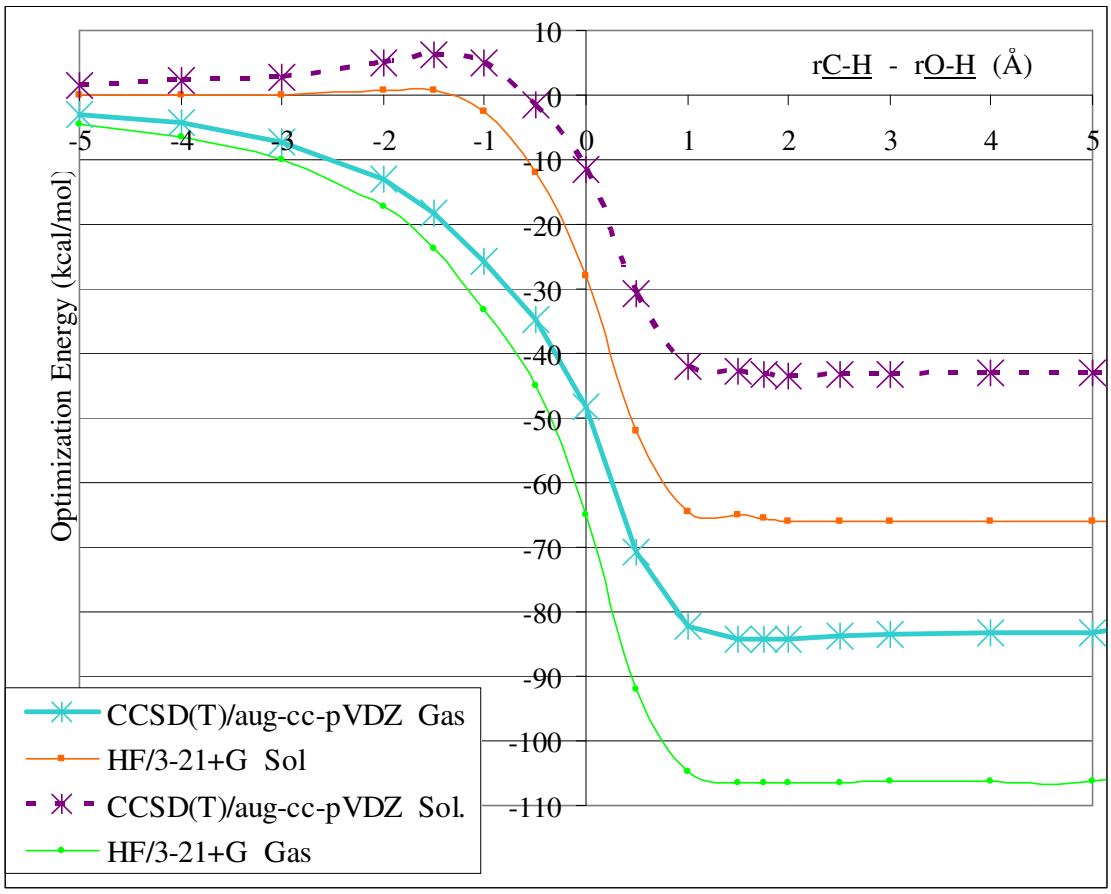

Figure 4.10 Reaction #5: $CHClO + OH^- \rightarrow CO + Cl^- + H_2O$ Proton Transfer from Formyl Chloride to OH^-. Solution-phase free energy and gas-phase potential energy vs. reaction coordinate. In this proton transfer reaction the reaction coordinate is obtained by taking the difference between the distances of the transferred proton to the formyl carbon and the hydroxide oxygen, respectively.

Reaction Free Energy (kcal/mol):

Theor.(explicit)	-43
Theor.(implicit)*	-43

(*) PCM (Pauling radii) CCSD(T)/aug-cc-pVDZ

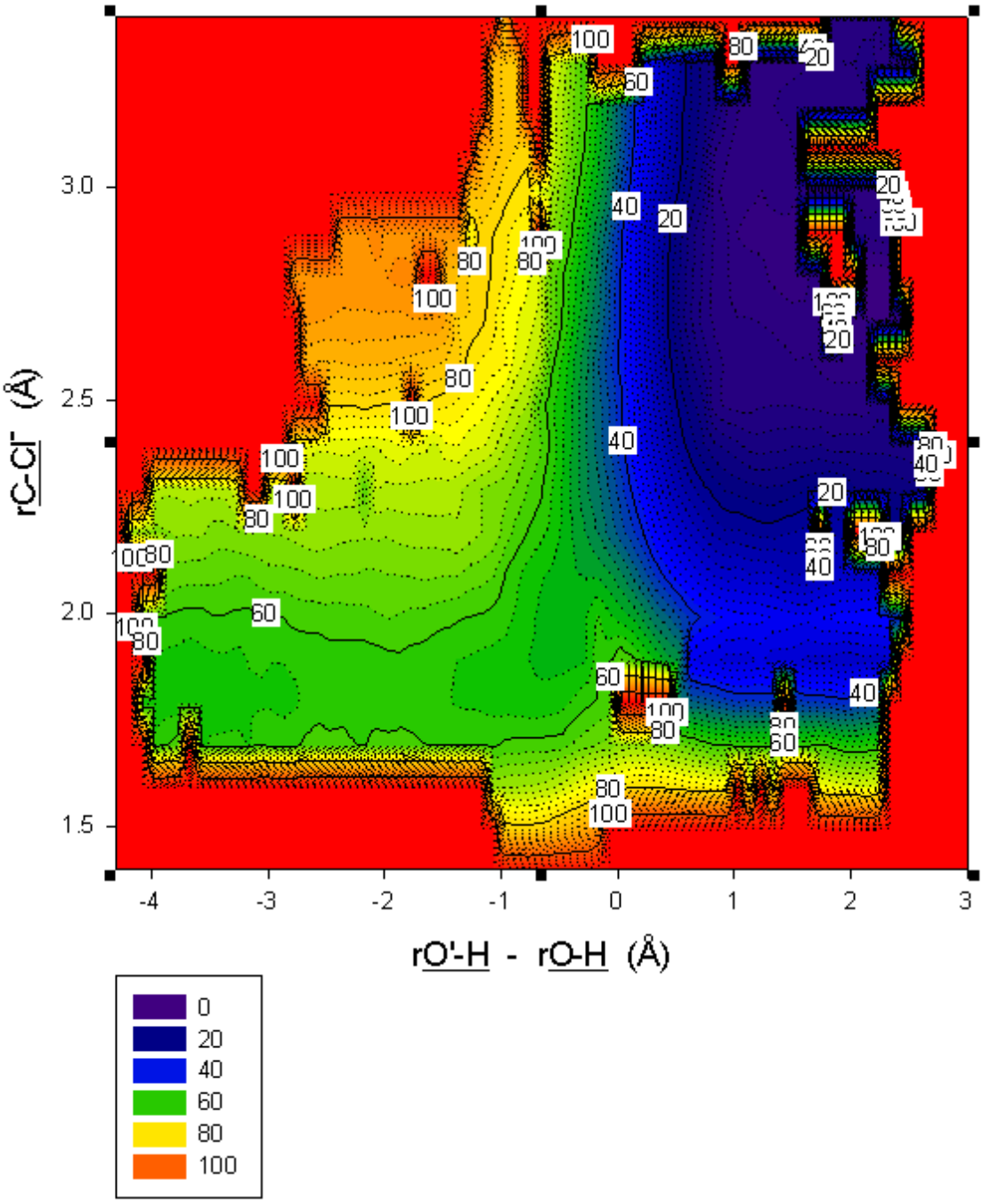

Figure 4.11 Reaction #5: $CHClO + OH^- \rightarrow CO + Cl^- + H_2O$ Two-dimensional solution-phase free energy profile for the fifth reaction. The reaction proceeds from bottom left to top right. Reaction Free Energy (kcal/mol): Theor.(explicit) -59 + 20 = -39

Theor.(implicit)* -43

(*) PCM (Pauling radii) CCSD(T)/aug-cc-pVDZ

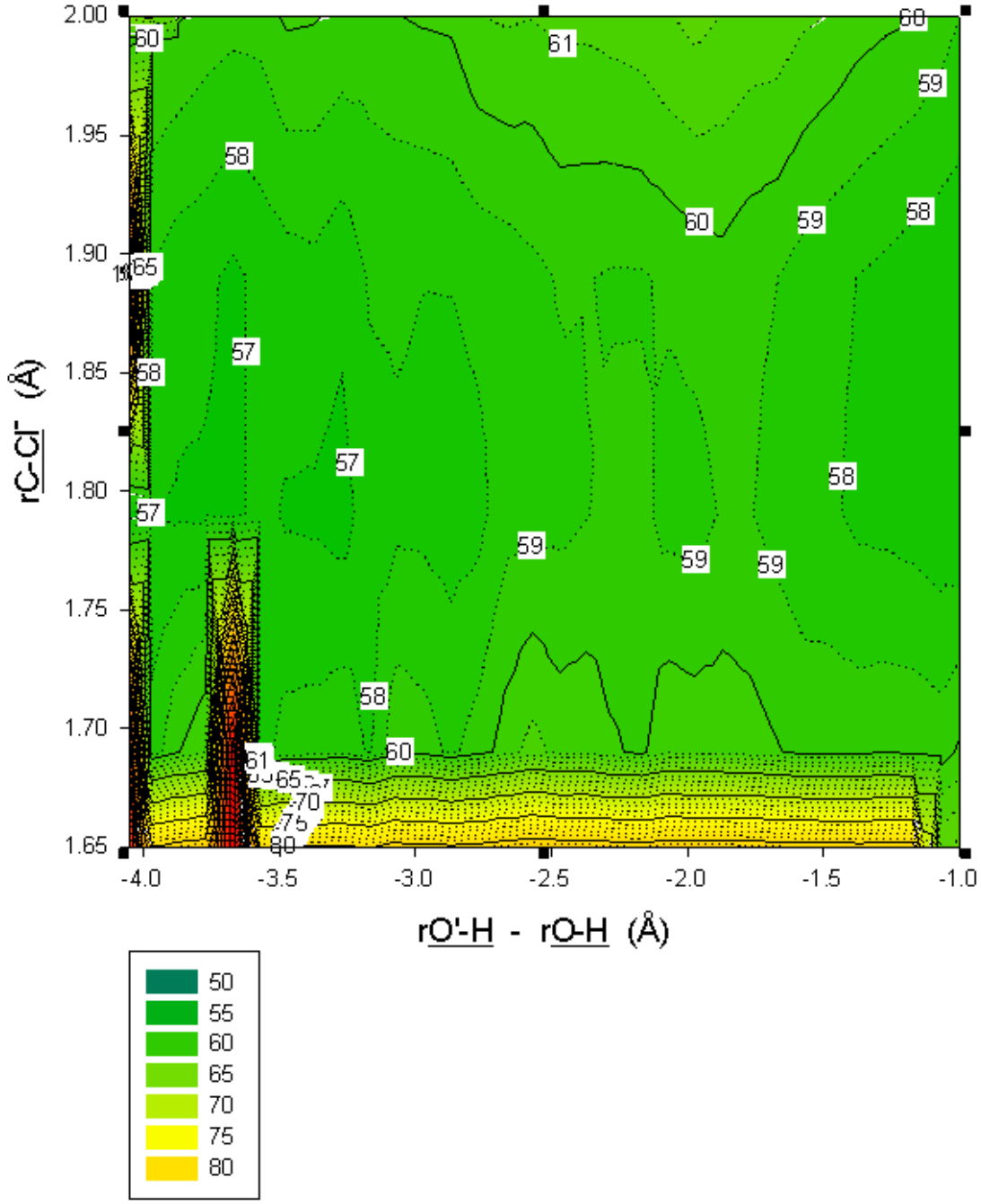

Figure 4.12 Reaction #5: $CHClO + OH^- \rightarrow CO + Cl^- + H_2O$ Small section of the two-dimensional solution-phase free energy profile for the fifth reaction. A 2 kcal/mol free energy of activation barrier to the reaction can be observed in the reactant channel.

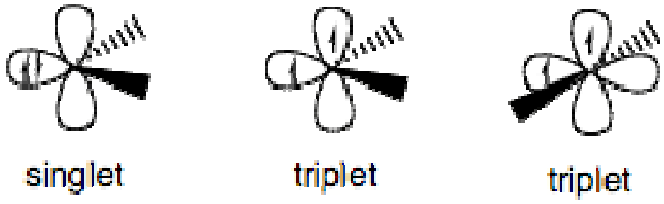

Figure 5.1 Source: Wikipedia: Carbene

Step #	ΔE_{act}
1	**30.4**
2	20.5
3	21.2
4	27.4
5	**16.3**
6	44.4
7	46.7
8	0
9	0

Calculations performed at the MP2/DZP//SCF/ DZP level.[1]

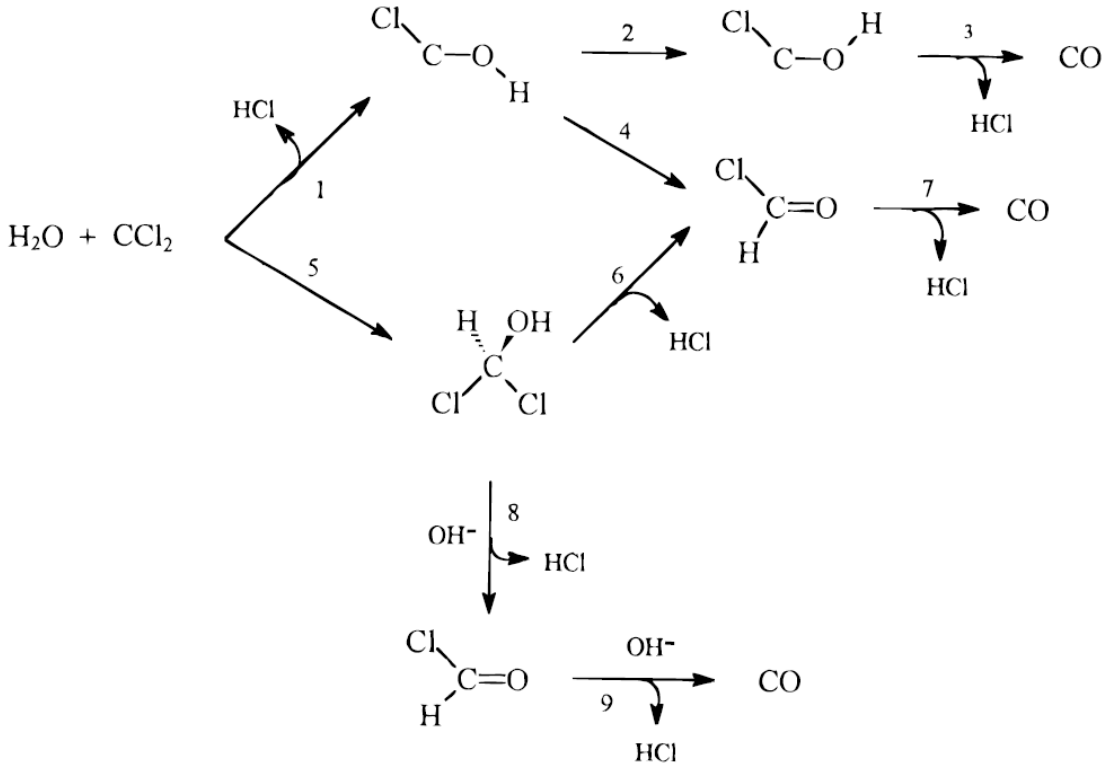

Figure 6.1 Alternative Mechanisms Following Reaction #3:

$CCl_2 + H_2O \rightarrow CHCl_2OH$

Two water carbene insertion mechanism proposed by Pliego *et al* in 1996.[25]

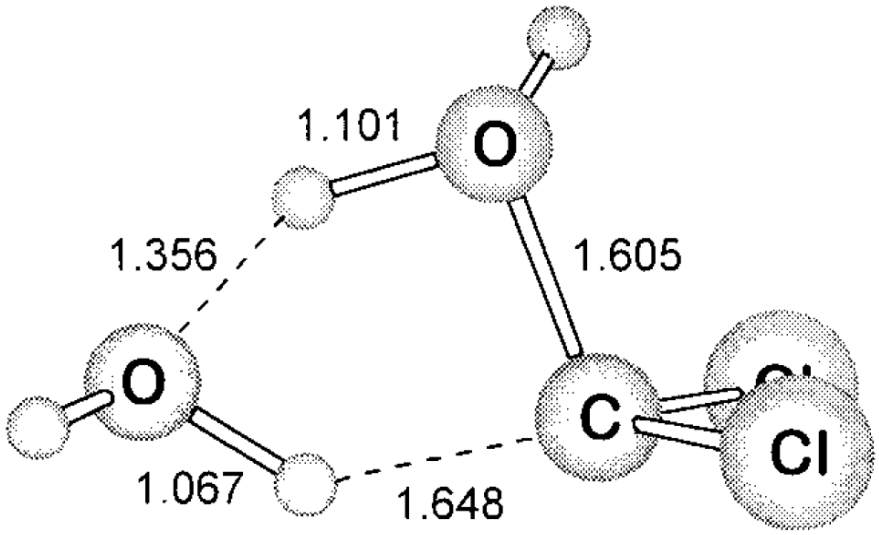

Figure 6.2 Alternative Mechanism for Reaction #3:

$CCl_2 + 2\,H_2O \rightarrow CHCl_2OH + H_2O$

Two water carbene insertion mechanism proposed by Pliego *et al* in 1998[31] and calculated in 1999.[72]

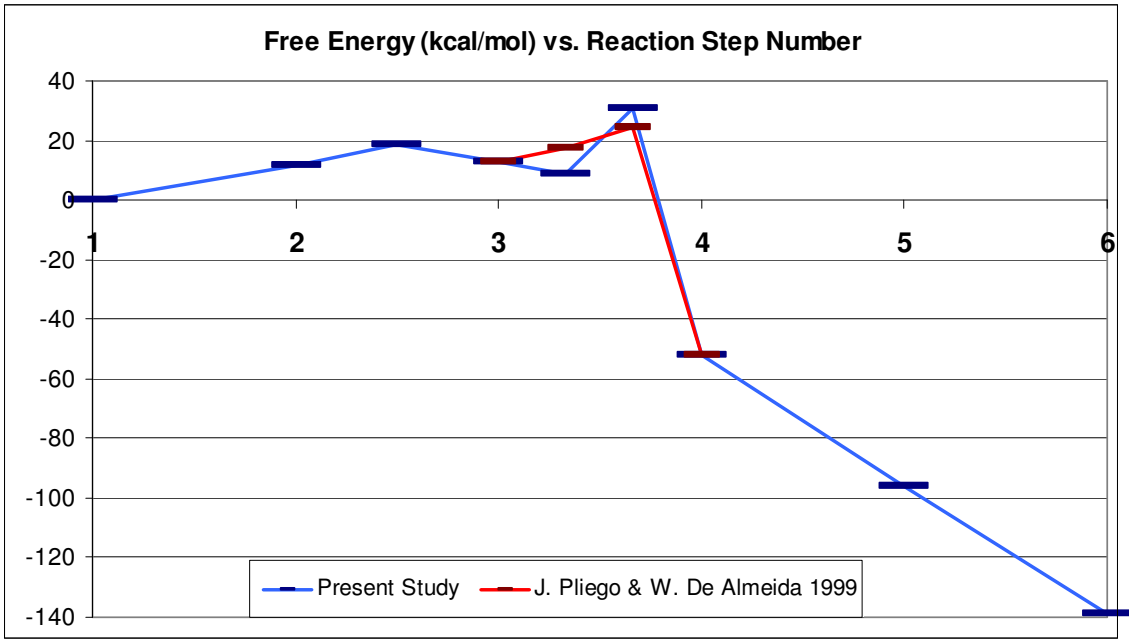

Figure 6.3 Free energy profile for the dehalogenation of chloroform in aqueous alkaline solution though to the production of carbon monoxide.

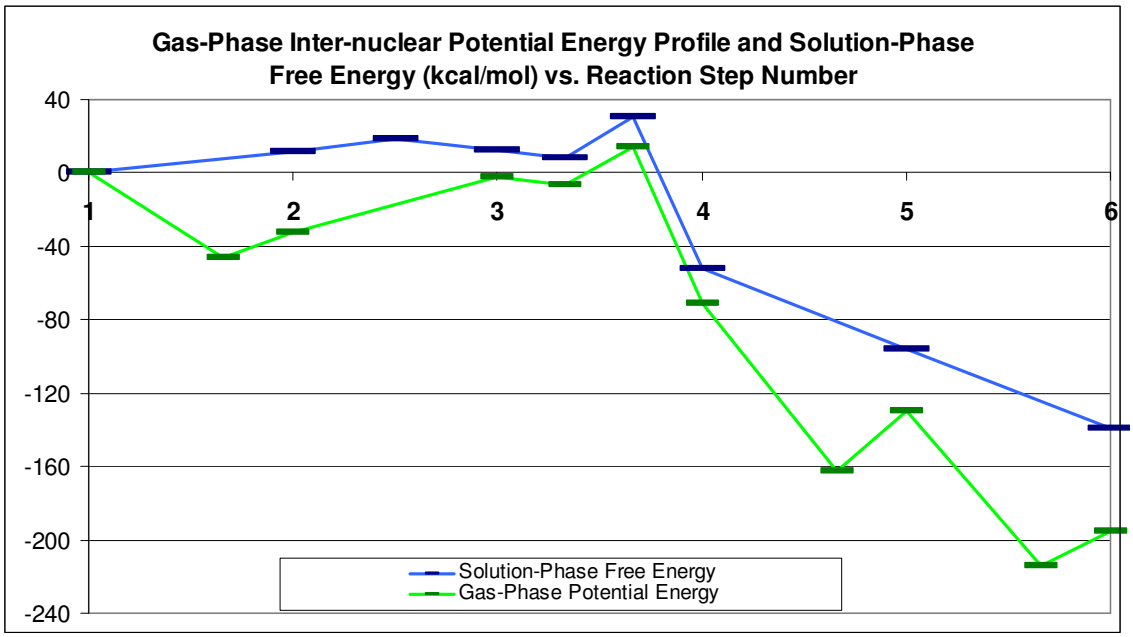

Figure 6.4 Gas-phase inter-nuclear potential energy and aqueous alkaline solution free energy profiles for the dehalogenation of chloroform in though to the production of carbon monoxide.

REFERENCES

1 E. Arcia, Y. Borisov, C. Cramer, T. Dunning, M. Dupuis, B. Garrett, J. Gao, K. Morokuma, T. P. Straatsma, J. Thompson, and D. Truhlar, *Chemical Fate of Contaminants in the Environment: Chlorinated Hydrocarbons in the Groundwater; Theory, Modeling and Simulation*, Published by the Pacific Northwest National Laboratory for the Environmental Molecular Sciences Laboratory 2002.

2 Y. Borisov, E. Arcia, S. Mielke, B. Garrett, and T. Dunning, J. Phys. Chem. A **105**, 7724 (2001).

3 L. Wade, *Organic Chemistry*, 4th ed. (Prentice-Hall, Inc., 1999).

4 P. Jeffers, L. Ward, L. Woytowitch, and N. Wolfe, Environ. Sci. Technol. **23**, 965 (1989).

5 M. Rossberg and e. al., in *Ullmann's Encyclopedia of Industrial Chemistry* (Wiley-VCH, Weinheim, 2006).

6 W. Mabey and T. Mill, J. Phys. Chem. Ref. Data **7 (2)**, 383 (1978).

7 S. Chou and W. Spoo, edited by A. F. T. S. A. D. Registry and U. S. D. o. H. a. H. Services (U.S. Government Printing Office, 1997).

8 H. Bir Singh, D. Fowler, and T. Peyton, Science **192**, 1231 (1976).

9 I. Fells and E. Moelwyn-Hughes, J. Chem. Soc. **72**, 398 (1959).

10 N. Sonoyama, K. Ezaki, and T. Sakata, Adv. Environ. Res. **6**, 1 (2001).

11 T. Ivahnenko and J. Barbash, edited by N. W.-Q. A. Program, U. S. G. Survey, and U. S. D. o. t. Interior (2004).

12 in *Eleventh Report on Carcinogens*, edited by N. T. Program.

13 E. Andrews and P. Novak, presented at the International In Situ and On-Site Bioremediation Symposium, 5th, San Diego, 1999 (unpublished).

14 R. Boopathy, Bioresource Technology **84**, 69 (2002); C. Guerrero-Barajas and J. Fied, Biodegradation **16**, 215 (2005).

15 K. Danielsen and K. Hayes, Environ. Sci. Technol. **38**, 4745 (2004); M. McCormick and P. Adriaens, Environ. Sci. Technol. **38**, 1045 (2004).

16 V. Molina, V. Montiel, M. Dominguez, and A. Aldaz, Electrochemistry Communications **5** (3), 246 (2003).

17 Q. Cooper, L. Stratmann, and J. Henry, in *The Material World* (BBC, London, 2005).

18 S. Belding.

19 L. Stratmann, *Chloroform The Quest For Oblivion*. (Sutton Publishing, UK, 2003).

20 Kotek, *Chloroform Human Health Fact Sheet*, Argonne National Laboratory (2005).

21 D. o. C. C. a. P. Carcinogenesis Program, edited by N. C. Institute (1976).

22 W. Choi and M. Hoffmann, Environ. Sci. Technol. **31**, 89 (1997).

[23] S. Kumaran, M. Su, K. Lim, J. Michael, S. Klippenstein, J. DiFelice, P. Mudipalli, J. Kiefer, D. Dixon, and K. Peterson, J. Phys. Chem. A **101**, 8653 (1997).
[24] J. Hine, J. Am. Chem. Soc. **72**, 2438 (1950).
[25] J. Pliego and W. De Almeida, J. Phys. Chem. **100**, 12410 (1996).
[26] J. Hine and A. Dowell, J. Am. Chem. Soc. **76**, 2688 (1954).
[27] J. Hine, A. Dowell, and J. Singley, J. Am. Chem. Soc. **78**, 479 (1956).
[28] J. Hine and P. Langford, J. Am. Chem. Soc. **80**, 6010 (1958).
[29] J. Horiuti, K. Tanabe, and K. Tanaka, J. Research Inst. Catalysis, Hokkaido University **3** (119), 147 (1955).
[30] J. Hine and S. Ehrenson, J. Am. Chem. Soc. **80**, 824 (1958).
[31] J. Pliego, M. Franca, and W. De Almeida, Chem. Phys. Lett. **285**, 121 (1998).
[32] S. Re and K. Morokuma, Theor. Chem. Acc. **112**, 59 (2004).
[33] M. Valiev, B. Garrett, M. Tsai, K. Kowalski, S. Kathmann, G. Schenter, and M. Dupuis, J. Chem. Phys. **127**, 051102 (2007).
[34] W. von E. Doering and K. Hoffmann, J. Am. Chem. Soc. **76** (23), 6162 (1954).
[35] J. Pliego and W. De Almeida, J. Chem. Soc., Faraday Trans. **93** (10), 1881 (1997).
[36] P. Hohenberg and W. Kohn, Phys. Rev. **136** (3B), B864 (1964); W. Kohn and L. Sham, Phys. Rev. **140** (4A), A1133 (1965).
[37] E. Schrödinger, Annalen der Physik **80** (4), 437 (1926); J. Rayleigh, *Theory of Sound*, 2 ed. (Macmillan, London, 1894).
[38] C. Møller and M. Plesset, Phys. Rev. **46**, 618 (1934).
[39] D. Hartree, Proc. Cambr. Phil. Soc. **24** (89), 111 (1928); V. Fock, Zs. Phys. **61**, 126 (1930); D. Hartree, Rep. Prog. Phys. **11**, 113 (1947).
[40] K. Kim and K. Jordan, J. Phys. Chem. **98** (40), 10089 (1994); P. Stephens, F. Devlin, C. Chabalowski, and M. Frisch, J. Phys. Chem. **98**, 11623 (1994); A. Becke, Phys. Rev. A. **38**, 3098 (1988); C. Lee, W. Yang, and R. Parr, Phys. Rev. B. **37**, 785 (1988).
[41] A. Becke, J. Chem. Phys. **98**, 1372 (1993).
[42] T. Dunning, J. Chem. Phys. **90**, 1007 (1989); R. Kendall, T. Dunning, and R. Harrison, J. Chem. Phys. **96**, 6796 (1992).
[43] R. Zwanzig, J. Chem. Phys. **22** (8), 1420 (1954); D. Beveridge and F. DiCapua, Annu. Rev. Biophys. Chem. **18**, 431 (1989); D. Beveridge and F. DiCapua, *Free energy via molecular simulation: A primer*. (Escom, Leiden, the Netherlands, 1989).
[44] A. Ben-Naim, *Solvation Thermodynamics*. (Plenum Press, New York, 1987).
[45] T. P. Straatsma, H. J. Berendsen, and J. P. Postma, J. Chem. Phys. **85** (11), 6720 (1986).
[46] M. Orozco and J. Luque, Chem. Rev. **100**, 4187 (2000).
[47] K. Lum, D. Chandler, and J. Weeks, J. Phys. Chem. B **103**, 4570 (1999).
[48] J. Chandrasekhar, D. Spellmeyer, and W. Jorgensen, J. Am. Chem. Soc. **106**, 903 (1984).
[49] W. Jorgensen, J. Gao, and C. Ravimohan, J. Phys. Chem. **89**, 3470 (1985).
[50] J. Gao and X. Xia, Science **258** (5082), 631 (1992).

[51] M. Field, P. Bash, and M. Karplus, J. Comput. Chem. **11**, 700 (1990).
[52] J. Gao, J. Phys. Chem. **96**, 537 (1992).
[53] J. Gao and M. Freindorf, J. Phys. Chem. A **101** (17), 3182 (1997).
[54] Z. Sun, H. Ge, X. Hu, and Y. Peng, Chem. Eng. Technol. **32**, 134 (2009).
[55] E. Robinson, J. Chem. S. **324**, 1663 (1961).
[56] L. Devi-Kesavan and J. Gao, J. Am. Chem. Soc. **125** (6), 1532 (2003).
[57] K. Byoun, Y. Mo, and J. Gao, J. Am. Chem. Soc. **123**, 3974 (2001).
[58] M. Freindorf and J. Gao, J. Comput. Chem. **17** (3), 386 (1996).
[59] W. Jorgensen and J. Madura, J. Am. Chem. Soc. **105**, 1407 (1983).
[60] T. Helgaker and P. Taylor, in *Advanced Series in Physical Chemistry Modern Electronic Structure Theory, Part II*, edited by D. Yarkony (World Scientific, 1995), Vol. 2; C. Cramer, *Essentials of Computational Chemistry*, 1 ed. (John Wiley & Sons, Ltd., 2002).
[61] E. Papajak, H. Leverentz, J. Zheng, and D. Truhlar, J. Chem. Theory Comput. **5**, 1197 (2009).
[62] E. Kryachko and T. Zeegers-Huyskens, Jounal of Molecular Structure **605**, 251 (2002).
[63] M. Born, S. Ingemann, and N. Nibbering, Int. J. Mass Spectrom. **194**, 103 (2000).
[64] M. Chase, C. Davies, J. Downey, D. Frurip, R. McDonald, and A. Syverud, J. Phys. Chem. Ref. Data **14** (1985).
[65] J. Pedley, *Thermochemical Data and Structures of Organic Compounds*. (College Station, TX, 1994); M. Frenkel, K. March, R. Wilhoit, G. Kabo, and G. Roganov, *Thermodynamics of Organic Compounds in the Gas State*. (College Station, TX, 1994); S. Lias, J. Bartmess, J. Liebman, J. Holmes, R. Levin, and W. Mallard, J. Phys. Chem. Ref. Data **17** (Supplement No. 1) (1988).
[66] J. Smith, J. Kim, and W. Lineberger, Phys. Rev. A **55** (2036) (1997).
[67] J. Paulino and R. Squires, J. Am. Chem. Soc. **113**, 5573 (1991).
[68] A. Geuther, Annalen der Chemie und Pharmacie **123**, 121 (1862).
[69] C. Gonzalez and H. Schlegel, J. Chem. Phys. **90**, 2154 (1989).
[70] C. Gonzalez and H. Schlegel, J. Phys. Chem. **94**, 5523 (1990).
[71] Y.-L. Li, P. Zuo, and D. Phillips, Molecular Simulation **30** (2), 173 (2004).
[72] J. Pliego and W. De Almeida, J. Phys. Chem. A **103**, 3904 (1999).
[73] J. March, *Advanced Organic Chemistry*. (McGraw-Hill, 1977).
[74] Herzberg and Shoosmith, Nature **183**, 1801 (1959); Herzberg, Proc. R. Soc. London, Ser. A **262**, 291 (1961); Herzberg and Johns, J. Chem. Phys. **54**, 2276 (1971).
[75] Andrews, J. Chem. Phys. **48**, 979 (1968).
[76] M. Fujitake and E. Hirota, J. Chem. Phys. **91**, 3426 (1989).
[77] D. Clouthier and J. Karolczak, J. Chem. Phys. **94**, 1 (1991).
[78] C. Barden and H. Schaefer, J. Chem. Phys. **112** (15), 6515 (2000).
[79] R. Schwartz, G. Davico, T. Ramond, and C. Lineberger, J. Phys. Chem. A **103**, 8213 (1999).
[80] W. Kirmse, *Carbene Chemistry*, 2nd ed. (Academic Press, 1971).
[81] D. Das and S. Whittenburg, Jounal of Molecular Structure **492**, 175 (1999).

[82] G. Tarczay, T. Miller, G. Czako, and A. Csaszar, Phys. Chem. Chem. Phys. **7**, 2881 (2005).

[83] M. Liu, C. Lee, A. Bezant, G. Tarczay, R. Clark, T. Miller, and B. Chang, Phys. Chem. Chem. Phys. **5**, 1352 (2003).

[84] P. Scharlin, Acta Chemica Scandinavica, Series A: Physical and Inorganic Chemistry **40** (3), 207 (1986).

[85] G. Sarapulova, L. Rozinova, V. Rozinov, and V. Kolbina, Russian Journal of Organic Chemistry **38** (9), 1266 (2002).

[86] Z. Margolin and F. Long, J. Am. Chem. Soc. **95** (9), 2757 (1973); K. Uneyama, *Organofluorine Chemistry*. (Blackwell Publishing, 2006).

[87] A. Lin, Y. Chiang, D. Dahlberg, and A. Kresge, J. Am. Chem. Soc. **105**, 5380 (1983).

[88] K.-Y. Wong, *Simulating Biochemical Physics with Computers*, Ph.D. Thesis, University of Minnesota, Twin Cities, 2008

APPENDIX A

Gas-Phase Data for the Molecules Taking Part in the Decomposition of Chloroform in an Alkaline Aqueous Solution

Table A.1 Reaction #1. Inter-nuclear potential energy of each molecule involved in the first reaction.

Reaction 1	$CHCl_3 + OH^- \rightarrow CCl_3^- + H_2O$			
	Inter-nuclear Potential Energy (Hartree)			
Method	CHCl3	OH-	CCl3-	H2O
HF/3-21G	-1410.08422	-74.86863	-1409.52703	-75.58596
HF/3-21G*	-1410.41061	-74.86863	-1409.82302	-75.58596
HF/3-21+G	-1410.11305	-74.99574	-1409.56400	-75.61934
HF/6-31G*	-1416.86971	-75.32660	-1416.27164	-76.01075
HF/aug-cc-pVDZ	-1416.94973	-75.39618	-1416.36256	-76.04184
B3LYP/aug-cc-pVDZ	-1419.35996	-75.81693	-1418.78651	-76.44464
MP2/aug-cc-pVDZ	-1417.54056	-75.63702	-1416.96090	-76.26091
CCSD(T)/aVDZ//MP2/aVDZ	-1417.60032	-75.64390	-1417.02164	-76.27390
CCSD(T)/aug-cc-pVDZ	-1417.60045	-75.64390	-1417.02199	-76.27390

Table A.2 Reaction #1. Molecular thermal enthalpy at 298.15 K of each molecule involved in the first reaction. Obtained from gas phase inter-nuclear potential energy and harmonic approximation. Calculated with Gaussian "freq" command.

Reaction 1 $CHCl_3 + OH^- \rightarrow CCl_3^- + H_2O$

Thermal Enthalpy at 298K (Hartree)

Method	CHCl3	OH-	CCl3-	H2O
HF/3-21G	-1410.05797	-74.85867	-1409.51581	-75.56040
HF/3-21G*	-1410.38388	-74.85867	-1409.81197	-75.56041
HF/3-21+G	-1410.08679	-74.98417	-1409.55282	-75.56041
HF/6-31G*	-1416.84250	-75.31478	-1416.26026	-75.98400
HF/aug-cc-pVDZ	-1416.92301	-75.38362	-1416.35116	-76.01503
B3LYP/aug-cc-pVDZ	-1419.33493	-75.80513	-1418.77556	-76.41964
MP2/aug-cc-pVDZ	-1417.51508	-75.62514	-1416.94964	-76.23580
CCSD(T)/aug-cc-pVDZ		-75.63219		-76.24887

Table A.3 Reaction #1. Molecular thermal free energy at 298.15 K of each molecule involved in the first reaction.

Reaction 1 CHCl3 + OH- --> CCl3- + H2O

Thermal Free Energy at 298K (Hartree)

Method	CHCl3	OH-	CCl3-	H2O
HF/3-21G	-1410.09164	-74.87835	-1409.55057	-75.58183
HF/3-21G*	-1410.41719	-74.87835	-1409.84657	-75.58183
HF/3-21+G	-1410.12047	-75.00376	-1409.58762	-75.61527
HF/6-31G*	-1416.87567	-75.33433	-1416.29436	-76.00537
HF/aug-cc-pVDZ	-1416.95626	-75.40315	-1416.38523	-76.03640
B3LYP/aug-cc-pVDZ	-1419.36858	-75.82469	-1418.81043	-76.44107
MP2/aug-cc-pVDZ	-1417.54856	-75.64471	-1416.98399	-76.25724
CCSD(T)/aug-cc-pVDZ		-75.65177		-76.27097

Table A.4 Reaction #2. Inter-nuclear potential energy of each molecule involved in the second reaction.

Reaction 2	CCl_3^- --> CCl_2 + Cl^-		
	Inter-nuclear Potential Energy (Hartree)		
Method	CCl_3^-	CCl_2	Cl^-
HF/3-21G	-1409.52703	-952.10380	-457.35359
HF/3-21G*	-1409.82302	-952.33002	-457.44412
HF/3-21+G	-1409.56400	-952.12649	-457.38086
HF/6-31G*	-1416.27164	-956.71226	-459.52600
HF/aug-cc-pVDZ	-1416.36256	-956.77192	-459.56364
B3LYP/aug-cc-pVDZ	-1418.78651	-958.44350	-460.29818
MP2/aug-cc-pVDZ	-1416.96090	-957.18442	-459.72276
CCSD(T)/aVDZ//MP2/aVDZ	-1417.02164	-957.23598	-459.73830
CCSD(T)/aug-cc-pVDZ	-1417.02199	-957.23629	-459.73830

Table A.5 Reaction #3. Inter-nuclear potential energy of each molecule involved in the third reaction.

Reaction 3	CCl_2 + H_2O --> $CHCl_2OH$		
	Inter-nuclear Potential Energy (Hartree)		
Method	CCl_2	H_2O	$CHCl_2OH$
HF/3-21G	-952.10380	-75.58596	-1027.82680
HF/3-21G*	-952.33002	-75.58596	-1028.04090
HF/3-21+G	-952.12649	-75.61934	-1027.86726
HF/6-31G*	-956.71226	-76.01075	-1032.83966
HF/aug-cc-pVDZ	-956.77192	-76.04184	-1032.91503
B3LYP/aug-cc-pVDZ	-958.44350	-76.44464	-1034.98919
MP2/aug-cc-pVDZ	-957.18442	-76.26091	-1033.55761
CCSD(T)/aVDZ//MP2/aVDZ	-957.23598	-76.27390	-1033.61254
CCSD(T)/aug-cc-pVDZ	-957.23629	-76.27390	

Table A.6 Reaction #4. Inter-nuclear potential energy of each molecule involved in the fourth reaction.

Reaction 4	$CHCl_2OH + OH^- \rightarrow CHClO + Cl^- + H_2O$				
	Inter-nuclear Potential Energy (Hartree)				
Method	$CHCl_2OH$	OH^-	$CHClO$	Cl^-	H_2O
HF/3-21G	-1027.82680	-74.86863	-569.94621	-457.35359	-75.58596
HF/3-21G*	-1028.04090	-74.86863	-570.05431	-457.44412	-75.58596
HF/3-21+G	-1027.86726	-74.99574	-569.97513	-457.38086	-75.61934
HF/6-31G*	-1032.83966	-75.32660	-572.78161	-459.52600	-76.01075
HF/aug-cc-pVDZ	-1032.91503	-75.39618	-572.82553	-459.56364	-76.04184
B3LYP/aug-cc-pVDZ	-1034.98919	-75.81693	-574.16197	-460.29818	-76.44464
MP2/aug-cc-pVDZ	-1033.55761	-75.63702	-573.30200	-459.72276	-76.26091
CCSD(T)/aVDZ//SPE	-1033.61254	-75.64390	-573.33763	-459.73830	-76.27390
CCSD(T)/aVDZ		-75.64390	-573.33766	-459.73830	-76.27390

Table A.7 Reaction #5. Inter-nuclear potential energy of each molecule involved in the fifth reaction.

Reaction 5	$CHClO + OH^- \rightarrow CO + Cl^- + H_2O$				
	Inter-nuclear Potential Energy (Hartree)				
Method	$CHClO$	OH^-	CO	Cl^-	H_2O
HF/3-21G	-569.94621	-74.86863	-112.09330	-457.35359	-75.58596
HF/3-21G*	-570.05431	-74.86863	-112.09330	-457.44412	-75.58596
HF/3-21+G	-569.97513	-74.99574	-112.11038	-457.38086	-75.61934
HF/6-31G*	-572.78161	-75.32660	-112.73788	-459.52600	-76.01075
HF/aug-cc-pVDZ	-572.82553	-75.39618	-112.75548	-459.56364	-76.04184
B3LYP/aug-cc-pVDZ	-574.16197	-75.81693	-113.33028	-460.29818	-76.44464
MP2/aug-cc-pVDZ	-573.30200	-75.63702	-113.05497	-459.72276	-76.26091
CCSD(T)/aVDZ//SPE	-573.33763	-75.64390	-113.07404	-459.73830	-76.27390
CCSD(T)/aVDZ	-573.33766	-75.64390	-113.07405	-459.73830	-76.27390